Distribution agreement

In presenting this thesis or dissertation as a partial fulfillment of the requirements for an advanced degree from Emory University, I hereby grant to Emory University and its agents the non-exclusive license to archive, make accessible, and display my thesis or dissertation in whole or in part in all forms of media, now or hereafter known, including display on the world wide web. I understand that I may select some access restrictions as part of the online submission of this thesis or dissertation. I retain all ownership rights to the copyright of the thesis or dissertation. I also retain the right to use in future works (such as articles or books) all or part of this thesis or dissertation.

Signature:

_____ _____

Alexander V. Fedotov Date

Regulatory mechanisms of heterochromatin dynamics

during *Caenorhabditis elegans* meiosis

By

Alexander V. Fedotov
Doctor of Philosophy

Graduate Division of Biological and Biomedical Sciences
Genetics and Molecular Biology

_____
William G. Kelly, Ph.D.
Advisor

_____
Victor Corces, Ph.D.
Committee Member

_____
John Lucchesi, Ph.D.
Committee Member

_____
Stephanie Sherman, Ph.D.
Committee Member

_____
Yun Tao, Ph.D.
Committee Member

Accepted:

_____
Lisa A. Tedesco, Ph.D.
Dean of the James T. Laney School of Graduate Studies

_____
Date

Regulatory mechanisms of heterochromatin dynamics

during *Caenorhabditis elegans* meiosis

By

Alexander V. Fedotov
B.Sc., Bashkir State University, 2004
M.Sc., Stephen F. Austin State University, 2006

Advisor: William G. Kelly, Ph.D.

An abstract of
A dissertation submitted to the Faculty of the
James T. Laney School of Graduate Studies of Emory University
in partial fulfillment of the requirements for the degree of
Doctor of Philosophy

Graduate Division of Biological and Biomedical Sciences
Genetics and Molecular Biology
2012

Abstract

Regulatory mechanisms of heterochromatin dynamics
during *Caenorhabditis elegans* meiosis
By Alexander V. Fedotov

Major changes to higher-order chromatin architecture are tightly linked to all key meiotic processes that ensure proper juxtaposition of homologous chromosomes and their precise segregation during gametogenesis. Heterochromatic domains pose specific challenge for the maintenance of genome stability during homologous recombination due to their repetitive nature. Our understanding of the principles that govern organization of these domains during meiosis is limited. The overall goal of the work described in my dissertation is to determine the mechanisms that regulate dynamics of histone H3 lysine 9 methylation (H3K9me2), a hallmark of heterochromatin, in *Caenorhabditis elegans* meiosis.

Using a combination of three-dimensional high-resolution microscopy, data mining, and cytogenetic approaches, I revealed previously unrecognized heterochromatin-specific reorganization events at the onset of meiosis that depend upon assembly of meiotic scaffold of chromosomes. I demonstrated that an early association of central region components of synaptonemal complex with chromatin takes place prior to pairing and alignment of homologs, and is mediated by dynein motors. This step of chromosomal axis morphogenesis is required for the establishment of H3K9me2-enriched chromatin compartments, which are later sequestered by the maturing proteinaceous scaffold. I also uncovered the existence of sex-specific differences in the organization of heterochromatin in the context of meiotic scaffold.

My studies therefore provide the first example of the histone modification defining an interface of juxtaposed homologs and point to combinatorial interactions of its regions. They also suggest that chromosomal scaffold itself is an active contributor to compartmentalization of meiotic chromatin, thus potentially playing a role in the prevention of non-allelic recombination, the regulation of genome recognition and defense mechanisms, and the mediation of genome topology.

Regulatory mechanisms of heterochromatin dynamics

during *Caenorhabditis elegans* meiosis

By

Alexander V. Fedotov
B.Sc., Bashkir State University, 2004
M.Sc., Stephen F. Austin State University, 2006

Advisor: William G. Kelly, Ph.D.

A dissertation submitted to the Faculty of the
James T. Laney School of Graduate Studies of Emory University
in partial fulfillment of the requirements for the degree of
Doctor of Philosophy

Graduate Division of Biological and Biomedical Sciences
Genetics and Molecular Biology
2012

ACKNOWLEDGEMENTS

I would like to thank my advisor Dr. William Kelly for giving me a chance to do research work under his guidance. His continuous enthusiasm, useful critiques, and assistance in keeping my project on schedule have been very much appreciated. I would like to express my deep gratitude to my committee members, Dr. Victor Corces, Dr. John Lucchesi, Dr. Stephanie Sherman, and Dr. Yun Tao, for their patience, sincerity and unwavering support of my scientific endeavors. I am indebted to all my coworkers in the laboratory for their persistent help, insightful discussions, and thoughtful criticism. The project would not have been possible without the resources and technical expertise of the Emory University Integrated Cellular Imaging Microscopy Core. I would also like to extend my thanks to all the faculty, staff, and students of the Biology Department and the Genetics and Molecular Biology Program of Emory University for their encouragement and friendships. Finally, I wish to thank my family for their love, wisdom and faith in me.

TABLE OF CONTENTS

LIST OF FIGURES

LIST OF ABBREVIATIONS

3C	Chromatin confirmation capture
AE	Axial element
AO	Acridine orange
CE	Central element
CHIP	Chromatin immunoprecipitation
CR	Central region
DSB	Double-stranded break
FISH	Fluorescence *in situ* hybridization
H2AK5ac	Histone H2A lysine 5 acetylation
H3K4me2	Histone H3 lysine 4 trimethylation
H3K9me2	Histone H3 lysine 9 methylation
HEAT	Huntingtin, elongation factor 3, protein phosphatase 2a, and the yeast kinase TOR1
Him	High incidence of males
HORMA	Hop1p, Rev7p and MAD2
HP1	Heterochromatin protein 1
KASH	Klarsicht, ANC-1, Syne Homology
LE	Lateral element
MSCI	Meiotic sex chromosome inactivation
MSUC	Meiotic silencing of unpaired/unsynapsed chromatin
NE	Nuclear envelope
PC	Pairing center
PCA	Principal component analysis
POL II	RNA Polymerase II
qRT-PCR	Quantitative real-time polymerase chain reaction
rDNA	Ribosomal DNA
RNAi	RNA interference
SC	Synaptonemal complex
SMC	Structural maintenance of chromosomes
SUN	Sad1p, UNC-84
TF	Transverse filament
WT	Wild type

CHAPTER 1

INTRODUCTION

1.1 Meiosis as a specialized type of cell division

Cell division – a process of creation of new cells from preexisting ones – is a basis of life. Every eukaryotic organism starts its life cycle as a single cell. Only through a number of sequential cell divisions does this cell gives rise to all other cell types in developing multicellular eukaryotes. Two types of cell divisions, mitosis and meiosis, are utilized during these developmental processes. The main features of mitosis are the induction of chromosome replication and distributive separation of condensed chromosomes into two new nuclei. As a result, mitotic division gives rise to two identical cells with the same complement of chromosomes in daughter cells as in the parent. Due to this fundamental aspect mitosis serves as the basis of uniparental, asexual, reproduction. The life cycle of the overwhelming majority of eukaryotes also incorporates sexual, or biparental, type of reproduction (John, 1990). This type involves two distinct events – (1) production of a special type of cells, termed gametes (or spores, eventually giving rise to gametes), with a chromosome number reduced by half (haploid) compared to the rest of cells (diploid) in the organism, and (2) a fusion of two of these cells, produced by different sexes of an organism, during fertilization. Fertilization leads to the restoration of the chromosomal complement and combination of two different genomes in one cell.

Thus, meiosis is a specialized cell division that leads to formation of haploid gametes from diploid cells (White, 1973). While some key features of meiosis – replication of chromosomes, their condensation and separation between two dividing cells via a microtubule-based apparatus –are highly similar to the ones of mitosis, meiosis is much more complex and often involves unique molecular machinery. During pre-meiotic S-phase, DNA replicates, resulting in chromosomes consisting of two sister chromatids. DNA replication is

followed by two divisions, the first of which (meiosis I) is characterized by juxtaposition and segregation of homologous chromosomes (homologs), and halving of the total number of chromosomes because each of the homologs moves to opposite poles of the dividing cell (Figure 1A). The second division (meiosis II) is essentially mitosis where sister chromatids separate into two different daughter cells (gametes).

The major challenge the cell faces during meiosis is the correct segregation of homologs in the first division (Sumner, 2003). The fidelity of this process is achieved by sequential occurrence of distinct meiosis-specific events during each of multiple meiotic stages, ensuring that each gamete will carry the correct haploid complement of chromosomes.

1.2 Specifics of prophase I events across model organisms

The first phase of meiosis is termed prophase I. Prophase I is the longest and most complex stage of meiosis. It is usually subdivided into five consecutive stages, based on the differences in the appearance of chromosomes during these stages under the light microscope (Zickler and Kleckner, 1998). Prior to entrance into the first stage, leptotene, chromosomes undergo compaction and appear as long and thin threads. Leptotene is followed by zygotene, at which chromosomes become thicker, acquire a compact configuration (termed “meiotic bouquet”) but without clear substructures, and engage in pairing with their homologs. By the next stage, pachytene, chromosomes are further compacted and homologs are tightly associated, forming bivalents. This association is achieved in part by crossovers or genetic recombination, in which double-stranded breaks (DSBs) of DNA molecules are made and the broken ends from two homologs are reconnected. Next comes diplotene, which is characterized by a loss of all contacts between homologs except for the crossover sites

(termed “chiasmata”). The last stage of prophase I is diakinesis, where bivalents achieve maximal condensation and the meiotic spindle starts to form.

Precise juxtaposition of homologs during prophase I is a fundamental process that ensures correct halving of chromosomal complement at later stages of meiosis. An initial step of juxtaposition involves a search for homology among the chromosomes, followed by the alignment of homologs that successfully identified each other. Despite several decades of intense research, the molecular mechanism of this initial event is probably the least understood (Dernburg, 2012). Recently identified meiosis-specific non-coding RNA, required for recognition between homologs in fission yeast *Schizosaccharomyces pombe* highlighted an unexpected contribution of RNA machinery to this enigmatic process (Ding et al., 2012). The molecular mechanisms of subsequent events of homolog juxtaposition have been characterized in greater detail in most of model systems.

Accurate juxtaposition of homologs depends on proper pairing, alignment, stabilization of close contacts by a proteinaceous matrix, and recombination. It has long been observed that the onset of meiosis coincides with dynamic reorganization of telomeric regions of homologs, resulting in their attachment to the nuclear envelope (NE) by the end of leptotene (Moses, 1968). These attachments are mediated via telomeres and telomere-associated proteins in yeast and mammals or specialized pairing center (PC) regions at one end of chromosomes bound by a family of Zinc-finger-containing proteins in the nematode *Caenorhabditis elegans* (Zickler and Kleckner, 1998; Alsheimer, 2009). Homologous pairing of chromosomal ends, a step that directly follows their attachment to the NE but precedes alignment of chromosomes along their length, has just begun to be understood in some organisms. It occurs during zygotene stage of prophase I and is mediated by conserved

families of nuclear envelope proteins, containing *S*ad1p, *UN*C-84 (SUN) (inner nuclear envelope) and *K*larsicht, *A*NC-1, *S*yne *H*omology (KASH) (outer nuclear envelope) domains (Hiraoka and Dernburg, 2009). These SUN/KASH bridges connect chromosomal ends to the cytoplasmic cytoskeletal network and orchestrate meiotic chromosomal movements via microtubule or actin cables (Koszul and Kleckner, 2009). While the precise role of these motions is not yet known, it has been demonstrated that they could increase the probability of the interhomolog contacts, thus promoting homologous pairing at the NE as well as in other regions (Brown et al., 2011; Lee et al., 2012).

A number of recent studies have shown that formation of close contacts between homologs in regions, distant from NE-attachment sites, occurs via two major pathways. Recombination-dependent pathways, prevalent in mammals, fungi and plants, require formation of double-stranded breaks (DSBs) and invasion of a single strand of one homolog into the DNA duplex of another homolog (Zickler, 2006). Recombination-independent pathways, which occur in fruit flies *Drosophila melanogaster* and *C. elegans*, rely on mediation of interhomolog interactions by specialized pairing sites/centers (Joyce and McKim, 2007).

Stabilization of the homolog alignment is achieved via establishment of the synaptonemal complex (SC), a proteinaceous structure that consists of two lateral elements, forming the axes of homologs, and central region components, that bridge homolog interfaces (Page and Hawley, 2004) (Figure 1B). In organisms that rely on recombination for alignment of homologs, generation of DSBs is also required for synapsis (assembly of SC) (Bishop et al., 1992; Baudat et al., 2000). However, synapsis and recombination are two independent events in *D. melanogaster* and *C. elegans* (Dernburg et al., 1998; McKim, 1998).

Meiotic recombination leads to the formation of physical links between homologs, enabling them to stay connected and orient properly on the meiotic spindle when the SC is disassembled. Recombination is initiated by a highly conserved topoisomerase-like protein Spo11 that generates DSBs which creates single-stranded DNA by a Rad50-Mre11 complex of proteins (Lichten, 2001; San Filippo et al., 2008). This strand is then covered by another complex of recombination proteins that contains the RecA homolog Rad51, and invades the opposing double-stranded homolog (Barzel and Kupiec, 2008). At the next step, DSB repair is channeled into either formation of crossovers or non-crossover products. Crossover generation is a tightly regulated process due to its potential contribution to genome instability. In most organisms, only a single crossover is formed per chromosomal arm, - a phenomenon known as crossover interference (Pawlowski and Cande, 2005). SC formation has long been known to regulate the distribution of crossover events, highlighting the coordination of these two events (Sym and Roeder, 1994).

Thus, it is this interplay of multiple events that ensures correct juxtaposition of homologues on the meiotic spindle after prophase I is complete.

1.3 *C. elegans* as a model system for studies of meiosis

Despite the diversity of meiotic events, the core machinery that regulates homolog juxtaposition is highly conserved in all groups of eukaryotic kingdoms, indicating that the basic aspects of meiosis were established in a common ancestor of eukaryotes. Meiosis in the nematode *C. elegans* shares key features with higher eukaryotes, but it is unique in several ways - and these provide certain advantages for research (Zetka, 2009). First, the spatial distribution of nuclei in the gonad correlates with the order of their progression through

prophase I (Kimble and White, 1981). As a result, each of the linearly aligned zones of the gonad corresponds to a particular substage of prophase I of meiosis: small nuclei in the distal portion of the meiotic zone of the gonad represent leptotene stage (formation of axes of chromosomes), more proximal nuclei with chromatin mass displaced to one pole represent zygotene (homolog pairing and alignment), nuclei with distinct bivalents represent pachytene (synapsis and crossover formation), and nuclei with condensed bivalents represent diplotene and finally nuclei with separated homologs, linked by chisamata represent diakinesis (Dernburg et al., 1998) (Figure 2). Second, the presence of Pairing Centers (PCs) allows the mechanisms of homologue alignment and synapsis to be analyzed independently from recombination (MacQueen et al., 2005). Third, *C. elegans* is a hermaphroditic species, thus allowing us to study both male- and female-specific meiosis in the same individual (Brenner, 1974). Fourth, it has shorter generation time compared to *Drosophila* and mammalian counterparts, making it a highly efficient system when using both forward and reverse genetic approaches (Lui and Colaiácovo, 2013). Fifth, chromosome nondisjunction, a hallmark of defects in homolog juxtaposition, is easily detected in *C. elegans* populations by an increase in the number of males, which carry a single X chromosome (XO) versus hermaphrodites, which carry two (XX) (Brenner, 1974). This phenotype, termed *h*igh *i*ncidence of *m*ales (Him) has formed the basis of mutant screens, aimed at identifying key components of meiotic machinery (Hodgkin et al., 1979). Finally, meiotic checkpoints of *C. elegans* seem to be less strict than in mammals, since mutantions in meiosis-specific genes that would exhibit complete gametogenic failure and sterility in mammals, can still often produce functional gametes in *C. elegans* (Colaiacovo, 2006). All these features make *C. elegans* a powerful model for studies of meiosis-specific processes.

1.4 Spatial organization of prophase I chromatin

Numerous electron and light microscopy studies have revealed that similar to mitotic prophase chromosomes, meiotic pachytene chromosomes comprise loops of chromatin, emanating from a proteinaceous scaffold. In mitotic chromosomes, this scaffold is formed by a family of chromosomal ATPases, named the Structural Maintenance of Chromosomes (SMC) (Hirano, 2002). Conserved from bacteria to humans, SMC proteins form two distinct complexes, differing in their composition and functions. The condensin complex, composed of two SMC subunits and non-SMC proteins and along with Topoisomerase II plays a role in condensation of chromosomes, acting as an intramolecular DNA crosslinker (Hirano, 2005). During meiosis, condensins mediate axis length compaction of prophase and metaphase chromosomes in budding yeast *Saccharomyces cerevisiae* (Yu and Koshland, 2003), *C. elegans* (Hagstrom et al., 2002; Chan et al., 2004), *D. melanogaster* (Hartl et al., 2008), mice *Mus musculus* (Lee et al., 2011), and other systems. The cohesin complex is formed by several kleisin and *H*untingtin, elongation factor 3 (*E*F3), protein phosphatase 2A (PP2*A*), and the yeast kinase *T*OR1 (HEAT)-domain proteins and in mitotic chromosomes tethers sister chromatids together after replication (Hirano, 2002). The meiotic cohesion complex has several meiosis-specific paralogs in most studied organisms, with Rec8 being the most well characterized among them (Barbero, 2012). In meiosis, cohesins assemble along the axial core during pre-meiotic S phase and are critical for the stepwise separation of homologs and sister chromatids at the meiotic spindles (Wood et al., 2010)

The major difference in organization of chromosomal scaffold between mitosis and meiosis lies in the formation of SC, a unique proteinaceous complex, present only during prophase I of meiosis (Page and Hawley, 2004). While the protein composition of the SC is

not evolutionary conserved, its ultrastructural features are highly similar across species (Zickler and Kleckner, 1999). Electron microscopy reveals a “ladder-like” structure of mature SC with a mesh of lateral elements (LEs) of the homologs serving as an attachment base for chromatin loops of sister chromatids, while fibrillar transverse filaments (TFs) along with central elements (CEs) interconnect them, forming a central region (CR) (von Wettstein et al., 1984). Different organisms have different numbers of axial and central region components. Axial elements (AEs) of yeast are represented by Hop1 and Red1 proteins (Hollingsworth et al., 1990; Smith and Roeder, 1997), and central region is composed of Zip1 filaments (Sym et al., 1993). The Synapsis Initiation Complex, consisting of Zip2, Zip3, and Zip4 proteins, promotes assembly of Zip1 and becomes a part of SC after completion of synapsis (Voelkel-Meiman et al., 2012). The SC of *D. melanogaster* is composed of cohesin-like axial element C(2)M and a transverse filament protein C(3)G (Page and Hawley, 2001; Manheim and McKim, 2003). In mammals (rodents), SYCP1 is a main component of TFs, while SYCP3 establishes AEs (Meuwissen et al., 1992; Lammers et al., 1994). A number of other proteins, specifically SYCP2 of AEs and SYCE1, SYCE2, SYCE3, and Tex12 of CR, also contribute to the formation of the SC, making its composition one of the most complex among studied model systems (Fraune et al., 2012).

Similar to most organisms, assembly of the SC is the culmination of homolog juxtaposition in prophase I of *C. elegans* and is indispensable for the establishment of crossovers (MacQueen et al., 2002). In *C. elegans*, the SC consists of four HORMA (named after the *Ho*p1p, *R*ev7p and *MA*D2 proteins)-domain-containing axial proteins HIM-3, HTP-1, -2, and -3 that form lateral elements (Zetka et al., 1999; Couteau and Zetka, 2005; Martinez-Perez and Villeneuve, 2005; Goodyer et al., 2008), and four proteins of the central

region of SC, SYP-1, -2, -3, and -4 (MacQueen et al., 2002; Colaiácovo et al., 2003; Smolikov et al., 2007a, 2007b, 2009). LEs form the basis of the chromatin loops of two sister chromatids, which are kept together by kleisin members of the cohesin complex (Pasierbek et al., 2001; Severson et al., 2009). Interestingly, assembly of some axial elements is dependent on cohesins, while others are themselves required for the association of cohesins with chromatin (Severson et al., 2009). Accordingly, the assembly of the axial elements takes place during or immediately after premeiotic S-phase and before homolog pairing or alignment (Zetka et al., 1999). Loading of CR components depends on the association of axial elements and cohesins with chromatin and thus follows completion of their assembly on chromatin (Couteau et al., 2004; Severson et al., 2009).

Several studies have shown that in *C. elegans* coordination of the assembly of the CR of the SC between homologs takes place during leptotene/zygotene stages of prophase I and is achieved via attachment of PC regions at one end of chromosomes to the NE, mediated by a family of zinc-finger-containing proteins (MacQueen et al., 2005; Phillips et al., 2005; Phillips and Dernburg, 2006; Penkner et al., 2007, 2009). Similar to other systems, SUN-1/ZYG-12 bridges within the NE connect chromosomal ends to dynein and cytoplasmic microtubule network, thus providing mechanical force for the chromosome motion, and having been shown to be required for proper synapsis (Sato et al., 2009; Wynne et al., 2012). Control of these early prophase events, mediated in part by a set of kinases, ensures assembly of SC between paired homologs (MacQueen and Villeneuve, 2001; Penkner et al., 2009; Harper et al., 2011; Labella et al., 2011).

Although the SC has been a target of extensive research efforts for more than a century, several fundamental questions regarding the timing and mechanism of SC formation remain.

It is currently unclear how chromatin loops are anchored to a protein axis and what forces regulate its assembly. While HORMA domain-containing axial elements are thought to mediate the linkage between chromatin and CR, the specific sites of their interactions with chromatin and underlying mechanisms of their assembly remain elusive. While it has previously been established that some chromatin loops protrude beyond the inner surface of the LE, the sequence of these regions remains to be determined. Our understanding of the sequence of events that leads to the establishment of the components of the central region of the SC is also not clear. Studies of SC assembly in diverse groups of organisms have indicated that loading of the central region of SC depends on the assembly of the axial elements and, more importantly, takes place after homologs have identified each other and achieved pairing and alignment. However, the mechanisms that prevent premature assembly of CR components between non-homologous regions remain elusive.

1.5 Chromatin features as factors in regulation of meiotic processes

It has long been appreciated that besides core meiotic machinery specific local and global features of meiotic chromatin contribute to proper homolog juxtaposition. The best documented examples of connections between chromatin features and homolog interactions come from studies on the regulation of recombination. During the past several decades it has been observed that DSBs are distributed unevenly within the genome. Chromatin organization itself plays a role in regulating DSBs numbers by making specific regions more or less accessible to the cleavage activity of Spo11, thus serving as a determinant of the sites of crossover events between homologs (Petes, 2001; Paigen and Petkov, 2010; Lichten and de Massy, 2011). The first nucleotide-resolution DSB map in *S. cerevisiae* (Pan et al., 2011)

and the first genome-wide map of DSB distribution in a mammal *M. musculus* (Smagulova et al., 2011) both revealed positioning of nucleosome and binding of chromatin-associated proteins, such as transcription factors, as key features of chromatin that influence DSB numbers and distribution.

Covalent modifications of histones represent a striking feature of chromatin that dramatically affects its organization. These modifications are dynamic, and enzymes that add or remove them, have been identified. A particular modification of histone can have two main functional consequences – it can either directly affect the contacts between nucleosomes, and/or serve as a recruitment platform for other nonhistone proteins (Kouzarides, 2007). Both of these events have the potential to affect higher-order architecture of chromatin. Remarkably, a set of genome-wide studies indicated that chromatin enriched for histone H3 lysine 4 trimethylation (H3K4me3), a histone modification associated with open chromatin, also demonstrated elevated levels of DSB formation in both yeast and mice (Borde et al., 2009; Buard et al., 2009). Remarkably, inactivation of Set1 in yeast or PRDM9 in mouse, both H3K4me3 methyltransferases, causes severe reduction or redistribution of DSBs in the genomes of both species (Borde et al., 2009; Brick et al., 2012). Histone H2A lysine 5 acetylation (H2AK5ac), a histone modification of unknown function, has been linked to global changes in chromatin organization, affecting distribution of crossover events in *C. elegans* (Wagner et al., 2010). The unique higher-order architecture of meiotic chromatin, in which the bulk of DNA is organized into an array of loops, also contributes to recombination patterns in yeast (Blat et al., 2002; Panizza et al., 2011), *C. elegans* (Mets and Meyer, 2009), and mammals (Kauppi et al., 2011). Evidence suggests that SC proteins play a direct role in the establishment of specific chromatin features. The axial element HTP-3 is

required for acquisition of H2AK5ac-associated chromatin configurations during DNA damage repair specifically at the axes of juxtaposed homologs in *C. elegans* (Couteau and Zetka, 2011). However, in contrast to interphase chromatin, our knowledge of organization of specific chromatin domains within the core of meiotic chromosomes is extremely scarce. Therefore, gaining insights into the principles of chromatin reorganization in the context of the assembly of meiotic scaffold holds enormous potential for our understanding of the mechanisms that govern homolog juxtaposition.

1.6 Heterochromatin in meiosis

Differentiation of mitotic chromosomes into regions of genetically active and inactive chromatin was first pointed out by the German cytologists Emil Heitz in 1928 (Passarge, 1979). He was also the one who coined the terms “euchromatin” and “heterochromatin”, correctly referring to the less and more condensed regions of interphase nucleus, respectively. Being extensively studied for almost a century, heterochromatin serves as a unique model of the effects of chromatin organization on biological processes, such as transcription, topology and DNA repair (Grewal and Jia, 2007). Since then two types of heterochromatin have been identified, constitutive and facultative. Chromatin regions that bear high density of repetitive DNA elements, such as telomeres, centromeres, and pericentromeric regions, remain condensed throughout the cell cycle and represent constitutive heterochromatin. Heterochromatin can also be temporarily established at loci that play an active role in regulation of development, but need to remain silent during specific time periods. These regions represent facultative heterochromatin.

While the mechanisms of constitutive heterochromatin formation vary across eukaryotic kingdoms, they all share several common themes. In most model systems, histone H3 lysine 9 methylation (H3K9me2) and Heterochromatin Protein 1 (HP1) are the hallmarks of this epigenetic phenomenon (Cowell et al., 2002). The initial targeting of constitutive heterochromatin is achieved via RNAi pathways, by "sensing" the presence of repetitive elements in the genome and through yet poorly characterized mechanism recruiting histone methyltransferase to the repeats (Beisel and Paro, 2011). Histone H3 methylated at lysine 9 serves as a binding platform for the chromodomain-containing HP1, which in turn recruits other chromatin-modifying factors that are involved in condensation of the targeted region. This condensation can preclude the access of canonical transcriptional machinery, thus leading to transcriptional repression of these regions (Martin and Zhang, 2005).

Repetitive regions of the genome pose a significant threat to genome stability during meiosis due to their potential for non-allelic recombination (Lichten et al., 1987; Kupiec and Petes, 1988; Schlecht et al., 2004; Henry et al., 2006). Remarkably, a specific set of chromatin-modifying factors ensures heterochromatinization of these regions in budding yeast and thus limits DSB formation (Gottlieb and Esposito, 1989; Mieczkowski et al., 2007; Vader et al., 2011). While formation of heterochromatin in budding yeast is achieved via the activity of histone deacetylases, studies in fission yeast and mammals have identified H3K9-specific N-methyltransferases participating in heterochromatin formation (Peters et al., 2001; Tachibana et al., 2007; Krauss, 2008). These enzymes are similar in that their C-termini all contain pre-SET, SET and post-SET domains, involved in chromatin binding and H3K9 methylation (Krauss, 2008). Remarkably, knock-out of enzymes responsible for H3K9me2 in

the mouse germline leads to defective pairing of homologs, delayed synapsis and progression of gametogenesis (Peters et al., 2001; Tachibana et al., 2007).

Heterochromatin in *C. elegans* has been studied less extensively when compared to fission yeast, fruit flies, or mammals. However, the existing knowledge highlights conservation of basic pathways of heterochromatin formation and maintenance in the nematode. Genome-wide studies of the distribution of H3K9me2 in somatic nuclei of *C. elegans* embryos and larvae revealed that this modification is enriched primarily at several different classes of repetitive elements (Gerstein et al., 2010). The contribution of RNAi machinery to maintaining the heterochromatic state of transposons has been demonstrated both in somatic tissues and in the cells undergoing meiosis (Sijen and Plasterk, 2003; Grishok et al., 2005). Intriguingly, transgenes in repetitive extrachromosomal arrays have also been shown to accumulate H3K9me2 in the meiotic cells of *C. elegans*, and similarly to repeats in other organisms require a homolog of HP1 for their silencing (Couteau et al., 2002; Kelly et al., 2002). There are 31 SET domain-containing methyltransferases in *C. elegans*, but only two of them, encoded by genes R05D3.11 (*met-2*) and F34D6.4 (*set-11*), have domain structures similar to H3K9-specific methyltransefrases in other organisms (Andersen and Horvitz, 2007). Recent studies demonstrated that MET-2 is a histone methyltransfrease, responsible for the bulk of H3K9me2 in mitotic and meiotic nuclei in *C. elegans* germline (Bessler et al., 2010). Interestingly, *met-2* mutants exhibited only mild defects in chromosome segregation, suggesting that the presence of H3K9me2 during meiosis is not required for the normal pairing, synapsis, and recombination of homologs (Bessler et al., 2010). The difference of these phenotypes from the ones observed in mammals could be attributed to several reasons: (1) a generally low content of repetitive elements in *C. elegans*

genome in comparison with mammalian genomes; (2) the reliance on specialized pairing sites, rather than recombination, for stabilization of homolog alignment; and (3) potentially mild effects of derepression of transposon-like elements on genome stability due to the redundant control of their activity by a robust RNAi machinery.

Heterochromatic regions could also play a direct role in promotion of homologous pairing. These unexpected findings came from the studies of chromatin reorganization at the onset of meiotic prophase I in wheat lines and wheat-rice hybrids (Colas et al., 2008). They demonstrated that subtelomeric repeats undergo dramatic expansion at the onset of meiosis, engage in contacts during pairing of homologs, and are required for proper synapsis. Remarkably, a specific chromosomal locus with functions in DNA replication, *Ph1*, is required for these events, linking homology recognition and heterochromatin (Prieto et al., 2004).

Taken together, these studies indicate that heterochromatic regions of the genome on one hand protect genome integrity by reducing the chance of non-homologous recombination at repetitive elements and silencing transposable elements. On the other hand, heterochromatin can play direct roles in unique chromatin reorganization events, encompassing juxtaposition of chromosomes, by providing a platform for the formation of structurally stable chromatin domains. These aspects of heterochromatin biology of meiotic chromatin and their contribution to key processes of meiosis have only just begun to be understood.

1.7 Meiotic sex chromosome inactivation (MSCI)

In mammals, X and Y chromosomes share only a short region of homology and are not fully synapsed (Turner, 2007). In *C. elegans*, sex is determined by the presence or absence of the

second X chromosome, so males have a single X, which lacks a homologous partner (Brenner, 1973). Does this unique status of sex chromosomes have an effect on the organization of their chromatin?

Studies of heterologous sex chromosomes from a variety of systems have indicated that they exhibit dramatically different patterns of histone modifications starting as early as prophase I of meiosis. The initial observations, made in the males of *C. elegans*, revealed that their lone X chromosome exhibits elevated levels of H3K9me2 during the pachytene stage of prophase I (Kelly et al., 2002; Reuben and Lin, 2002; Bean et al., 2004). This process was shown to be dependent on the components of a small RNA-mediated pathway that are also involved in the organization of chromatin domains of holocentric chromosomes during the formation of kinetochores of meiotic spindle (Maine et al., 2005; Claycomb et al., 2009; She et al., 2009). Similar observations have been since made in *M. musculus* and chicken *Gallu gallus*, where heterologous sex chromosomes are decorated with H3K9me2 during prophase I (and at prometaphase I, in mammals) of meiosis (Khalil et al., 2004; Schoenmakers et al., 2009).

In contrast to *C. elegans*, heterologous sex chromosomes in vertebrates undergo another round of chromatin reorganization events, linked to unrepaired DSBs. This involves association of the DNA damage repair protein BRCA1 with the XY pair, which in turn recruits ATR kinase to phosphorylate the histone variant H2AX at serine 139 (Mahadevaiah et al., 2001; Turner et al., 2004). A set of other histone modifications are also acquired by the XY pair, including H2A and H2B ubiquitination, but the mechanistic details of this process remain unclear (Baarends et al., 1999, 2005).

Remarkably, the *C. elegans* X in males, the heterologously synapsed ZW sex chromosomes in birds (to a lesser degree), and partially synapsed XY pair in mammals become heavily condensed and compartmentalized, forming so called sex body (Solari, 1974; Kelly et al., 2002). This condensation is thought to cause their depletion of RNA Pol II and subsequent transcriptional inactivation in meiosis – hence the name of this phenomenon, MSCI (Meiotic Sex Chromosome Inactivation) (Turner, 2007). Despite the conserved nature of this phenomenon and elevated interest to this process in recent years, the causative role of these chromatin reorganization events on transcriptional inactivation of sex chromosomes remains yet to be demonstrated unequivocally (Burgoyne et al., 2009).

1.8 Quality control of meiotic processes

Two distinct proapoptotic surveillance systems are known to control the fidelity of prophase I of meiosis. Both of them rely on coupling mechanisms, called checkpoints, which allow the temporal detection of aberrant chromatin with the progression of meiosis (Hochwagen and Amon, 2006). The first checkpoint, identified in *S. cerevisiae, D. melanogaster,* and *C. elegans*, is DNA damage-induced and senses unrepaired single-stranded or double-stranded breaks (Lydall et al., 1996; Ghabrial and Schüpbach, 1999; Gartner et al., 2000). This mechanism couples the detection of these lesions to the meiotic arrest of the germ cells with the aberrant chromatin and/or their elimination through apoptosis. Therefore, DNA damage-induced checkpoints guard the genome integrity by preventing chromosome fragmentation and missegregation during meiosis. In *S. cerevisiae* and *C. elegans*, another checkpoint signal comes from unsynapsed chromatin and is detected by a synapsis-dependent checkpoint (Bhalla and Dernburg, 2005; Wu and Burgess, 2006) (Bhalla and Dernburg, 2005). This

checkpoint eliminates nuclei with unsynapsed chromatin, but in *C. elegans* the activation of programmed cell death is triggered only in cases when chromosomes maintain a functional connection to NE. These data suggests a complex signaling machinery, coordinating proper pairing and synapsis of homologs and thus preventing the production of aneuploid gametes. The molecular mechanisms of action of these checkpoints remain poorly understood.

Sex chromosomes, due to their unique juxtaposition status, present a challenge for the meiotic checkpoint machinery. While our knowledge of mammalian checkpoint machinery is still fragmentary and the dissection of its interplay with sex chromosomes is currently difficult (Handel and Schimenti, 2010), recent studies in *C. elegans* indicated that checkpoint activation by an unpaired X chromosome during spermatogenesis is precluded, thus preventing erroneous elimination of spermatocytes through apoptotic pathways (Jaramillo-Lambert and Engebrecht, 2010). Accordingly, the unsynapsed status of Z and W sex chromosomes in some oocytes was recently shown to be refractory to triggering programmed cell death in birds as well (Guioli et al., 2012). The intriguing nature of these findings prompts further investigation into the relationship between the status of sex chromosomes and meiotic quality control machinery.

RATIONALE

Our previous studies have shown that the single X chromosome in males, unpaired X chromosomes in PC mutant hermaphrodites, extrachromosomal duplications, and extrachromosomal transgenic arrays exhibit elevated levels of H3K9me2 in pachytene of prophase I in *C. elegans* meiosis. All these aberrant chromosomes/chromosomal fragments share a particular feature that sets them apart from the normal chromatin – they either lack

their homologous partner or fail to pair, synapse, and recombine with it. Therefore, the specific contribution of each of these events to the appearance of heterochromatic domains remained unclear. The existence of a vast collection of *C. elegans* meiotic mutants, specifically defective for each of the numerous events during homolog juxtaposition, and the powerful molecular genetics and cytological analysis techniques available for this organism enable us to manipulate and monitor the status of chromosomes at the onset of *C. elegans* meiosis. These features of *C. elegans* as a genetic model system put us in an unprecedented position to explore the regulatory mechanism of heterochromatin dynamics during *C. elegans* meiosis with the final goal of understanding principles of chromatin organization in the context of the assembly of meiotic scaffold.

SIGNIFICANCE

Although abnormalities in meiosis progression have long been implicated in development of meiotic arrest and sterility in humans, the underlying reasons for a majority of these defects remain unclear (Hassold et al., 2007). Recent advances in understanding the epigenetic basis of meiotic repression of aberrant chromatin in lower organisms generated a new wave of interest into human meiosis. As a result, several studies found that asynapsed arms of chromosomes undergo patterns of chromatin reorganization, reminiscent of MSCI, in infertile male carriers of reciprocal translocations (Oliver-Bonet et al., 2005; Ferguson et al., 2008). Assessing the consequences of other meiotic defects in human subjects remains challenging, however, due to a difficult chronology of meiotic events and lack of easy access to the cells of interest (Vallente et al., 2006). At the same time, gaining insights into the principles of chromatin reorganization in the context of the assembly of the meiotic scaffold

is critical for our understanding of the mechanisms that ensure homolog juxtaposition and fidelity of meiosis.

Simplified, yet highly conserved, features of meiosis in *C. elegans* allowed us to dissect the heterochromatin-specific reorganization events at the onset of meiosis that accompany the process of homolog juxtaposition. In this work I show that the establishment of heterochromatic domains requires an early association of SC central region components with chromatin that occurs prior to pairing of homologs, and this association is mediated by dynein-dependent events. Continuation of SC assembly leads to a disappearance of these domains, which may indicate their sequestration by the proteinaceous SC scaffold. Taken together, these findings suggest that, in contrast to euchromatic regions, heterochromatic domains acquire specific positions within the chromosomal core during juxtaposition of homologs and thus reveal compartmentalization of meiotic chromatin architecture. I also demonstrate the existence of sex-secific differences in organization of heterochromatin in the context of meiotic scaffold.

The importance of these findings is three-fold. First, I demonstrate for the first time that, similarly to interphase nuclei, heterochromatic regions of the genome could serve as a platform for recruitment of meiotic scaffold, thus establishing the unique compartmentalized architecture of meiotic chromatin. These results highlight the importance of understanding principles of the higher-order organization of meiotic chromatin in our quest for dissecting the mechanisms of crossover formation and other aspects of homolog juxtaposition. Similar studies in vertebrates could facilitate research on the etiology of meiotic dysfunctions and birth defects in human subjects. Second, the outcomes of this project shed light on the potential contribution of higher-order chromatin architecture to manifestations of MSCI

phenomena, thus prompting detailed investigation of this process in similar context in mammals. Third, described dimorphism in heterochromatin reorganization events during homolog juxtaposition in spermatogenesis versus oogensis may help us understand the elusive reasons of variations in degree of fidelity of meiotic processes in male versus female sexual environments.

Figure 1. Main events of meiosis and features of meiotic chromosomes.

(A) Steps of meiotic chromosome segregation.

(B) Model of the synaptonemal complex structure. A cross section of the segment of the mature synaptonemal complex is shown. Chromatin loops of homologous chromosomes are anchored to the lateral elements (LE). Central region elements (CREs) are assembled between the aligned homologs.

A

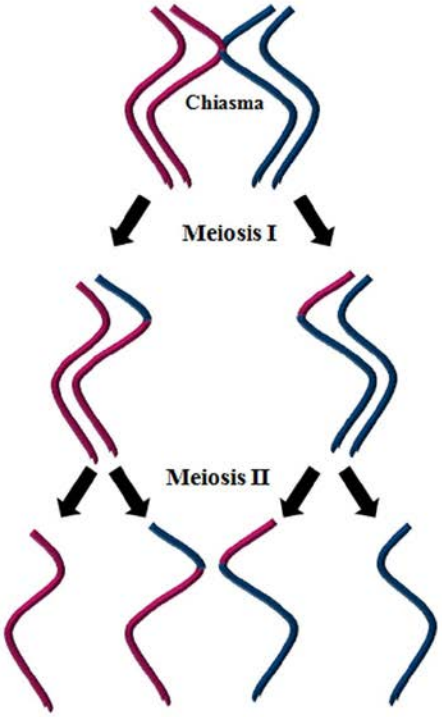

B

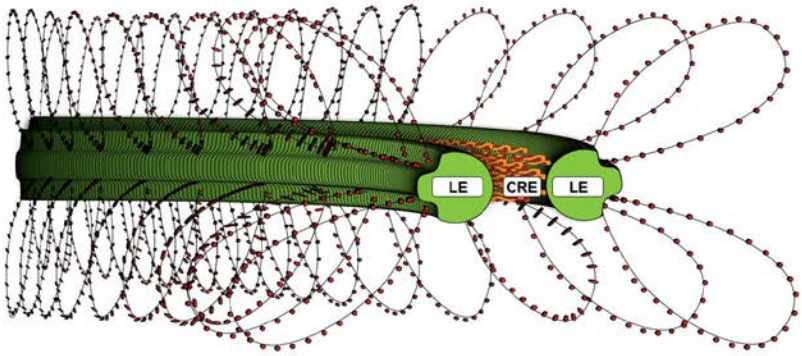

Figure 2. Schematic diagram of the main events of prophase I in the gonad of an adult *C. elegans* hermaphrodite. Prophase I is subdivided into 5 substages: leptotene (condensation of replicated chromosomes and DSBs formation), zygotene (alignment and pairing of homologous chromosomes), pachytene (SC is complete and crossover formation takes place), diplotene (SC disassembly, visible chiasmata), and diakinesis (final condensation of chromosomes).

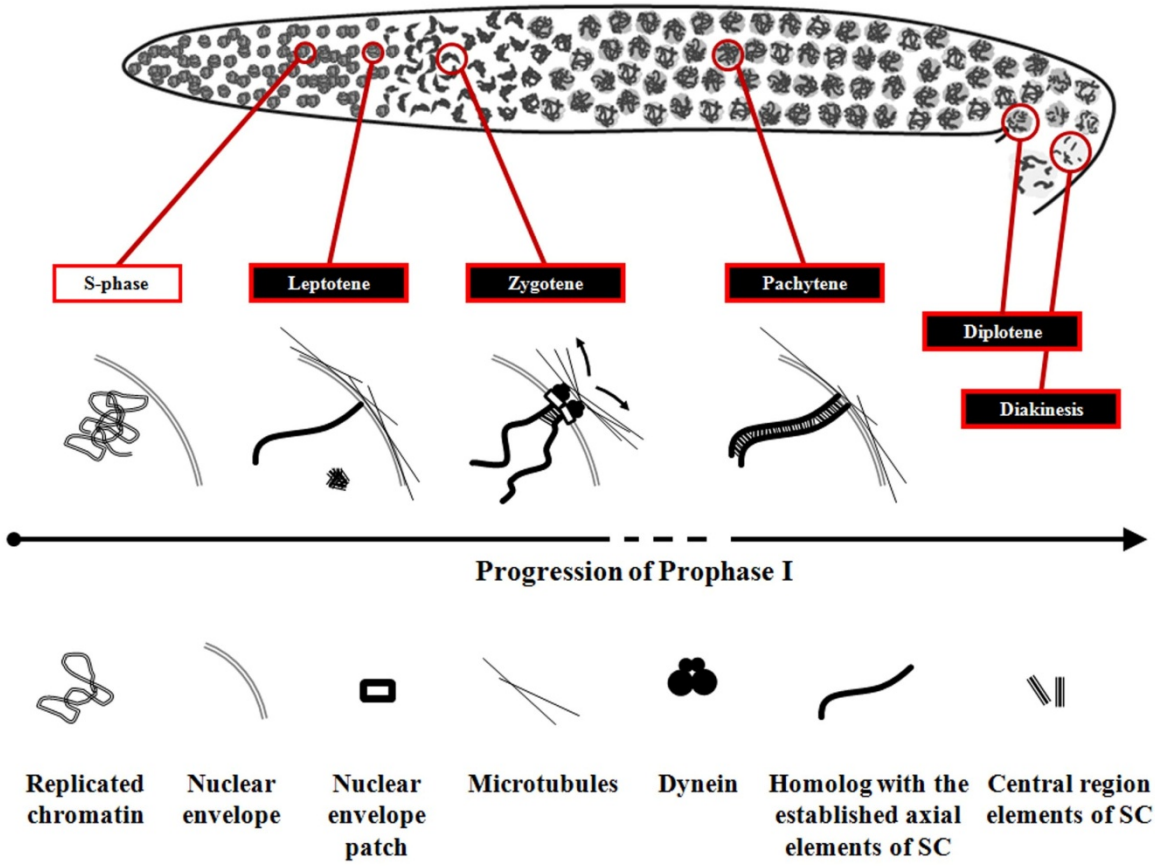
S-phase
Leptotene
Zygotene
Pachytene
Diplotene
Diakinesis
Progression of Prophase I
Replicated chromatin
Nuclear envelope
Nuclear envelope patch
Microtubules
Dynein
Homolog with the established axial elements of SC
Central region elements of SC

CHAPTER 2

THE CONSEQUENCES OF THE APPEARANCE OF HETEROCHROATIC DOMAINS ON UNIVALENTS FOR MEIOTIC PROCESSES

2.1 Introduction

Studies of mouse strains, defective for proper synapsis or recombination of autosomes, have revealed that MSCI could be a manifestation of a broader phenomenon, named Meiotic Silencing of Unpaired/Unsynapsed Chromatin (MSUC) (Turner, 2007). This process was shown to rely on the similar to MSCI mechanisms and was proposed to cause cell death through interference with expression of meiotic genes (Burgoyne et al., 2009). Moreover, it was recently shown that defects in synapsis of autosomes could interfere with MSCI and thus contribute to meiotic failure of aberrant meiocytes (Mahadevaiah et al., 2008). The phenomena described resemble modifications of chromatin features of aberrant chromosomes in prophase I of *C. elegans* (Kelly and Aramayo, 2007). These similarities prompted us to investigate the consequences of the appearance of H3K9me2 on unpaired chromosomes during oogenesis and spermatogenesis in *C. elegans*.

2.2 Results

Appearance of H3K9me2 on univalents in PC mutants does not trigger elevated levels of apoptosis

Based on the phenotypes of asynapsis mutants in mammals, we hypothesized that enrichment of H3K9me2 on unpaired/unsynapsed chromosomes in *C. elegans* also leads to their targeting for elimination via apoptotic machinery. To test this hypothesis, we compared the levels of apoptosis using Acridine Orange (AO) staining in the gonads of age-matched adult hermaphrodite worms of wild-type and the following mutant backgrounds: *zim-2(tm574)* (two unpaired univalents of chromosome V, exhibiting enrichment for H3K9me2), *met-2(n4256)* (no detectable H3K9me2 in meiotic cells), *zim-2(tm574); met-2(n4256)* (two

unpaired univalents of chromosome V, no enrichment for H3K9me2) (Figure 3A). We predicted that if our hypothesis was correct, we would observe a decrease in the number of apoptotic bodies in the double mutant *zim-2(tm574); met-2(n4256)* compared to *zim-2(tm574)*.

Our results indicated that depletion of H3K9me2 enrichment on univalents does not have a significant effect on the levels of apoptosis during oogenesis. The number of AO-positive bodies was elevated in *zim-2(tm574)* mutant alone, consistent with previous reports on the activation of DNA damage checkpoint upon defects in pairing/synapsis of single pair of chromosomes (Bhalla and Dernburg, 2005) (Figure 3B). *met-2(n4256)* mutants by themselves had levels of apoptosis comparable to wild type, suggesting that absence of H3K9me2 in prophase I does not trigger programmed cell death (Figure 3B). Double mutant *zim-2(tm574); met-2(n4256)* had numbers of apoptotic bodies similar to *zim-2(tm574)* alone (Student's t-test, $p>0.05$) (Figure 3B). These data indicated that removal of H3K9me2 from unpaired/unsynapsed chromosomes does not abrogate activation of apoptotic response to aberrant chromatin.

Transcriptional status of univalents exhibiting enrichment for H3K9me2

Recent observations of transcriptional silencing of aberrant chromosomes in prophase I of meiosis prompted us to investigate the effect of appearance of H3K9me2 signal on the transcriptional status of univalents in *C. elegans* adult hermaphrodites. We examined the levels of transcripts, originating from genes residing on chromosome V with different patterns of expression: F26D2.2 (*syp-1*, encodes a component of the CR of SC), expressed during meiosis; T06E6.2a (*cyb-3*, encodes Cyclin-3), expressed in oocytes; F11A3.1 (*acs-14*,

encodes Acyl-CoA synthetase), expressed in hermaphrodite somatic tissues (Figure 4A-C, schematics). The ubiquitously expressed T04C12.6 (*act-1*, actin) was used as an endogenous control. Expression patterns of the genes were based on published microarray data (Reinke et al., 2000, 2004) and *in situ* hybridization data from The Nematode Expression Pattern Database of the Kohara lab (http://nematde.lab.nig.ac.jp). Similarly to the apoptosis experiment outlined above, transcripts levels were measured by quantitative real-time polymerase chain reaction (qRT-PCR) in age-matched adult hermaphrodite worms of wild-type and the following mutant backgrounds: *zim-2(tm574)* (two unpaired univalents of chromosome V, exhibiting enrichment for H3K9me2), *met-2(n4256)* (no detectable H3K9me2 in meiotic cells), *zim-2(tm574); met-2(n4256)* (two unpaired univalents of chromosome V, no enrichment for H3K9me2).

Our results indicated that enrichment of H3K9me2 on univalents does not affect the levels of transcripts originating from genes on these chromosomes either at the onset of meiosis, during maturation of oocytes, or in somatic cells of an adult *C. elegans*. None of the examined genes showed significant up-regulation of expression levels in mutants that lacked H3K9me2 on univalents compared to the ones with H3K9me2 enrichment on them (Figure 4A-C). In the case of the gene with somatic expression pattern, its transcript levels were down-regulated upon removal of H3K9me2 from chromatin (Student's t-test, $p<0.05$) (Figure 4C). These data showed that the appearance of H3K9me2 on prophase I univalents does not down-regulate their transcriptional status either during meiosis or later, in somatic cells.

Levels of H3K9me2 at selected loci on univalent chromosome V of C. elegans mutants

Next we compared levels of H3K9me2 at selected loci in the genome of *C. elegans* wild type and *zim-2(tm574),* carrying unpaired/unsynapsed univalents of chromosome V in prophase I of meiosis, using chromatin immunoprecipitation (ChIP) assays. Recent genome-wide studies of H3K9me2 distribution in *C. elegans* L3 larvae and embryos using ChIP-chip indicated that H3K9me2 is specifically enriched at four classes of repetitive elements: tandem repeats, inverted repeats, transcribed and non-transcribed mobile elements (Figure 5A) (Gerstein et al., 2010). Therefore, we examined the levels of H3K9me2 in several sites on chromosome V, half of which represented repetitive regions, while others were located in gene bodies or intergenic spaces in close proximity (several kilobases) to the repeats.

Our ChIP results revealed that, similarly to larvae and embryonic stages, adult hermaphrodites also have H3K9me2 enrichment specifically on repetitive elements in examined regions of chromosome V (Figure 5B). Remarkably, we did not detect significant increase in the levels of H3K9me2 in *zim-2(tm574)* mutant compared to wild type (Figure 5B).

2.3 Discussion

While it has been previously proposed that appearance of H3K9me2 on the lone male X chromosome during spermatogenesis is the determining factor in its transcriptional repression, our studies indicated that H3K9me2 does not seem to significantly affect the transcriptional status of autosomal univalents during oogenesis in adult hermaphrodites. This chromatin feature also does not appear to impact the ability of the apoptotic machinery to detect unpaired/unsynapsed autosomes either. Similar results were recently obtained by

examination of apoptotic levels and transcriptional status of unpaired X chromosomes during oogenesis in adult *C. elegans* hermaphrodites, revealing the generality of our findings (Jaramillo-Lambert and Engebrecht, 2010; Checchi and Engebrecht, 2011). In contrast, mRNA levels of an X-linked gene, normally expressed during oogenesis in wild-type XX hermaphrodites, were dramatically downregulated during oogenesis of sexually transformed XO hermaphrodites (Bean et al., 2004). These studies indicate that a lone sex chromosome, entering prophase I of spermatogenesis or oogenesis, could have a different organization of chromatin, when compared to chromosomes that normally do have a homologous partner at the onset of meiosis, yet fail to align with each other due to a defect in pairing. It is also possible that the observed effect is limited to X-linked loci and the general transcriptional repression of the male X chromosome during meiotic stages.

Our data also has direct implications for understanding some of the phenomena related to MSCI in mammals. For instance, while the appearance of BRCA1 and phosphorylated H2AX was shown to coincide with the establishment of the transcriptionally repressed state of sex chromosomes or unsynapsed chromosomes in pachytene of mouse meiosis, direct genetic evidence of the effect of these chromatin reorganization events on transcription or apoptotic pathways is lacking (Burgoyne et al., 2009). Therefore, in light of our finding, caution should be exercised when addressing the causality of these events, as MSCI and MSUC might be very different mechanistically. Taken together, our attempts to investigate the consequence of appearance of heterochromatic domains on univalents for transcription and apoptosis in *C. elegans* did not provide supporting evidence that these phenomena are directly related.

2.4 Materials and Methods

Strains

Standard techniques were used for worm culture (Brenner, 1974). All worms were raised at 20°C, unless otherwise specified. Worms of N2 strain var. Bristol were used as wild type reference. The following alleles were used in the study: *zim-2(tm574), met-2(n4256),* and *zim-2(tm574); met-2(n4256).*

Apoptosis assay

Apoptosis assays were performed essentially as previously described (Gumienny et al., 1999; Kelly et al., 2000). To determine the number of apoptotic corpses in *C. elegans* gonads, 48-hr post-L4 hermaphrodites were picked into 100µL of 25µg/mL AO in M9 and incubated for one hour in the dark at room temperature. Worms were then transferred to bacteria lawns and allowed to recover for 20 min. Worms were mounted in 60µg/mL levamisole in M9 on agar pads and apoptotic bodies were visualized using differential interference contrast and epifluorescence microscopy. At least ten gonads were scored per each genotype. Statistical analysis was performed using Student's t-test.

Determination of the levels of mRNA transcripts using qRT-PCR

To determine the levels of mRNA transcripts, 50 24 hr-post L4 hermaphrodites were collected per sample. A total of three samples were analyzed per each genotype. RNA was isolated from tissues using TRIzol® (Ambion®)-based lysis approach. DNA was digested using RNase-Free DNase I (Qiagen®). RNA clean-up was preformed using RNeasy® MiniKit (Qiagen®). cDNA synthesis was performed using SuperScript™ III First-Strand Synthesis System for RT-PCR (Invitrogen™). qRT-PCR was performed in three replicates per each biological sample using iQ™ SYBR® Green Super Mix (Bio-Rad®) on 7500 Real-Time PCR

System (Applied Biosystems®).The following PCR program was used: 95°C for 3 min, 40 cycles of 95°C for 10 sec, 55°C for 30 sec. Sequences of primers used were as follows: 5'-CATCCTTCTTGGGTATGGAG-3' (forward, T04C12.6), 5'-TTCATGGTTGATGGGG CAAG-3' (reverse, T04C12.6), 5'-ACCATTCAGAAGCTTGCATG-3' (forward, T06E6.2a), 5'-GAAGAGTTCACGCTCCATGG-3' (reverse, T06E6.2a), 5'-ATGAA GATTGTGGAACCAGG-3' (forward, F11A3.1), 5'-AATGTCTCCAGTGTGAAGCC-3' (reverse, F11A3.1), 5'-AGATCTCTGCTATGCAGTTG-3' (forward, F26D2.2), 5'-CGGATTCCACGATATCGATG-3' (reverse, F26D2.2). Calculations of the relative amount of the transcript were performed using the comparative C_T method (Applied Biosystems®). Statistical analysis was performed using Student's t-test.

ChIP assays

ChIP was performed essentially as described in (Katz et al., 2009). Three samples of gravid adult worms, washed off five 10-cm plates with M9 were used a starting material. Worms were lysed and fixed in 1% formaldehyde. Samples were sonicated on Sonic Dismembrator Model 500 (Fisher Scientific) for 200 sec (4 sec on, 10 sec off) at 20% amplitude to yield an average DNA fragment length of 250 base pairs. The following antibodies were used for immunoprecipitation: mouse anti-H3K9me2 (ab1220, Abcam®), rabbit anti-pan-H3 (ab1791, Abcam®). Mouse pre-immune serum was used as a control (ZYMED Laboratories, Inc., 1:10 dilution). Immunoprecipitation was performed using ChIP Assay Kit (Millipore®). qRT-PCR was performed in two technical replicates per each sample using SsoFast™ EvaGreen® Supermix (Bio-Rad®) on CFX96™ Real-Time PCR System (Bio-Rad®). The following PCR program was used: 95°C for 3 min, 40 cycles of 95°C for 10 sec and 55°C for 30 sec. Sequences of primers used were as follows: 5'-TGTGCTACACATGTCCGTGA-3'

(forward, AF168), 5’-GGCCTACACTCCTCACTTCG-3’ (reverse, AF168), 5’-CGACCGGTACATAAGCGAAT-3’ (forward, AF169), 5’-TCCGCTTCCAATACAA CTCA-3’ (reverse, AF169), 5’- GGCCAACGACTGGTGACTAT -3’ (forward, AF184), 5’-TCGAATTGTGTTTCAGCTTCA-3’ (reverse, AF184), 5’- AGGGGGTTACAGGAAAG GAA-3’ (forward, AF185), 5’-CACTTTTTGAAGCGGGTTGA-3’ (reverse, AF185), 5’-GGAGCTGGCTTCTCGTTACA-3’ (forward, AF200), 5’-TCCAGAACACCAAGGAA ACC-3’ (reverse, AF200), 5’- TTCTGGCTGAAGCGTTAAAAA-3’ (forward, AF201), 5’-TAAAATCCCCTAGGCAAACG-3’ (reverse, AF201). Statistical analysis was performed using Student’s t-test.

Figure 3. Enrichment of H3K9me2 on univalents does not impact apoptotic processes.

(A) Detection of apoptotic corpses based on their morphological features. Gonadal arm of a 48-hr-post L4 wild-type hermaphrodite, stained with AO and visualized using epifluorescence (left) or differential interference contrast (right) microscopy. Dashed arrow indicates progression of meiosis. Small arrows point to two apoptotic corpses. Scale bar, 30 μm.

(B) Measurements of apoptosis levels in the gonads of wild type, *zim-2(tm574*, *met-2(n4256)*, and *zim-2(tm574);met-2(n4256)* adult hermaphrodites.

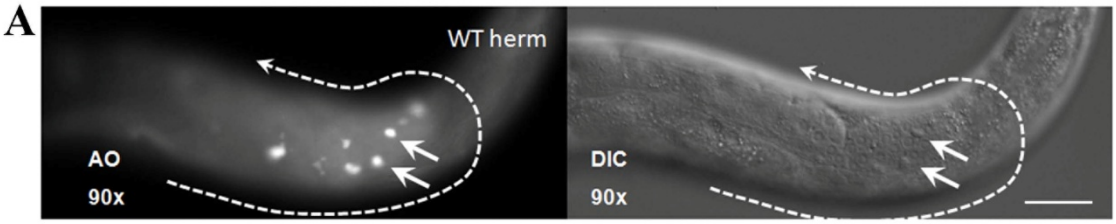
A
WT herm
AO
90x
DIC
90x

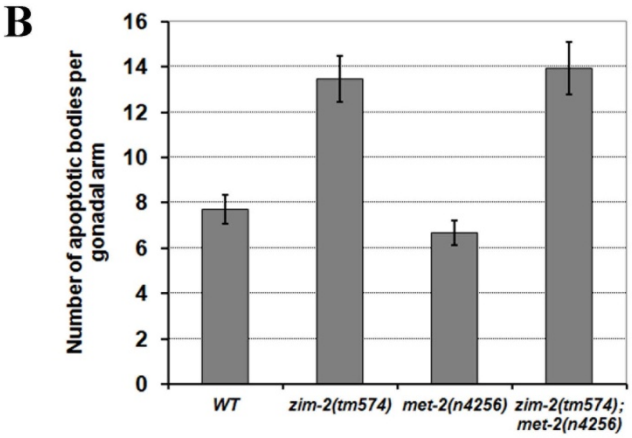
B
Number of apoptotic bodies per gonadal arm
16
14
12
10
8
6
4
2
0
WT
zim-2(tm574)
met-2(n4256)
zim-2(tm574); met-2(n4256)

Figure 4. Enrichment of H3K9me2 on univalents does not impact their transcriptional status.

(A) Results of quantification of mRNA transcript levels of *syp-2* gene (F26D2.2), expressed in the prophase I cells of wild type, *zim-2(tm574)*, *met-2(n4256)*, and *zim-2(tm574);met-2(n4256)* adult hermaphrodites, by qRT-PCR.

(B) Transcript levels of *cyb-3* gene (T06E6.2a), expressed in the maturing oocytes.

(C) Transcript levels of *acs-14* gene (F11A3.1), expressed in the somatic cells of adult hermaphrodites.

Schematic diagrams of gene expression patterns in the adult hermaphrodites are shown above each graph [adapted from (Zarkower, 2006)].

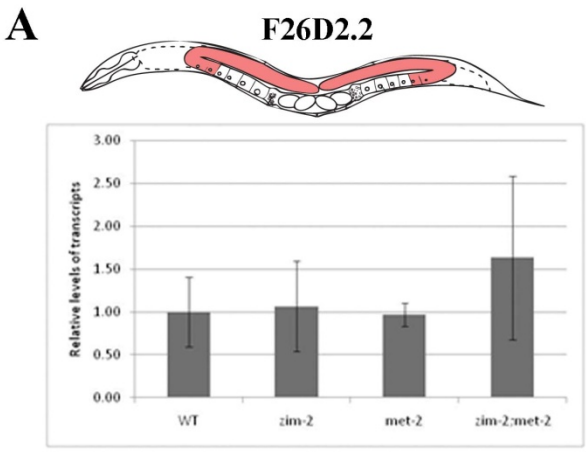
A
F26D2.2
Relative levels of transcripts
3.00
2.50
2.00
1.50
1.00
0.50
0.00
WT
zim-2
met-2
zim-2;met-2

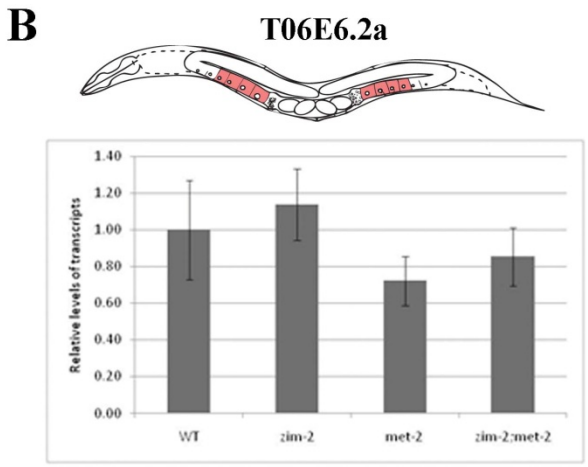
B
T06E6.2a
Relative levels of transcripts
1.40
1.20
1.00
0.80
0.60
0.40
0.20
0.00
WT
zim-2
met-2
zim-2;met-2

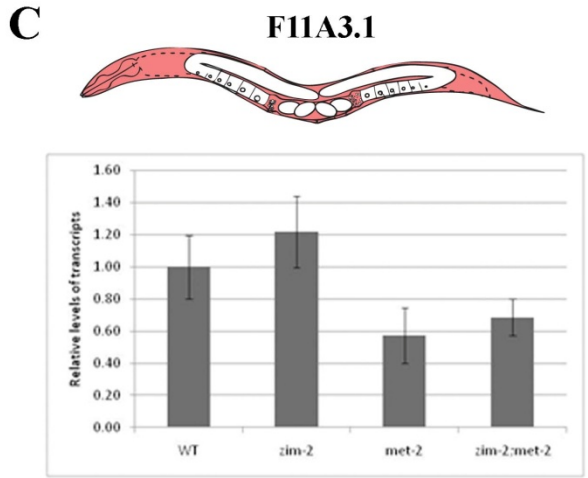
C
F11A3.1
Relative levels of transcripts
1.60
1.40
1.20
1.00
0.80
0.60
0.40
0.20
0.00
WT
zim-2
met-2
zim-2;met-2

Figure 5. H3K9me2 is enriched in repetitive elements in adult *C. elegans* genome.

(A) MODEncode data on the distribution of H3K9me2 in a locus, enriched for complex repeats and transposons, in L3 stage *C. elegans* larvae (Contrino et al., 2012).

(B) Verification of enrichment of H3K9me2 mark on repetitive elements by analysis of selected loci on chromosome V of wild type and *zim-2(tm574)* adult hermaphrodites using ChIP. AF168, AF184, AF200 – repetitive regions; AF169, AF185, AF201 – non-repetitive control regions.

A

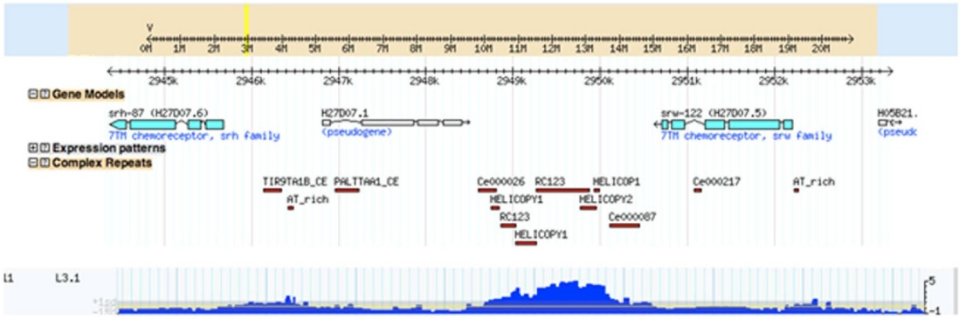
V
2945k
2946k
2947k
2948k
2949k
2950k
2951k
2952k
2953k
Gene Models
srh-87 (H27D07.6)
7TM chemoreceptor, srh family
H27D07.1
(pseudogene)
srw-122 (H27D07.5)
7TM chemoreceptor, srw family
Expression patterns
Complex Repeats
AT_rich
RC123
HELICOPY1
HELICOPY2
L1
L3.1

B

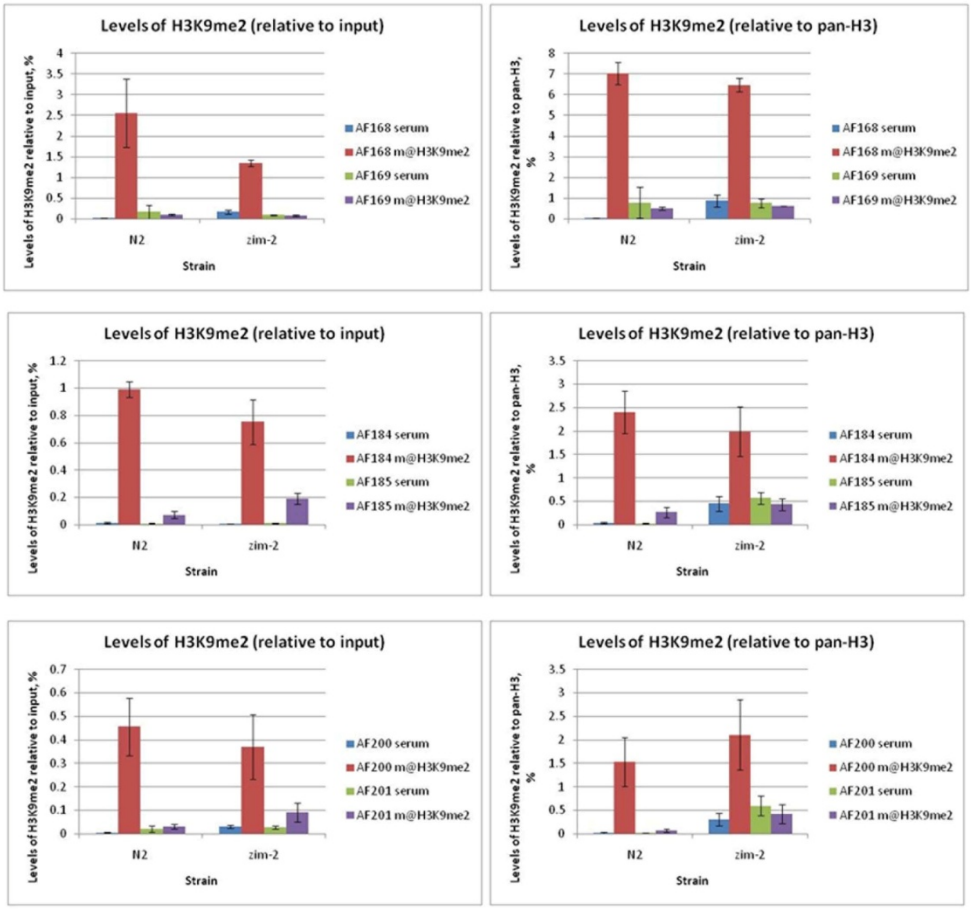
Levels of H3K9me2 (relative to input)
Levels of H3K9me2 relative to input, %
Strain
N2
zim-2
AF168 serum
AF168 m@H3K9me2
AF169 serum
AF169 m@H3K9me2
Levels of H3K9me2 (relative to pan-H3)
Levels of H3K9me2 relative to pan-H3, %
AF184 serum
AF184 m@H3K9me2
AF185 serum
AF185 m@H3K9me2
AF200 serum
AF200 m@H3K9me2
AF201 serum
AF201 m@H3K9me2

CHAPTER 3

SYNAPTONEMAL COMPLEX ASSEMBLY LEADS TO COMPARTMENTALIZATION OF HETEROCHROMATIC DOMAINS IN *C. ELEGANS* MEIOSIS

(as submitted, with modifications)

3.1 Introduction

Acquisition of specific chromatin features by the aberrant chromatin in prophase I of meiosis is a conserved phenomenon. In mammals and birds homologs that failed to properly juxtapose are marked by heterochromatin-associated modifications of histone H3, ubiquitination and sumoylation of histone H2A, and phosphorylation of histone variant H2AX (Inagaki et al., 2010). In *C. elegans*, unpaired homologs, chromosomal duplications, or the lone X chromosome in XO males, are enriched for H3K9me2, a hallmark of heterochromatin (Kelly and Aramayo, 2007). These unique chromatin features are most readily observed in pachytene nuclei – a stage significantly downstream from the initiation of pairing, synapsis, or recombination events. However, it remains unclear which process specifically triggers the appearance of these modifications. For instance, in *C. elegans*, abrogation of pairing leads to defects in a number of subsequent chromatin remodeling events, including failure to properly align homologs, repair DSBs, assembly of the central region of the SC (Phillips et al., 2005; Phillips and Dernburg, 2006). As a result, any of these defects could potentially cause the observed H3K9me2 phenotype. Therefore, it is necessary to separately test contribution of each of these processes for our understanding of the molecular mechanism of the described phenomenon.

Investigation of the mechanisms of chromatin reorganization on aberrant homologs in mammals is challenging due to the early apoptosis of nuclei, carrying unpaired/unsynapsed chromosomes, or complete sterility of mutants, lacking the essential components of the meiotic machinery (Burgoyne et al., 2009). *C. elegans*, on the contrary, is a highly suitable model for these studies due to progression of meiosis through all the stages independent from the degree of pairing/synapsis defects, and the existence of an extensive collection of meiotic

mutants (Lui and Colaiácovo, 2013). Thus, we set out to determine what factor(s) and processes are specifically linked to H3K9me2 enrichment on unpaired chromosomes in *C. elegans*. We screened *C. elegans* mutants that carried mutations in key meiotic genes for changes in H3K9me2 patterns in pachytene nuclei. Examined mutants carried null alleles of the respective meiotic genes, except for *sun-1(jf18)* and *zyg-12(or577)*, which are hypomorphic alleles. To determine whether the examined defects were limited to H3K9me2 patterns or caused broader impacts on chromatin in general, we also analyzed patterns of H3K4me2, a histone modification primarily associated with euchromatic regions of the genome.

3.2 Results

Diverse meiotic defects lead to a few common types of H3K9me2 patterns in pachytene chromatin

To test whether the acquisition of heterochromatic domains by unpaired chromosomes in *C. elegans* is X chromosome-specific, we examined the H3K9me2 immunofluorescence patterns in a *zim-2(tm574)* mutant with defective pairing of chromosome V. Pachytene nuclei of this mutant display an enrichment of H3K9me2 signal on two autosomes, while the other autosomes and X chromosomes have wild-type (WT) levels of H3K9me2 (Jaramillo-Lambert and Engebrecht, 2010). Fluorescent *in situ* hybridization analysis using a probe specific to the 5S ribosomal DNA (rDNA) locus on the right arm of LG V revealed that the enriched H3K9me2 signal was restricted to this chromosome in the *zim-2(tm574)* mutant (Figure 6). These data show that changes in H3K9me2 signal distribution in meiotic chromatin resulting from defective pairing is not sex chromosome-specific.

Clustering analysis distinguished four distinct types of pachytene H3K9me2 patterns in the examined mutants – with H3K9me2 foci similar in their volume and surface area to WT or smaller, slightly larger, and considerably larger than WT (Figure 7). Three of the patterns were represented by large clusters, containing a number of diverse mutants, while one type – Cluster 4, with the highest standard deviation of the volume of H3K9me2 foci and the most extreme differences in their surface area – was represented by three pairing center mutants. These results, and other results presented below, suggest that the H3K9me2 patterns observed in pachytene nuclei are regulated by a complex network of earlier meiotic events. Importantly, PCA and clustering analysis of H3K4me2 patterns did not yield stable clustering solution based on the measured features (data not shown). The meiotic defects in the examined mutants therefore did not significantly affect appearance of H3K4me2-enriched chromatin in pachytene nuclei. To identify the molecular events leading to particular H3K9me2 patterns, we examined features of H3K9me2 signal distribution in each of the identified clusters.

DSB intiation, processing, and repair defects do not affect H3K9me2 distribution on pachytene chromosomes

The absence of DSBs or defects in their processing and repair disrupt chromosome pairing and synapsis in *S. cerevisiae* and *M. musculus* and trigger the arrest of meiotic progression (reviewed in Yang and Wang, 2009; Hochwagen and Amon, 2006). In contrast, *C. elegans* mutants defective in recombination pathways exhibit normal pairing and homologous synapsis with wild type dynamics, indicating that synapsis is independent of recombination in this organism (Dernburg et al., 1998). This feature provides an advantage for testing the

role of DSBs in the regulation of H3K9me2 separately from pairing or synapsis defects. We performed H3K9me2 pattern clustering analysis in strains carrying *atl-1(tm853), brc-2(tm1086), rad-54(ok615), spo-11(ok79), zhp-3(ok1993),* and *rad-51(lg8701)* alleles. This mutant set defines genes involved in the generation, recognition, and repair or processing of meiotic DSBs (Alpi et al., 2003; Martin et al., 2005; Aoki et al., 2000; Jantsch et al., 2004). These mutants formed the largest cluster (Cluster 1) on the phylogram in the pattern analysis, and importantly they clustered with the wild type pattern (Figure 7). No significant changes to the volume or the distribution of H3K9me2 foci on pachytene chromosomes were detected in these mutants when compared to wild type (Figure 10). Pachytene H3K9me2 patterns are thus not influenced by defective generation, processing, or repair of DSBs on paired and synapsed chromosomes. Moreover, *zim-2(tm574);spo-11(ok79)* double mutants retain elevated levels of H3K9me2 on chromosome V despite the absence of DSBs (Fedotov and Kelly, unpublished). Therefore, recombination defects most likely do not directly contribute to the establishment of heterochromatic domains.

Pairing centers are dispensable for the establishment of heterochromatic domains on univalents

The *mnDp66;meDf2* strain carries a terminal deficiency that includes the X chromosome pairing center (Villeneuve, 1994). As a consequence X chromosomes remain unpaired and unsynapsed, a phenotype similar to *him-8(e1489)* allele despite having an intact copy of the *him-8* gene (MacQueen et al., 2005). We examined the X chromosomes in the *mnDp66;meDf2* strain and found that, similar to *him-8(e1489)* (Kelly et al., 2002), both X chromosome univalents were dramatically enriched in H3K9me2 (Figure 11). This indicates

that pairing center loci *per se* are dispensable for this process; i.e., the physical presence of unaligned pairing center elements is not required for H3K9me2 enrichment on the unpaired chromosomes. Since the increase in levels of H3K9me2 signal in the terminal deficiency strain occurred in the presence of the functional HIM-8, this finding also suggests that pairing center proteins are not directly involved in regulation of H3K9me2 dynamics.

Although the *mnDp66;meDf2* and *him-8(e1489)* mutants were located in the same cluster on the constructed phylogram, some features of their H3K9me2 patterns differed (Cluster 4, Figure 7). For instance, the average ratio of the largest to the smallest H3K9me2 foci was consistently higher in the deficiency strain. Recent work on meiotic chromosome painting in *C. elegans* has revealed that in contrast to *him-8(e1489),* X chromosomal territories in pachytene nuclei of *mnDp66;meDf2* germline undergo wild type-like extension (Nabeshima et al., 2011). Therefore, the observed differences in the measured features of H3K9me2 foci of these two mutants suggest that our image analysis approach allows detection of subtle changes in H3K9me2 patterns that parallel changes in particular chromatin reorganization events.

H3K9me2 distribution is affected by synapsis defects

The rest of the examined mutants formed two large clusters on the phylogram – Clusters 2 and 3 (Figure 7). These clusters represented a collection of mutants with a diverse set of meiotic aberrations that affect all chromosomes, including defects in axial element assembly, attachment of chromosomes to the nuclear envelope, chromosome pairing, or loading of the central region components of the SC. Interestingly, none of these mutants exhibited the dramatic increase in the volume of H3K9me2 foci observed in the single pairing center

mutants (e.g., *him-8(e1489)* or *zim-2(tm574)*, Figure 7). Instead, the total volume of H3K9me2 foci, compared to WT, was decreased in Cluster 2, and only slightly increased in Cluster 3 (Figure 7). That the wide variety of meiotic defects in these mutants resulted in only two types of H3K9me2 patterns suggested that there were common meiotic aberrations that affected H3K9me2 distribution in each cluster.

A unifying feature for mutants from Cluster 2 is that all have been shown to exhibit extensive asynapsis of homologs in pachytene nuclei (Zetka et al., 1999; Couteau et al., 2004; Goodyer et al., 2008; Severson et al., 2009). Mutants that fail to load the SC central element due to a defect in one of its components [*syp-1(me17)* and *syp-2(ok307)*], or because they are defective for the assembly of axial elements or cohesins [*him-3(gk149)*, and *rec-8;coh-3;coh-4*] did not exhibit prominent heterochromatic domains and instead had only a few small H3K9me2 foci (Figure 10, 12, 13, 14). Quantitative analysis of the overall volume of H3K9me2 foci ruled out that this was an artifact of an anti-H3K9me2 signal dispersed among many chromosomes, as the total volume of H3K9me2 foci was consistently below the wild-type levels (data not shown).

Most of the mutants in Cluster 3 likewise share a common aberration in synapsis – they inappropriately assemble SC tracks between nonhomologous chromosomes (heterologous synapsis) and/or on univalents (Couteau and Zetka, 2005; Penkner et al., 2007; Sato et al., 2009). Using antibodies against SYP-1, one of the central region components of the SC, we examined the relationship between synapsis and H3K9me2 distribution in these mutants. We observed that H3K9me2 foci in these mutants were enriched primarily on the regions that had weak patches of SYP-1 tracks or lacked them, whereas fully synapsed regions with robust SYP-1 tracks were devoid of H3K9me2 signal (Figure 13, 14).

Taken together, results of the clustering analysis indicated that specific aspects of SC formation rather than the pairing or recombination defects are linked to the regulation of H3K9me2 distribution. To further investigate this hypothesis, we further examined the interplay between the regulatory hierarchy of synapsis and H3K9me2 pattern dynamics.

Euchromatic regions are not affected by the same chromatin organization defects as heterochromatic

In agreement with the results of the clustering analysis, direct assessment of H3K4me2 patterns of the examined mutants revealed that in most cases they were highly similar (Figure 10). As mentioned earlier, in wild-type pachytene nuclei autosomes exhibit robust staining with anti-H3K4me2 antibodies and the only chromosomal pair that lacks extensive H3K4me2 signal is the transcriptionally inactive X. All mutants had the wild type distribution of H3K4me2 signal, although H3K4me2 staining appeared in thinner tracks in mutants from Cluster 2, which is consistent with the presence of univalents. Notably, both unpaired chromosomes in *zim-2(tm574)* mutant had levels of H3K4me2 similar to other autosomes. The similarities of H3K4me2 patterns across the mutants suggested that euchromatic regions of chromatin are not directly affected by the same chromatin reorganization defects that impact H3K9me2-enriched chromatin.

Central region components of the SC associate with chromatin prior to the establishment of pairing of homologs

Immunolocalization studies indicated that SC central region components loading is initiated at early stages of *C. elegans* meiotic prophase, and that synapsis is largely complete by

pachytene stage with thick SC tracks lining the homolog interface (MacQueen et al., 2002). In an effort to understand the sequence of chromatin reorganization events during SC assembly, we performed high-resolution analysis of key steps in the synapsis process. Based on the immunofluorescence staining of SYP-1 we were able to distinguish five main states of SC central elements (synapsis zones) in early prophase: (1) one-to-two SYP-1 foci (polycomplexes) in the nucleoplasm but not colocalized with chromatin; (2) several SYP-1 foci and weak patches associated with chromatin; (3) partially established but incomplete SYP-1 tracks associated with chromatin and displaced to one pole of the nucleus; (4) fully established SYP-1 tracks associated with chromatin and displaced to one pole of the nucleus; and, (5) fully established tracks associated with chromatin and fully dispersed within the nucleus (Figure 17A). Meiotic progression in the *C. elegans* gonad takes place along a spatiotemporal gradient; quantification of the number of nuclei along the distal-proximal axis of the gonad based on the stage of SC assembly revealed five consecutive zones within which each state was predominant (Figure 17B).

Next we utilized a comprehensive set of molecular and cytological markers for detailed analyses of chromosome dynamics events during each of the identified synapsis zones of the gonad. Pairing center proteins ZIM-3 (pairing center region of chromosomes I and IV) and HIM-8 (pairing center region of chromosome X) were used to determine the pairing status of homologs, while 5S rDNA *F*luorescence *in situ h*ybridization (FISH) probes distal to the pairing center probed chromosome alignment.

In accordance with previous findings, more than 90% of nuclei in the most distal meiotic zone of the wild type gonad had one or two SYP-1 foci adjacent to but not clearly associated with any chromatin mass. These nuclei exhibited two HIM-8 foci and two separated 5S

rDNA FISH signals, indicating the absence of chromosome pairing and alignment (Figure 18AI, BI, C, D). The SYP-1 foci in these nuclei most likely represent so called polycomplexes, or aggregates of SC central elements. Foci of ZIM-3 were not yet detectable at this stage. Most nuclei in this region are known to contain newly-synthesized DNA and thus had undergone meiotic S-phase (Jaramillo-Lambert et al., 2007; Sato et al., 2009). Together these findings indicate that nuclei in this region have entered the leptotene stage of meiotic prophase.

The second zone in our analysis, up to 5 nuclear diameters in length, harbored nuclei where separate patches of SYP-1 foci were detected in association with chromatin (Figure 17B). Surprisingly, we observed only a minimal increase in the number of paired and/or aligned chromosomes in this zone. More than 80% of nuclei in this zone lacked detectable ZIM-3 foci, and remainder exhibited three-to-four foci per nucleus, showing that pairing of chromosomes I and IV had not yet initiated (Figure 18AII, C). Two separate foci of HIM-8 were also detected in more than 80% of nuclei in this zone, so this zone also precedes X chromosome pairing (Figure 18AII, C). Importantly, the chromosomes in this zone remained dispersed, and lacked the clustered appearance that correlates with successful pairing of homologs (Figure 18AII). Homologs remained unaligned in this zone as well, as evidenced by lack of pairing of the 5S rDNA FISH signals in 94% of nuclei (Figure 18BII, D). Interestingly, in 3% of nuclei we detected colocalization of SYP-1 and one of the unpaired FISH signals, clearly verifying association of SYP-1 with unpaired chromatin (Figure 18BII, D). While it is commonly accepted that the establishment of the central elements of the SC takes place after homolog axes are formed and their intimate homolog association is achieved (eg., Kleckner, 2006), these finding show that an initial association of SYP-1 with chromatin

occurs in nuclei that have not yet achieved either pairing or homolog alignment and are only transitioning into an early zygotene stage of meiosis.

The next more proximal zone of the gonad is characterized by short tracks of SYP-1 assembled on chromatin (Figure 17B). Nuclei in this zone exhibited displacement of chromatin mass to one pole of the nucleus and acquisition of a basket-like configuration of chromatin (or crescent-like when acquired three-dimensional data stacks are projected onto a single imaging plane) (Figure 17B). This chromatin conformation is typical for nuclei undergoing pairing of their homologs during the zygotene stage of prophase. More than 90% of nuclei in this zone had bright ZIM-3 foci, of which almost 80% exhibited complete pairing (Figure 18AIII, C). More than 80% of X chromosomes were also paired, as evidenced by a single focus of HIM-8 per nucleus (Figure 18AIII, C). Consistent with the onset of homologous synapsis, 64% of nuclei had a single 5S rDNA FISH signal that associated with a thick SYP-1 track, located between aligned chromosomes (Figure 18BIII, D). However, a few nuclei retained two foci of 5S rDNA FISH signal, both associated and unassociated with SYP-1 tracks. Remarkably, close examination confirmed that the chromatin-associated SYP-1 tracks in these cases were on univalents physically separated from their homolog along their entire lengths in the nucleoplasm (Figure 18BIII, inset). These cases further indicate that components of the central region of SC can associate with unpaired and unaligned univalents. In addition, in those cases when 5S rDNA FISH signals were paired but not colocalized with SYP-1 tracks, fully formed SCs were observed on other bivalents in the same nucleus. The establishment of the mature SC between homologs thus appears to proceed on a chromosome-to-chromosome basis, rather than being uniformly controlled within each nucleus.

Consistent with the non-uniform SC assembly described above and observed by others (MacQueen et al., 2002; Colaiácovo et al., 2003; Smolikov et al., 2007a), the next more proximal zone had a mix of nuclei with partially and fully established SYP-1 tracks (Figure 17B). Here most of the chromosomes were fully paired, aligned and synapsed, as indicated by two ZIM-3 foci, a single HIM-8 focus, and single 5S rDNA FISH foci colocalizing with robust tracks of SYP-1 (Figure 18AIV-D). Most of these nuclei demonstrated decreased intensity of ZIM-3 foci and less chromatin polarization compared to the zygotene zone, signifying transition to the pachytene stage of prophase I (Figure 18AIV, C). The ZIM-3 foci disappeared as nuclei entered pachytene, which maintained uniformly paired HIM-8 and 5S rDNA FISH signals, with complete and thickened SYP-1 tracks between homologs that were uniformly dispersed in the nuclear periphery (Figure 18AV-D).

Initiation of the assembly of SC on univalents coincides with the appearance of heterochromatic domains

To examine any role that SC dynamics may play in H3K9me2 patterns, we next compared SYP-1 and H3K9me2 patterns in each of the synapsis zones examined above (Figure 19). The distribution of H3K9me2 in wild-type meiotic nuclei undergoes dramatic changes in every examined zone. Nuclei in the most distal leptotene zone exhibited few H3K9me2 foci scattered throughout the chromatin mass (Figure 19I). A dramatic change to this pattern was observed in nuclei transitioning into zygotene, where there is a striking increase in the number and intensity of H3K9me2 foci on chromosomes. This striking change in H3K9me2 distribution coincides with the initial redistribution of SYP-1 from polycomplexes to regions on the chromosomes, suggesting a potential link between these two events (Figure 19II).

These changes in both H3K9me2 and SYP-1 patterns were observed in all nuclei in this zone of the gonad, indicating tight synchronization.

H3K9me2 foci disappear upon completion of homologous synapsis

Strikingly, the progression of SC assembly between homologs that takes place in the zygotene zone of the gonad had an opposite correlation with H3K9me2 distribution. In cases where we detected robust SYP-1 tracks along the length of chromosomes, the number of H3K9me2 foci dramatically decreased (Figure 19III). In contrast, nuclei with SYP-1 distribution indicative of the transition-to-zygotene state (i.e., few foci in the nucleoplasm and weak patches on chromatin) still exhibited numerous bright foci of H3K9me2 (Figure 19III). In nuclei where a subset of chromosomes in the nucleus had established continuous SYP-1 tracks, these synapsed regions lacked detectable H3K9me2 foci, while unsynapsed chromosomes in the same nucleus retained H3K9me2 foci (Figure 19III). This indicates that it is the progression of synapsis along each chromosome, rather than a global signal, that drives the disappearance of the H3K9me2 foci in zygotene chromatin.

In agreement with the anti-correlation between synapsis and H3K9me2 foci, chromosomes transitioning from zygotene to pachytene largely lacked dispersed H3K9me2 foci, with only a few bright punctae remaining at the ends of synapsed homologs (Figure 19IV). In pachytene nuclei, chromosomal axes remained mostly devoid of H3K9me2 foci, with the enrichment of H3K9me2 at the ends of synapsed chromosomes more pronounced (Figure 19V). This presumably represents the previously described enrichment of this mark at telomeres (Reuben and Lin, 2002).

Collectively, these data demonstrate that the initial assembly of SC central elements on chromosomes coincides with dramatic changes in patterns of H3K9me2 distribution observable by immunofluorescence. These results suggest an important role for SC proteins in regulating H3K9me2 patterns, and hence meiotic chromatin architecture, prior to the actual assembly of the SC between paired and aligned homologs. They further indicate that the process of SC assembly may further reorganize heterochromatic domains during alignment and synapsis of homologs.

To determine whether SC-related chromatin reorganization in early prophase I has a similar effect on euchromatic regions of the genome, we examined changes in the appearance of H3K4me2 pattern along the five identified zones of the gonad. We did not detect any dramatic changes to the appearance of H3K4me2-enriched chromatin at any of the examined zones (Figure 15). H3K4me2 was distributed with varying degrees of intensity along the length of all the autosomes during and between leptotene, zygotene and pachytene stages. Intriguingly, in zones where the SC had fully assembled on chromosomes we observed several cases where chromatin along the interface of the aligned and presumably synapsed homologs was devoid of H3K4me2 staining (Figure 16A, B). This could suggest that the chromatin regions where the SC assembles has less H3K4me2-marked chromatin, or that the assembly of the SC provides a steric block to antibody accessibility to chromatin marks along the axes. The latter, if true, would suggest that the decrease in H3K9me2 observed with SC assembly is due to preferential sequestration of genomic regions carrying this chromatin mark, rather than its selective removal.

Individual unsynapsed chromosomes exhibit heterochromatic domains in early prophase I

The pairing center mutant *zim-2(tm574)* has defective SC assembly on chromosome V due to defective pairing of the homologs (Phillips *et al*., 2006), yet both homologs show robust enrichment of H3K9me2 in pachytene. We examined this mutant to determine if the pre-pairing SC central element association with chromosomes still occurred, and if the other leptotene and zygotene chromosome dynamics were affected. We analyzed H3K9me2 and SYP-1 dynamics in the five zones of prophase I in *zim-2(tm574)* mutants (Figure 21I-V). We found that the dynamics of pairing of ZIM-3, HIM-8 foci and 5S rDNA signals, along with the distribution of SYP-1 foci in leptotene and transition to zygotene zones remained undistinguishable from wild type (Figure 20A, B). Correspondingly, H3K9me2 patterns at these stages underwent similar to wild type changes and nuclei transitioning to zygotene acquired numerous foci of H3K9me2 (Figure 21II). Zygotene nuclei demonstrated successful pairing of ZIM-3 and HIM-8 foci, and initiation of the establishment of SYP-1 tracks between the aligned chromosomes, and this was accompanied by disappearance of H3K9me2 foci along the length of the synapsed axes (Figure 20A, B, 21III).

As expected, the chromosome V 5S rDNA signals remained unpaired in the zygotene zone and did not colocalize with SYP-1 tracks, indicating the failure of chromosome V homologs to align and synapse (Figure 20B). Remarkably, the chromosome V chromatin retained the H3K9me2 foci normally observed in the preceding zone, suggesting that in the absence of a functional pairing center, synapsis-related chromatin reorganization events do not progress and the heterochromatin domains of the univalent remain exposed (Figure 3CIII). Importantly, a small fraction of nuclei in this zone also exhibited colocalization of

anti-SYP-1 with the 5S rDNA FISH probe, showing that some degree of SYP-1 association with chromatin had occurred on the univalents of chromosome V (Figure 20B).

Persisting asynapsis delays the transition from zygotene to pachytene. Hence, the most proximal zone in this mutant, corresponding to mid-pachytene in wild type, contained a mix of nuclei either transitioning into pachytene or nuclei exhibiting typical early pachytene features (Figure 20A, B). The pachytene-like nuclei demonstrated the most prominent H3K9me2 signals on chromosome V univalents, indicating that a dramatic expansion of the abnormally retained H3K9me2 signals occurs upon entrance into pachytene (Figure 21V). Importantly, we also noticed that more than half of the 5S rDNA FISH probes in this proximal zone were colocalized with thick SYP-1 tracks, reminiscent of tracks on properly synapsed homologs (Figure 20B). This class of univalents had presumably undergone fold-back synapsis. However, enrichment of the H3K9me2 signal on these univalents was unaffected by SYP-1 loading. Two different interpretations of this result are possible. First, the level of SC, aberrantly assembled on univalents, might be insufficient to affect H3K9me2 on them in a way it does on normally paired and synapsed chromosomes. Second, the timing of SC assembly between chromosomes might be critical for the normal disappearance of H3K9me2 signals – normal assembly initiating in zygotene is sufficient to remove the signal, while delayed assembly, observed in the case of *zim-2(tm574)* mutant, is not (Figure 21V).

Limiting SC components in the nucleus leads to persistence of heterochromatic domains on chromosomes

To investigate whether depletion of SC from the interface of synapsed homologs can affect H3K9me2 patterns, we sought to phenocopy the synapsis defects of *zim-2(tm574)* mutant

without affecting other aspects of chromosome dynamics. Recent work showed that limited asynapsis of chromosomes can be achieved by partial depletion of one of the SC central element components (Hayashi et al., 2010). We found SYP-1 RNAi to be largely ineffective in wild type animals, so we developed conditions to achieve partial depletion of SYP-2 by weak RNAi. The efficacy of SYP-2 RNAi was monitored based on the number of DAPI-stained bodies in diakinesis and the detection of SYP-1 tracks on chromosomes, since SYP-1 loading is dependent on SYP-2 (Colaiácovo et al., 2003). Wild-type diakinesis nuclei contain six bivalents, whereas *syp-2* (*ok307)* mutants exhibit 12 univalents (Colaiácovo et al., 2003). Weak *syp-2(RNAi)* animals had a mixture of bivalents and univalents in diakinesis, indicating we had achieved limited asynapsis of homologs (Figure 26A).

Chromosome pairing and alignment dynamics and H3K9me2 patterns in leptotene and transition to zygotene zones were similar to wild type in the weak *syp-2(RNAi)* animals (Figure 20C, D, 22I, II). Zygotene nuclei, however, had shorter SYP-1 tracks on chromosomes and an increased number of H3K9me2 foci despite normal pairing processes, consistent with a limited pool of SYP-2 and a consequential delay in the assembly of the SC central elements (Figure 22III). Nuclei transitioning to pachytene displayed two ZIM-3 foci and a single HIM-8 focus, indicative of successful completion of homolog pairing (Figure 20C). However, an increased number of nuclei in this zone had a polarized chromatin configuration, short SYP-1 tracks, and unpaired 5S rDNA FISH signals compared to wild type (Figure 20D). These results confirmed that a limited pool of SYP-2 leads to a partial defect in synapsis and a subsequent delay in progression into pachytene. These changes also affected H3K9me2 patterns – we detected a high number of H3K9me2 foci on unsynapsed regions of chromatin in this zone in contrast to almost complete disappearance of H3K9me2

signal on the late zygotene chromosomes in wild type nuclei (Figure 22IV, compare with Figure 19IV). Therefore, mild depletion of SYP-2 prevented timely establishment of SYP-1 tracks between several homologs and caused consequential persistence of H3K9me2 foci – a feature, observed in the gonads of *zim-2(tm574)* mutant.

Pachytene zone nuclei in the SYP-2-depleted gonads had either polarized or typical pachytene dispersed chromatin configuration, and demonstrated the most dramatic difference from wild type in H3K9me2 patterns (Figure 22V). Chromosomes in this zone had fewer SYP-1 tracks than in wild type, and decreased pairing level of chromosome V, indicating that significant portion of chromosomes remained unaligned and unsynapsed (Figure 20D). Correspondingly, regions that lacked SYP-1 tracks acquired elevated levels of H3K9me2 signal, similar to the *zim-2(tm574)* mutant (Figure 22V). This confirms that defective SC assembly correlates with H3K9me2 enrichment, and further that multiple regions of unsynapsed chromatin on multiple chromosomes can simultaneously accumulate robust H3K9me2 enrichment.

SC-dependent chromatin reorganization at the onset of meiosis is required for the establishment of heterochromatic domains

The results of weak SYP-2 RNAi demonstrated that heterochromatic domains can persist on mutiple chromosomes that fail to synapse, and a robust enrichment of H3K9me2 signal at these domains can occur at many sites in pachytene nuclei. Oddly, meiotic mutants that cause extensive asynapsis clustered separately from those with a dramatic H3K9me2 response (Figure 7, Cluster 2 vs. Cluster 4). How can SC central elements be both *refractory* to H3K9me2 enrichment and *required* for the enrichment to occur?

We hypothesized that the initial assembly of the SC central components prior to pairing and alignment we observed at the onset of meiosis is required for the establishment of the H3K9me2 patterns and thus affects their downstream dynamics. We therefore examined H3K9me2 patterns during early prophase in the complete absence of SYP proteins using robust depletion of SYP-2 by RNAi. Complete abrogation of chromosome synapsis under the conditions employed was confirmed by severe polarization of chromatin configuration throughout most of prophase I, persistence of ZIM-3 and HIM-8 foci, an absence of SYP-1 tracks on chromosomes in zygotene and pachytene zones, and the presence of 12 univalents in diakinesis (Figure 23 A, B, Figure 26A).

Remarkably, examination of H3K9me2 patterns in these animals revealed significant differences from the dynamics we observed in wild type nuclei (Figure 24, compare with Figure 19). Whereas in wild type the number of H3K9me2 foci increased as the nuclei initiated a transition to zygotene (Figure 19II), this increase was not observed in *syp-2(RNAi)* nuclei (Figure 24II). This pattern remained unchanged throughout early prophase I, and pachytene nuclei in these animals displayed a few small H3K9me2 foci on unsynapsed chromosomes (Figure 24V). This indicates that the chromatin reorganization events that accompany the transition from leptotene to zygotene stages require the SYP proteins. Remarkably, this requirement precedes the completion of pairing and assembly of the SC, indicating that the SC central element components participate in the axis morphogenesis of unsynapsed univalents, and the reorganization of chromatin that accompanies these events.

To test whether the H3K9me2 response observed on the univalents in pairing center mutants also requires SC components, we performed strong SYP-2 RNAi in the *zim-2(tm574)* mutant. While *zim-2(tm574)* animals mostly have five bivalents and two univalents

in diakinesis, diakinesis nuclei of *zim-2(tm574)*; *syp-2(RNAi)* animals predominantly had twelve univalents, confirming high efficacy of SYP-2 RNAi (Figure 26B). The *zim-2(tm574);syp-2(RNAi)* animals had also acquired features similar to strong *syp-2(RNAi)* animals in all of the examined zones of the gonad (Figure 23 C, D). We did not detect any SYP-1 tracks on chromosomes and nuclei no longer had bright patches of H3K9me2 on two univalents, a characteristic feature of *zim-2(tm574)* mutant (Figure 25). The overall H3K9me2 pattern in this zone was thus closer to that of *syp-2(RNAi)* animals than to wild type or *zim-2(tm574)* with numerous small H3K9me2 foci spread along univalents (Figure 25). Importantly, similar phenotypes were observed with depletion of the axial component HIM-3 by RNAi in *zim-2(tm574)* mutants, suggesting that the observed effects on heterochromatin dynamics are not specific to a particular component of the SC, but related to axis-specific defects (Figure 27). Taken together, these results indicate that appearance of heterochromatic domains on unaligned chromosomes in zygotene and pachytene stages depends on the ability of SC central components to assemble on them. The foci that transiently appear at the onset of meiosis during transition to zygotene also require the central region proteins and their presumed early role in axial morphogenesis. Therefore, the massive H3K9me2 heterochromatic domains that become enriched on chromosome V in *zim-2* mutants, for example, may arise from further expansion of early prophase foci that persist in absence of pairing, and this expansion is normally prevented by the later assembly of the SC along the paired and aligned homologs.

Assembly of SC between non-homologs in early prophase I leads to disappearance of heterochromatic domains

Results of clustering analysis indicated that mutants that initiate early non-homologous synapsis of chromosomes (e.g., SC assembly between non-homologs prior to pachytene stage in *sun-1(jf18)* mutant) had only a small increase in the volume of H3K9me2 foci in their pachytene nuclei (Figure 1, Cluster 3). We hypothesized that the modest increase in the volume of H3K9me2 foci in Cluster 3 mutants is a result of two events: (1) extensive ectopic assembly of SC between non-homologous chromosomes, leading to the global disappearance of heterochromatic domains in early stages of prophase, coupled with; (2) persistence of heterochromatic domains on those regions of chromatin where SYP-1 track assembly is incomplete. We argued that if our hypothesis were true, then triggering non-homologous synapsis of univalents in early prophase would lead to the disappearance of heterochromatic domains in pachytene nuclei. To test this hypothesis, we took advantage of a recent observation that deletion (e.g., the *ieDf2* deficiency mutant) or RNAi-mediated depletion of all four pairing center proteins dramatically increases the extent of non-homologous synapsis and leads to the assembly of robust SYP-1 tracks on all 12 univalents (Harper et al., 2011). Importantly, this aberrant synapsis initiates prematurely at early stages of prophase I and is fully manifest by the time the nuclei reach pachytene. Therefore, to establish the role that timing of SC assembly plays in sequestration of H3K9me2 foci, we examined the effects of early non-homologous synapsis in the *ieDf2* mutant on H3K9me2 dynamics. Quantification of the synapsis dynamics in this strain indicated that more than half of unaligned FISH signals nevertheless colocalized with SYP tracks by the time nuclei were transitioning to pachytene, indicating extensive heterologous synapsis (Figure 28A). We found that the

H3K9me2 pattern upon entry into meiosis in the *ieDf2* mutant is largely similar to wild type – we detected few H3K9me2 foci on chromatin in leptotene nuclei (Figure 29I). The next zone of the gonad also demonstrated the normal initiation of SYP-1 association with chromatin and a corresponding increase in the number of H3K9me2 foci (Figure 29II).

However, zygotene nuclei displayed a delay in SYP-1 track assembly – one to two robust SYP-1 stretches were detected on unpaired and unaligned chromosomes at this stage, while the rest remained unsynapsed (Figure 29III). Consistent with this delay in SC assembly, nuclei from this zone retained numerous H3K9me2 foci (Figure 29III). The extent of synapsis increased in nuclei in subsequent zones, and H3K9me2 foci disappeared from those univalents that assembled prominent SYP-1tracks, confirming disappearance of heterochromatic domains upon non-homologous fold-back synapsis of chromosomes at early prophase I (Figure 29IV). By the time nuclei reached pachytene, the number of H3K9me2 foci had decreased dramatically, and only a few patches of H3K9me2 foci were left on self-synapsed univalents. However, the signal from those H3K9me2 foci that remained had dramatically increased (Figure 29V).

Consistent with our other findings, robust depletion of SYP-2 by RNAi in *ieDf2* strain reduced the number of H3K9me2 foci on chromosomes in all zones of the gonad to the levels observed in Cluster 4 mutants (Figure 30, compare to Figure 24). Similar effects on H3K9me2 pattern were obtained for other Cluster 3 mutants (Figure 31). For instance, hypomorphic alleles *jf18* of SUN-1 protein leads to defective establishment of NE patches and premature initiation of SC assembly between non-homologs. As a result, most chromosomes in this mutant are devoid of H3K9me2 singal, with only few unsynapsed/partially synapsed regions exhibiting bright H3K9me2 staining. Strong SYP-2

RNAi in this mutant also leads to disappearance of these H3K9me2 domains from chromosomes. In summary, these results show that early full assembly of the SC, even between non-homologous regions of chromosomes, also leads to the disappearance of heterochromatic domains. Any H3K9me2 foci that remain on unsynapsed chromatin as it traverses early prophase thereafter become targeted for significant H3K9me2 enrichment, as long as that chromatin was made competent for such enrichment by the initial reorganization that depends on SC central components.

The association of SC central elements with univalent chromatin requires dynein function

Recent work has demonstrated that loading of the SC central region components between homologs in early stages of prophase I is dependent on cytoskeletal forces, since this loading can be abrogated by inactivating dynein motors (Sato et al., 2009). We therefore sought to assess whether the effects of dynein-mediated asynapsis on H3K9me2 patterns would be similar to the ones we achieved by directly eliminating structural components of the SC. We initially determined that subjecting animals to weak RNAi against dynein light chain *(dlc-1)* for as long as 24 hours at 16°C did not result in any dramatic defects in SYP-1 assembly (Figure 32). Consistent with previous findings (Sato et al., 2009), when *dlc-1* RNAi animals were shifted to 25°C for 12 hours and dissected immediately we observed that nuclei in the regions spanning leptotene and zygotene zones of the gonad failed to distribute SYP-1 into chromatin and exhibited SYP-1 aggregates (Figure 32). Strikingly, gonads of animals that were shifted up for 12 hours and recovered at 16°C for 3 hours exhibited a narrow region where SYP-1 still remained in distinct aggregates (Figure 32). Amazingly, a narrow and proximally advancing zone of affected nuclei with SYP-1 aggregates was also clearly visible

after recovery for 6 and 12 hours (Figure 32). Importantly, meiotic nuclei distal to the affected zone exhibited normal dynamics of SC assembly (Figure 32). The spacing of these nuclei was also similar to wild type. These results indicated that the temperature sensitive processes revealed by *dlc-1* RNAi can be restored to essentially wild type function upon recovery at permissive temperatures. However, a narrow band of nuclei that encountered the restrictive temperature at the onset of SYP-1 redistribution appears to have irreversibly lost their competence for SYP-1 assembly regardless of their position within the gonad. Quantification of the number of nuclei carrying one or two bright SYP-1 foci revealed that the differences in their numbers at one recovery time point versus another are not statistically significant (Student t-test, $p>0.05$) (Figure 32). These results suggest that once SYP-1 association with chromatin is abrogated at a specific stage in nuclei entering meiosis, it does not resume even at lesser rates despite re-establishment of normal dynein function. Consistent with these findings, animals that were recovered for 24 hours after the 12 hr shift-up still had bright SYP-1 polycomplexes in nuclei in the proximal diplotene zone, and diakinetic oocytes displayed12 DAPI-stained bodies confirming the irreversible abrogation of synapsis in these nuclei (Figure 32).

SC-dependent dynamics of heterochromatic domains can be uncoupled from other chromatin reorganization events

We examined the pairing status of the chromosomes in the irreversibly asynapsed nuclei and adjacent cells after temperature downshift. Despite the extensive asynapsis in the affected nuclei, these nuclei exhibited normal levels of chromosome pairing, as evidenced by the presence of a single HIM-8 and two ZIM-3 foci (Figure 34A). Consistent with the observed

degree of asynapsis, 5S rDNA FISH revealed that despite the paired status, the majority of these nuclei harbored unaligned chromosomes (Figure 34B). Examination of H3K9me2 distribution in the affected region of the gonad revealed that its pattern was similar in all nuclei that contained SYP-1 polycomplexes with a few small foci distributed across the chromatin (Figure 35III). This pattern is close to the one observed in Cluster 3 mutants with extensive asynapsis, further indicating that it is specifically the failure of SC to initiate assembly on chromatin at the onset of meiosis, rather than any other asynapsis-related defects that affects H3K9me2 distribution.

Interestingly, we noticed that in *dlc-1* RNAi animals subjected to 25°C for 12 hours without recovery, some adjacent nuclei just proximal to the region with SYP-1 polycomplexes contained foci of SYP-1 associated with chromatin (Figure 33A). This pattern of SYP-1distribution was reminiscent of the appearance of SYP-1 in wild type leptotene-to-zygotene transition stage nuclei. When the “proximally adjacent nuclei” were examined in animals that were recovered for 3 hours, several nuclei also exhibited this pattern of SYP-1 distribution. Notably, instead of a normal gradient of transition from a few SYP-1 foci associated with chromatin to short tracks assembled between bivalents, nuclei that had initiated dissociation of SYP-1 aggregates immediately preceded nuclei with robust tracks of SYP-1 on chromatin (Figure 33A). This lack of intermediate assembly stages indicates that these “proximally adjacent nuclei” became arrested in the leptotene-to-zygotene stage of SC element redistribution from polycomplexes to the chromatin during the temperature shift. These nuclei may represent the most advanced stage of the SC-dependent chromatin reorganization process that requires normal dynein function.

After a 12 hour recovery period, however, the majority of proximally adjacent nuclei exhibited robust SYP-1 tracks. Pairing center foci and 5S rDNA FISH signals in this region indicated that during this 12-hour recovery period the assembly of the SC resumed and chromosomes successfully completed homologous synapsis (Figure 34A, B). Only few nuclei (immediately next to the region with SYP-1 aggregates) remained at the early stages of SC assembly and had short tracks of SYP-1 distributed across chromatin (Figure 35II, IV). Polarized localization of the chromosomes and bright paired foci of HIM-8 and ZIM-3 indicated that these nuclei were transitioning from zygotene to pachytene stage (Figure 34A). Remarkably, these nuclei also exhibited dramatic upregulation of the number of H3K9me2 foci on their chromatin, similar to that observed in nuclei transitioning from leptotene to zygotene in wild type gonads (Figure 35II, IV, compare with Figure 19II). All other nuclei within and proximal to this region that had undergone full synapsis had H3K9me2 foci restricted to the ends of the chromosomes (Figure 35I, V). These results indicate that full assembly of SC after chromosomes have achieved pairing, but before they fully transitioned into pachytene-like conformation, is sufficient for disappearance of heterochromatic domains. Therefore, the observed dynamics of H3K9me2 foci is coupled to SYP-1 assembly between homologs, rather than to a particular stage of meiosis.

3.3 Discussion

Initiation of the assembly of central elements of SC in C. elegans takes place prior to pairing and alignment of univalents

Components of the SC demonstrate properties to self-assemble into homopolymeric tracks, ensuring high processivity of the synapsis process (Yuan et al., 1998; Ollinger et al., 2005).

This polymerization is insensitive to homology and mutants defective for pairing of homologs or carrying chromosomal rearrangements assemble SC between non-homologous regions of chromosomes in *S. cerevisiae*, *C. elegans*, *M. musculus*, and a variety of plant species (reviewed in Pawlowski and Cande, 2005; Bhalla and Dernburg, 2008). The potential for non-homologous synapsis raises the question of the mechanism that ensures assembly of SC between homologs. The current model, based on the extensive immunofluorescence microscopy data, suggests that loading of central region components is restricted to chromosomes that have successfully paired and aligned, thus ensuring that only homologous segments of aligned chromosomes are available for synapsis (reviewed in Tsai and McKee, 2011).

Our study of the dynamics of SC assembly in *C. elegans* using high-resolution immunofluorescence microscopy suggests a different order of these events. Analysis of nuclei at the earliest stages of SC appearance indicates that association of the SC central region protein SYP-1 with chromatin initiates in nuclei transitioning from leptotene to zygotene stages. Cytological data and molecular markers demonstrate that homologs have not yet achieved pairing or alignment during this period. SYP-1 patches associated with unaligned homologs are present in zygotene nuclei as well. Remarkably, transverse filaments of SC have been previously detected on the axes of unaligned segments of paired chromosomes in zygotene stage of plant and insect species using electron microcopy (Moens, 1968, 1969). Accordingly, our findings provide the first evidence of initiation of central region components assembly on univalents that have not yet undergone significant juxtaposition, thus placing the formation of nascent SC upstream of the pairing and alignment events. It is currently unclear whether these early structures represent single- or

double-width segments of the SC complex, associated with one of the axes. Significance of these results in the context of regulation of SC assembly is highlighted below.

Role of dynein motors in initiation of SC assembly

Another aspect of initiation of SC assembly that we investigated was its regulation by the dynein motors. Interactions of meiotic chromosomes with cytoskeleton and cytoskeletal motors, resulting in dramatic chromosome motions at the onset of meiosis, have been reported in diverse groups of organisms (Koszul and Kleckner, 2009). However, the biological significance of meiotic chromosome movement has been a topic of debate. It has recently been proposed that in *C. elegans* dynein-dependent motions of chromosomal regions associated with NE patches are required for testing the affinity of homologous versus non-homologous PC interactions (Sato et al., 2009; Wynne et al., 2012). According to this model, stably paired homologs are able to resist the tension imposed by dynein motors at the NE, thus indirectly triggering the initiation of the assembly of SC at the PC regions. At the same time, our findings on SC dynamics prior to pairing events suggest a different mechanism of dynein contribution to "licensing" of homologous synapsis.

Our data indicates that dynein may play two distinct roles in promoting assembly of SC between homologs. We demonstrated that dynein activity, required for association of nascent SC with unpaired chromosomes, is critical only during a very narrow temporal window at the onset of prophase I, and is not recoverable once disrupted. These results implicate dynein in a quality control mechanism that assesses proper connection between the cytoskeleton and NE-attached chromosomal ends prior to their engagement in pairing and synapsis processes. This assessment could be implemented through the proposed dynein-mediated tension, required to

trigger a cascade of signaling events at NE patches that in turn leads to a suppression of the inhibitory effect of NE patches on SC assembly. This interpretation of our data is consistent with a previous observation that the disruption of dynein interactions with ZYG-12 in a temperature-sensitive mutant *zyg-12(ct350)* leads to the failure of SC assembly in most nuclei (Sato et al., 2009). In light of these findings, it seems likely that recently described modulations of NE patches by PLK-2 and CHK-2 kinases, required for proper synapsis and pairing, represent downstream signaling events, triggered upon the establishment of ZYG-12-dynein-microtubules bridge (Penkner et al., 2009; Harper et al., 2011; Labella et al., 2011).

Besides complete abrogation of SC assembly, we observed that temporary disruption of dynein function resulted in the persistence of early states of SC formation in a narrow band of nuclei just proximal to the ones that failed to initiate synapsis. These results indicate that dynein is also required for normal progression of early stages of SC assembly, while later stages being much less sensitive to dynein depletion.

Taken together, our findings support a model in which dynein (1) restricts initiation of SC assembly to chromosomes that established a connection with the cytoskeleton and (2) subsequently promotes progression of synapsis by facilitating alignment of homologs (Figure 7D). The alignment occurs after homologous interactions are stabilized at the PCs and may be mediated by dynein-dependent motions of the PC regions of chromosomes. This movement could specifically facilitate homologous contacts of chromosomal axes by increasing the frequencies of interactions between chromosomes that are paired at one end. These interhomolog interactions are then stabilized by nascent components of central region of SC, pre-assembled on the unaligned axes. The stabilization could be achieved through interdigitation of transverse filaments of opposing axes or assembly of central elements of

SC at the locked ends of filaments. Once mature SC is formed at several sites, it completes its self-polymerization along the entire length of the chromosomal bivalent.

This model is supported by several lines of evidence from other systems. First, dynein-dependent chromosome motions were shown to increase frequencies of homologous contacts between chromosomal arms and centromeres in *S. pombe* (Ding et al., 2004). Second, initiation of synapsis at several sites along chromosomal axes has been observed in numerous species using EM and immunofluorescence microscopy (reviewed in Zickler and Kleckner, 1999). Interestingly, nucleation of SC assembly at several sites distant from PC region has been recently proposed in *C. elegans* as well (Hayashi et al., 2010). Third, EM studies of zygotene chromosomes in the Easter lily *Lilium longiflorum* demonstrated several instances when the nascent tripartite SC is more than two times wider than the mature one, potentially revealing a stage of SC formation when filaments of two axes just captured each other (Moens, 1968). In summary, the proposed model of the promotion of SC assembly by dynein motors provides a unified explanation of the mechanisms that drive juxtaposition of chromosomes in those organisms that do not utilize recombination pathways to mediate pairing and alignment of homologs.

Heterochromatic domains dynamics reveals compartmentalization of chromatin upon synapsis of homologs

The mechanism of reorganization of chromatin during juxtaposition of homologs represents a fundamental question of particular interest, since these events have direct functional consequences for the establishment of homologous interactions, recombination and formation of crossovers. It has been demonstrated that the alignment of chromosomes is accompanied

by several global chromatin reorganization events, including repositioning of lateral element of SC to one side of sister chromatids, changes to the degree of chromatin compaction, and recruitment of DSB-generating machinery (reviewed in Westergaard and von Wettstein, 1972; Kleckner, 2006; Lichten and de Massy, 2011). At the same time, our knowledge of governing principles of organization of chromatin at the interface of juxtaposed homologs is very limited.

Our investigation of the dynamics of H3K9me2-enriched regions of chromosomes during the homolog juxtaposition revealed a dramatic reorganization of these regions at the onset of meiosis and its dependence on the central element proteins of the SC. We observed that the establishment of heterochromatic domains depends on an initial association of the SC central region components with the chromatin. We have also shown that maturation of the SC upon alignment and synapsis of homologs coincides with the disappearance of heterochromatic domains. Although this disappearance could result from actual removal of the H3K9me2 mark (or the nucleosomes carrying this mark), it is likely that the assembly of the dense and extensive proteinaceous complex of the SC “sequesters” this mark in fixed samples from the antibody probes used in these studies. Interestingly, our data suggests that both homologous and non-homologous synapsis could lead to this sequestration effect, and the critical point is the timing when the SC assembles on chromosomes. In cases when synapsis is delayed and occurs late, SC tracks established during progression of nuclei through pachytene are not capable of sequestering H3K9me2 foci. In contrast, early assembly of SC even between non-homologous regions leads to the disappearance of these domains. A potential explanation of this observation could lay in the recently described general extension of chromosome territories during the transition from zygotene to pachytene stages of meiosis (Nabeshima et

al., 2011). The SC assembled during pachytene may not efficiently sequester these domains from either antibody accessibility or methyltransferase-mediated expansion.

Based on our findings, we propose a model in which the initial binding of the SC central region elements to blocks of axial elements, promoted by dynein-dependent processes, assembles them into larger domains of the maturing chromosomal axis, thus forming H3K9me2-enriched compartments of chromatin at the bases of the loops (Figure 36). Maintenance of the initial H3K9me2-enriched regions of chromatin and these H3K9me2-enriched compartments during the progression of nuclei through prophase stages could be achieved via RNAi-mediated mechanism of recruitment of the histone methyltransferase MET-2, responsible for all levels of H3K9me2 in the gonad (Bessler et al., 2010). The resulting H3K9me2-enriched interface on one univalent is then juxtaposed with that of its homolog and is thus sequestered during the continuation of SC polymerization. The nature of the expansion of heterochromatic domains during transition of nuclei from zygotene to pachytene stages of prophase and the contribution of MET-2 to these processes remains to be elucidated.

The enrichment of heterochromatic marks such as H3K9me2 in meiotic chromatin in response to defective synapsis is a conserved process (reviewed in Turner et al., 2005; Inagaki et al., 2010). Our initial studies suggested this might be an integral component of the meiotic surveillance machinery, recognizing unsynapsed regions, yet further studies in *C. elegans* have not supported this idea. For example, the complete loss of H3K9me2 in meiotic chromatin in *met-2* mutants is unaccompanied by significant meiotic defects, with the exception of a subtle increase in the rate of non-disjunction (Bessler et al., 2010). This indicates that an increase in H3K9me2 within unsynapsed chromatin is not providing an

important signal that is interpreted by the meiotic surveillance processes. Rather, the subtle defects associated with the loss of H3K9me2 enrichment are more consistent with the dynamics of meiotic chromatin reorganization. H3K9me2 may thus be considered a useful marker for monitoring how the chromatin along the chromosomal axes becomes organized, but whether it is an essential component or how that organization occurs is unclear at this time.

Importantly, we did not observe changes in H3K4me2 patterns in response to synapsis. These results might indicate that assembly of the SC specifically involves regions enriched for H3K9me2, with euchromatic regions being omitted or prevented from entanglement in SC assembly. Moreover, antibodies directed against the higher methylated state of H3K9, H3K9me3, show no obvious dramatic changes to its pattern during progression through stages of prophase I (Bessler et al., 2010). Intriguingly, genome-wide examination of H3K9me2 and H3K9me3 distributions in *C. elegans* revealed that they are differentially enriched in different types of elements in the genome, potentially explaining differences in their response to chromatin reorganization upon synapsis (Gerstein et al., 2010).Thus, chromatin reorganization events that are coupled to SC dynamics appear to be specific for regions marked by H3K9me2.

It has recently been proposed that repetitive regions of the genome provide a basis for hierarchical folding of chromatin fibers in mitotic chromosomes by serving as driving force for formation of internal organizer modules (Tang, 2011). Remarkably, the existing evidence in several mammalian species points to repeat sequences acting as anchor points for binding of the axial elements and thus forming the base of the meiotic chromatin loops (Pearlman et al., 1992; Ortiz et al., 2002; Hernández-Hernández et al., 2008). Our model of meiotic

heterochromatin topology is also consistent with recent findings of compartmentalization of interphase chromatin in *C. elegans*, where subdomains of chromosome arms associated with NE were specifically enriched in repetitive sequences marked with H3K9me2, while active genes were residing in the gaps between the subdomains (Ikegami et al., 2010). Similar conclusions have been obtained for arrangement of *Drosophila* and human genomes, where heterochromatic domains are proposed to contribute to a hierarchical chromosomal organization by folding genomic regions into physical modules and tethering them to the nuclear envelope-associated scaffold (Guelen et al., 2008; Lieberman-Aiden et al., 2009; Sexton et al., 2012).

Our studies therefore provide the first example of histone modification defining a specific compartment of meiotic chromatin and reveal higher-order combinatorial interactions of its regions. Overall, the proposed aspects of the compartmentalized organization of meiotic chromosomes suggests that SC itself is an active contributor to the partitioning of meiotic chromatin into domains with different features, thus potentially playing a role in prevention of non-allelic recombination, genome recognition and defense mechanisms, and the mediation of genome topology.

3.4 Materials and Methods

Strains and worm culture

Standard techniques were used for worm culture (Brenner, 1974). All worms were raised at 20°C, unless otherwise specified. Worms of N2 strain var. Bristol were used as wild type reference. The following alleles were used in the study: *atl-1(tm853), brc-2(tm1086), msh-5(me23), rad-51(lg8701), rad-54(ok615), spo-11(ok79), zhp-3(ok1993), him-8(e1489), zim-*

2(tm574), him-3(gk149), htp-3(y428), syp-1(me17), syp-2(ok307), syp-3(ok758), rec-8(ok978);coh-3(gk112);coh-4(tm1857), htp-1(gk150), rec-8(ok978), sun-1(jf18), zyg-12(or577), zim-1(tm1813), mnDp66;meDf2, ieDf2.

Indirect immunocytochemistry

Dissected gonads of age-matched 24 hours-post L4 adults were used for staining procedures. Whole-mount fixation and incubation with antibodies was performed as previously described (Bean et al., 2004). The following primary antibodies were used at the indicated dilutions: mouse anti-H3K9me2 (Abcam®, ab1220, 1:500), rabbit anti-H3K4me2 (Millipore® 07-030, 1:500), guinea pig anti-SYP-1 (a gift from A. Villeneuve, 1:200), guinea pig anti-ZIM-3 (a gift from A. Dernburg, 1:200), and rabbit anti-HIM-8 (a gift from A. Dernburg, 1:200). The following secondary antibodies at respective dilutions were used: Alexafluor™ 594 goat anti-rabbit IgG (Invitrogen™, 1:500), Alexafluor™ 488 goat anti-mouse IgG (Invitrogen™, 1:500), Alexafluor™ 594 donkey anti-guinea pig IgG (Invitrogen™, 1:500).

Image acquisition and analysis

Images were acquired on a Leica DMRA microscope (Leica Microsystems, equipped with a cooled CCD camera (QImaging), with a 40× 1.4 or 100× 1.35 NA objectives and a voxel size of 150 nm in the x, 150 nm in the y, and 200 nm in the z planes. Image acquisition was performed using Simple PCI software (Hamamatsu Corporation). Images were processed and deconvolved using measured point spread function using Huygens Essential (Scientific Volume Imaging) deconvolution software. For demonstration purposes, acquired Z-stacks were projected on a single image plane using maximum projection algorithm of the SoftWorx (Applied Precision) software. For three-dimensional surface rendering of nuclei, images were subjected to semi-automated background subtraction, segmentation, volume

rendering and surface rendering using Metamorph (Molecular Devices) and Imaris (Bitplane Scientific Software) software packages. Quantification of chromosome pairing was performed in five designated zones of the goad on a total of ten gonads per strain. Statistical comparison between mutant and wild type strains was performed using Student's t-test.

Principal component and clustering analyses

Dissected gonads, stained with anti-H3K9me2, anti-H3K4me2 antibodies and DAPI in three independent experiments were used in the analysis.

The pattern of anti-H3K9me2 antibody localization on chromosomes of meiotic nuclei is often diffuse or speckled, which made visual interpretation of changes in the pattern between mutants challenging. Automated image analysis methods facilitate extraction of information from fluorescence microscopy images and aid in quantitative characterization of protein localization in cells. We therefore implemented a semi-automated image processing and analysis pipeline for comparison of the acquired three-dimensional datasets (Glory and Murphy, 2007). A set of quantitative morphological features, defining the overall appearance and relative size of surface-rendered H3K9me2 foci, was extracted after images were restored and subjected to segmentation algorithms. The following features were measured: total volume of H3K9me2 foci, mean volume of H3K9me2 foci, standard deviation of the volume of H3K9me2 foci, ratio of the largest volume of H3K9me2 to the smallest one, total surface area of H3K9me2 foci, mean surface area of H3K9me2 foci, standard deviation of the surface area of H3K9me2 foci, ratio of the largest surface area of H3K9me2 to the smallest one. For each of the experiments, at least ten gonads per strain were examined.

To identify key features that contributed to the difference in H3K9me2 patterns among wild-type and mutant strains, the obtained feature set was z-score normalized and subjected to principal component analysis (PCA) using *FactoMineR* package/R. The first two principal components accounted for 91.76% of variance in the dataset (Figure 8B). These components most strongly correlated with two features – average standard deviation of the volume of H3K9me2 foci in the nucleus (first component, correlation coefficient 0.96) and average ratio of the largest to the smallest surface area of H3K9me2 focus per nucleus (second component, 0.48**)** (Figure 9D). Since the first two components summarized most of the information extracted from H3K9me2 patterns, we limited our downstream analysis to these components. In order to group mutants that shared similar patterns of H3K9me2, we next performed hierarchical clustering analysis using Euclidean distances and Ward's algorithm. Clustering analysis was performed on the first two principal components using *ape*/R. The resulting clustering solution was visualized as a phylogram with size and color gradient of the nodes representing two features that most strongly correlated with the principle dimensions of variability in the dataset, and thus directly characterized the main differences in H3K9me2 patterns between the mutants (Figure 7, 8B, 9C). We assessed the uncertainty in the results of the clustering algorithm by random sampling of the dataset and conducting multiple rounds of clustering analysis using *pvclust*/R (Suzuki and Shimodaira, 2006). This multiscale bootstrap resampling favored partitioning of the phylogram into four clusters (N = 10,000, $p < 0.05$) (Figure 8A). To identify objects that did not lie well within their clusters, we calculated the silhouette width of each cluster using *silhouette*/R (Rousseeuw, 1987). High values of the obtained silhouette widths and the absence of misclassified replicates supported our conclusion that the obtained clustering solution is of high quality (Figure 9A, B).

FISH analysis

Combined FISH/immunocytochemistry was performed essentially as in (Bean et al., 2004). The 5S rDNA probe was generated by amplification of a 1 kb region of the 5S rDNA locus using published primers. The probe was labeled with DIG-11-dUTP using the DIG-Nick Translation Kit (Roche Applied Science). FISH was carried out as described (Bean et al., 2004). A 1:200 dilution of anti-Digoxigenin-Fluorescein antibody (Roche Applied Science) was used for probe detection. Quantification of colocalization of the FISH signal and SYP-1 tracks was performed in five designated areas of the gonad on a total of 10 gonads per strain. Statistical comparison between mutant and wild type strains was performed using Student's t test.

RNAi conditions

RNAi experiments were performed as previously described (Li and Kelly, 2011). For weak SYP-2 RNAi, L1s were plated on feeding plates with 1mM IPTG and containing bacteria expressing SYP-2 dsRNA or harboring empty L4440 vector. For strong SYP-2 RNAi, L1 were soaked in 1µg/µL of dsRNA overnight at 20°C and then placed on RNAi feeding plates. Animals were used for analysis 24 hours post L4 stage. For DLC-1 RNAi, L1 animals were placed on feeding plates with 1mM IPTG and containing bacteria expressing DLC-1 dsRNA or harboring an empty L4440 vector, grown to L4 stage at 16°C and incubated at 25°C for 12 hours. Then animals were recovered on DLC-1 feeding plates for 0, 3, 6, 12, or 24 hours at 16°C and dissected immediately.

Figure 6. Univalents of chromosome V are enriched for H3K9me2 in pachytene nuclei of *zim-2(tm574)* mutant.

Representative maximum intensity projection image of pachytene nuclei from wild-type and *zim-2(tm574) C. elegans* gonads, probed with anti-H3K9me2 antibodies (green) and FISH specific for the 5S rDNA locus on the right arm of LG V (white). DNA was stained with DAPI (blue). Arrows indicate the enrichment of H3K9me2 in the chromatin of the unsynapsed LG V univalents. Scale bar, 2 μm.

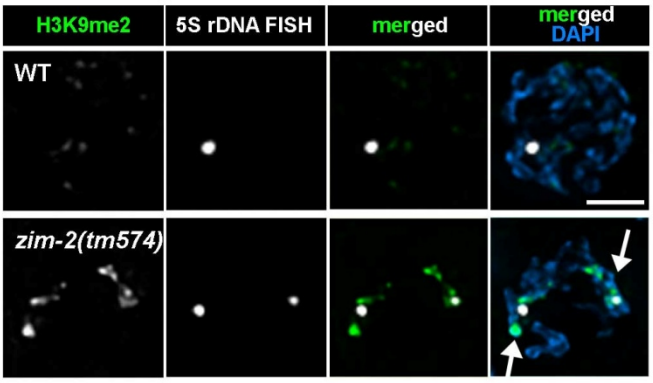
H3K9me2
5S rDNA FISH
merged
merged
DAPI
WT
zim-2(tm574)

Figure 7. Phylogram of the results of PCA and clustering analysis of H3K9me2 patterns in WT and mutant pachytene nuclei.

Numbers on the genotype labels indicate independent immunofluorescence experiments. The diameter of the circles at the tips of the phylogram and their shade indicate the change in two features of H3K9me2 pattern that most strongly correlated with principal dimensions of variability in the dataset. Clusters that demonstrated high certainty of existence are shown by colored circles (multiscale bootstrap resampling, N = 10,000, $p<0.05$). Scale bar, Euclidean distance of one.

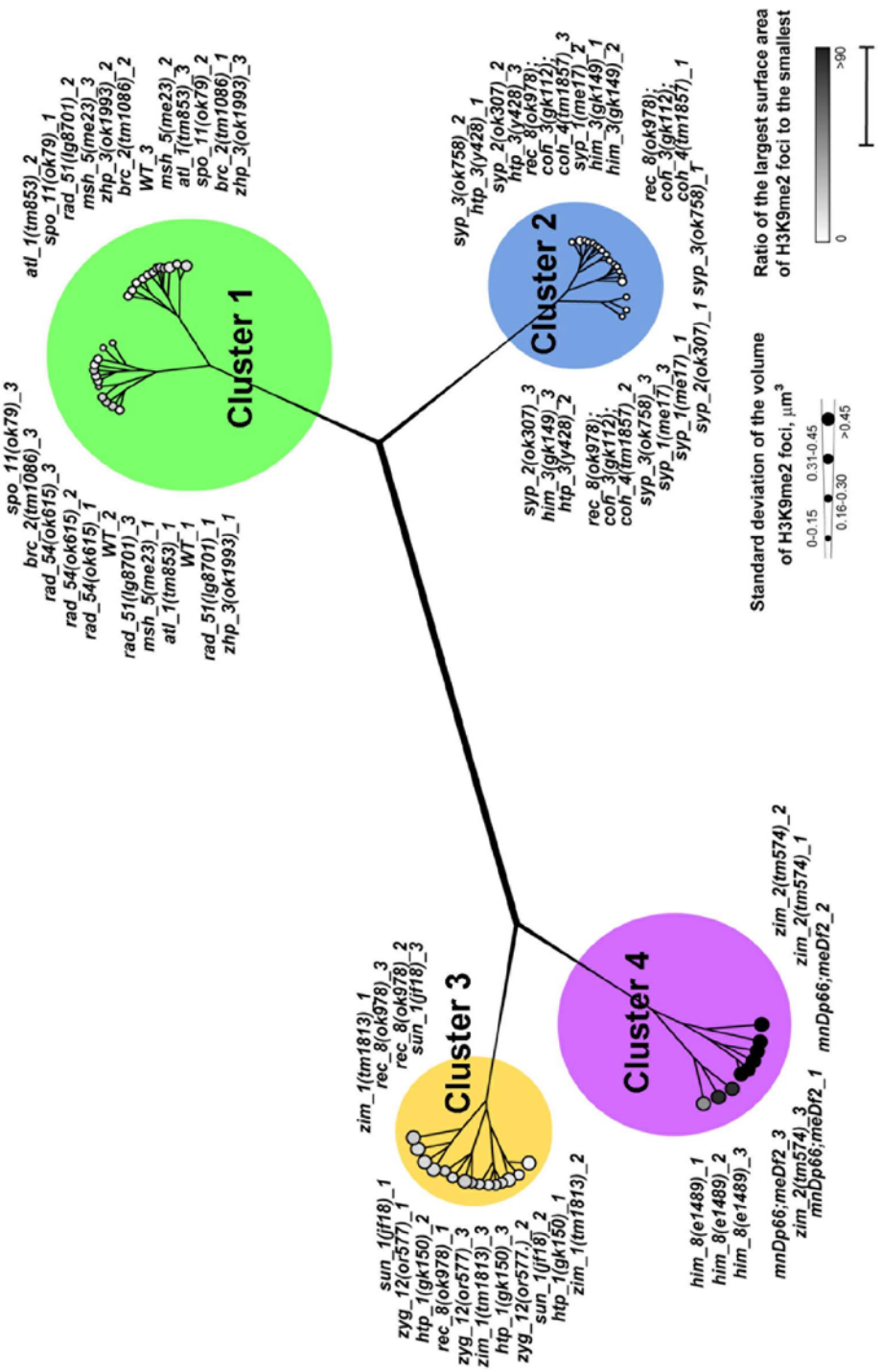
Cluster 1
Cluster 2
Cluster 3
Cluster 4
atl_1(tm853)_2
spo_11(ok79)_1
rad_51(lg8701)_2
msh_5(me23)_3
zhp_3(ok1993)_2
brc_2(tm1086)_2
WT_3
msh_5(me23)_2
atl_1(tm853)_3
spo_11(ok79)_2
brc_2(tm1086)_1
zhp_3(ok1993)_3
spo_11(ok79)_3
brc_2(tm1086)_3
rad_54(ok615)_3
rad_54(ok615)_2
rad_54(ok615)_1
WT_2
rad_51(lg8701)_3
msh_5(me23)_1
atl_1(tm853)_1
WT_1
rad_51(lg8701)_1
zhp_3(ok1993)_1
syp_3(ok758)_2
htp_3(y428)_1
syp_2(ok307)_2
htp_3(y428)_3
rec_8(ok978);
coh_3(gk112);
coh_4(tm1857)_3
syp_1(me17)_2
him_3(gk149)_1
him_3(gk149)_2
rec_8(ok978);
coh_3(gk112);
coh_4(tm1857)_1
syp_2(ok307)_3
him_3(gk149)_3
htp_3(y428)_2
rec_8(ok978);
coh_3(gk112);
coh_4(tm1857)_2
syp_3(ok758)_3
syp_1(me17)_3
syp_2(ok307)_1
syp_3(ok758)_1
zim_1(tm1813)_1
rec_8(ok978)_3
rec_8(ok978)_2
sun_1(jf18)_3
sun_1(jf18)_1
zyg_12(or577)_1
htp_1(gk150)_2
rec_8(ok978)_1
zyg_12(or577)_3
zim_1(tm1813)_3
htp_1(gk150)_3
zyg_12(or577)_2
sun_1(jf18)_2
htp_1(gk150)_1
zim_1(tm1813)_2
him_8(e1489)_1
him_8(e1489)_2
him_8(e1489)_3
mnDp66;meDf2_3
zim_2(tm574)_3
mnDp66;meDf2_1
zim_2(tm574)_2
zim_2(tm574)_1
mnDp66;meDf2_2
Standard deviation of the volume of H3K9me2 foci, µm³
0-0.15
0.16-0.30
0.31-0.45
>0.45
Ratio of the largest surface area of H3K9me2 foci to the smallest
0
>90

Figure 8. Steps of the principal component and clustering analysis of H3K9me2 patterns in the examined mutants (Part 1).

(A) Results of the bootstrap analysis of the obtained clustering solution. Values represent approximate unbiased *p*-value, indicating how strongly the cluster is supported by data. Clusters with *p*-values higher than 0.95 are highlighted by rectangles.

(B) Percent of variety, associated with each principal component of the data set. First two components, used for the downstream analysis, are highlighted in red.

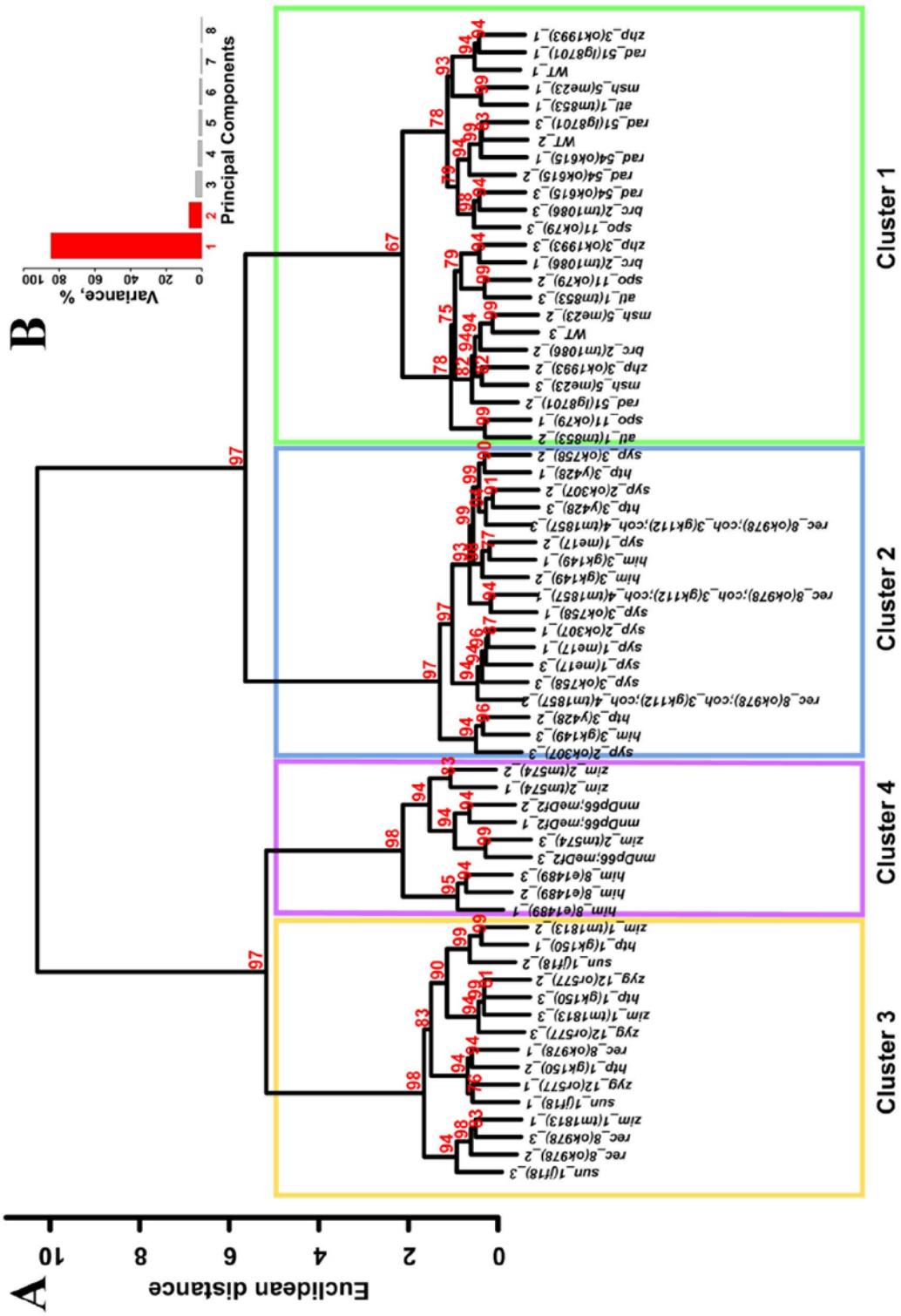
A
Euclidean distance
0
2
4
6
8
10
B
Variance, %
0
20
40
60
80
100
Principal Components
1
2
3
4
5
6
7
8
Cluster 1
Cluster 2
Cluster 4
Cluster 3

Figure 9. Steps of the principal component and clustering analysis of H3K9me2 patterns in the examined mutants (Part 2).

(A) Determination of the optimal number of clusters in the dataset, based on the average *silhouette* width of a cluster.

(B) Evaluation of the quality of the obtained clustering solution, based on the average *silhouette* width of each of the identified clusters.

(C) Distribution of individual H3K9me2 patterns of the mutants in the plane of the first two principal components. Data points are colored according to their respective cluster.

(D) Correlation of the measured parameters with the first two principal components. Two parameters with the highest correlation coefficients are highlighted in red.

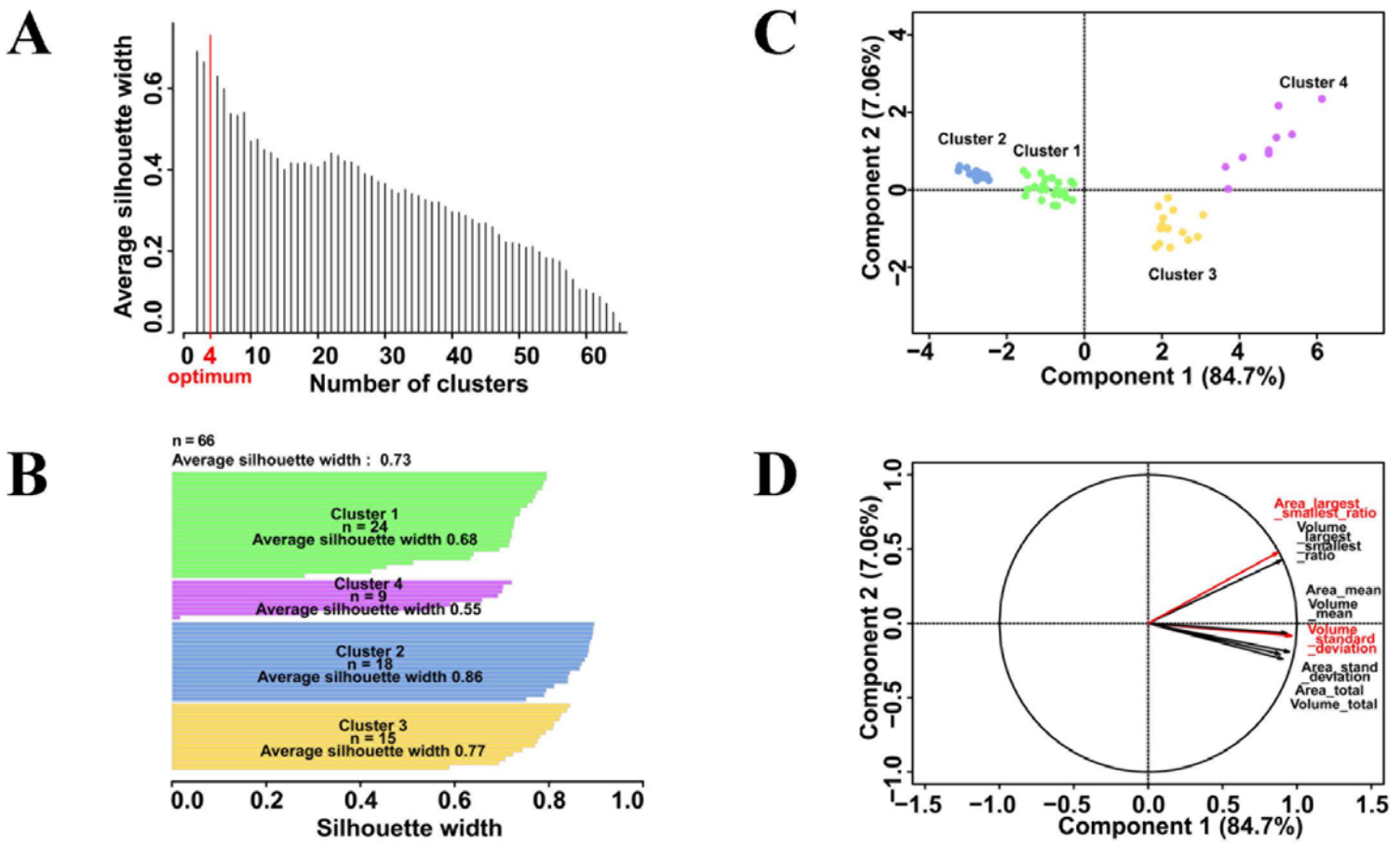
A
Average silhouette width
0.0
0.2
0.4
0.6
0 4 10 20 30 40 50 60
optimum
Number of clusters
B
n = 66
Average silhouette width : 0.73
Cluster 1
n = 24
Average silhouette width 0.68
Cluster 4
n = 9
Average silhouette width 0.55
Cluster 2
n = 18
Average silhouette width 0.86
Cluster 3
n = 15
Average silhouette width 0.77
0.0 0.2 0.4 0.6 0.8 1.0
Silhouette width
C
Component 2 (7.06%)
−4 −2 0 2 4
Cluster 4
Cluster 2
Cluster 1
Cluster 3
−4 −2 0 2 4 6
Component 1 (84.7%)
D
Component 2 (7.06%)
−1.0 −0.5 0.0 0.5 1.0
Area_largest_smallest_ratio
Volume_largest_smallest_ratio
Area_mean
Volume_mean
Volume_standard_deviation
Area_stand_deviation
Area_total
Volume_total
−1.5 −1.0 −0.5 0.0 0.5 1.0 1.5
Component 1 (84.7%)

Figure 10. H3K9me2 and H3K4me2 patterns in representative nuclei from each of the clusters of mutants on the phylogram.

Each panel shows three-dimensional surface rendering of H3K9me2 foci (green) and DNA (blue) or maximum intensity projection image of a single pachytene nucleus probed with anti-H3K9me2 (green), anti-H3K4me2 (yellow) antibodies or DAPI (blue). Arrows in *zim-2(tm574)* shows LG V univalents with enriched H3K9me2 but normal H3K4me2 signals. Grid spacing on the representations of surface-rendered images, 0.5 µm. Scale bar, 2 µm.

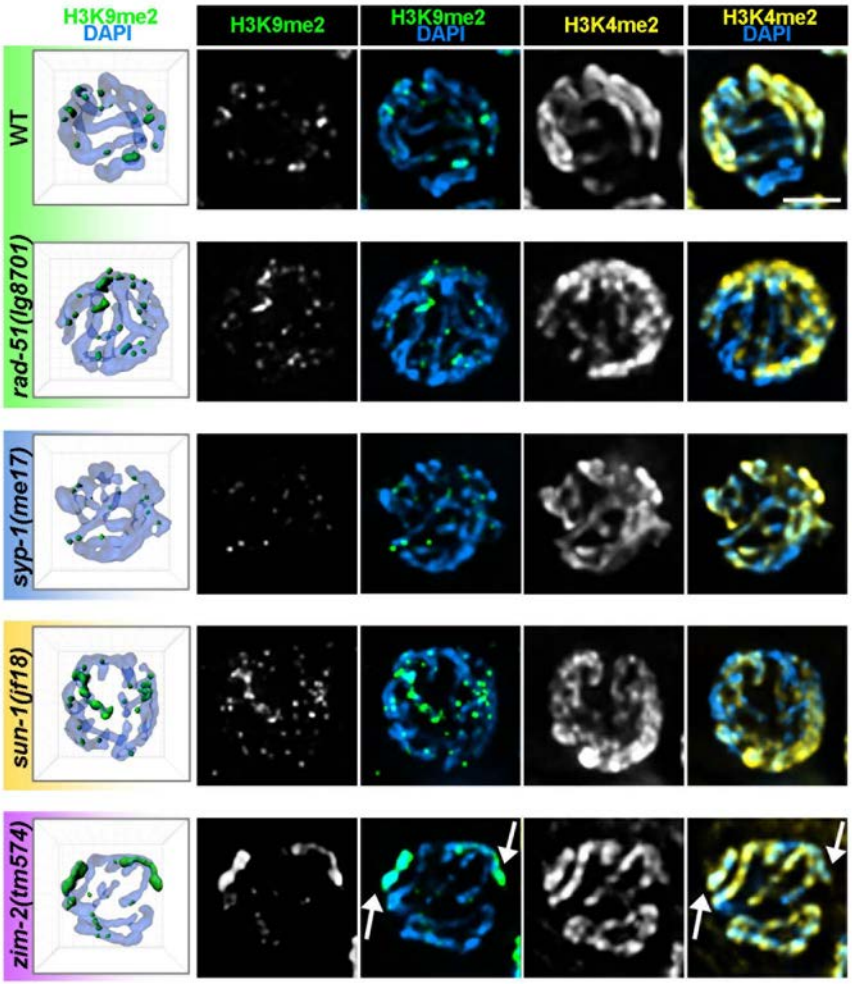
H3K9me2
DAPI
H3K9me2
H3K9me2
DAPI
H3K4me2
H3K4me2
DAPI
WT
rad-51(lg8701)
syp-1(me17)
sun-1(jf18)
zim-2(tm574)

Figure 11. Representative examples of H3K9me2 and H3K4me2 patterns in mutants from Cluster 1 (normal synapsis) and Cluster 4 (defective synapsis of a single pair of chromosomes) of the phylogram.

Maximum intensity projection image of pachytene nuclei, stained with anti H3K9me2 antibodies (green) and anti-H3K4me2 (yellow) antibodies. DNA is visualized with DAPI (blue). Scale bar, 5 μm.

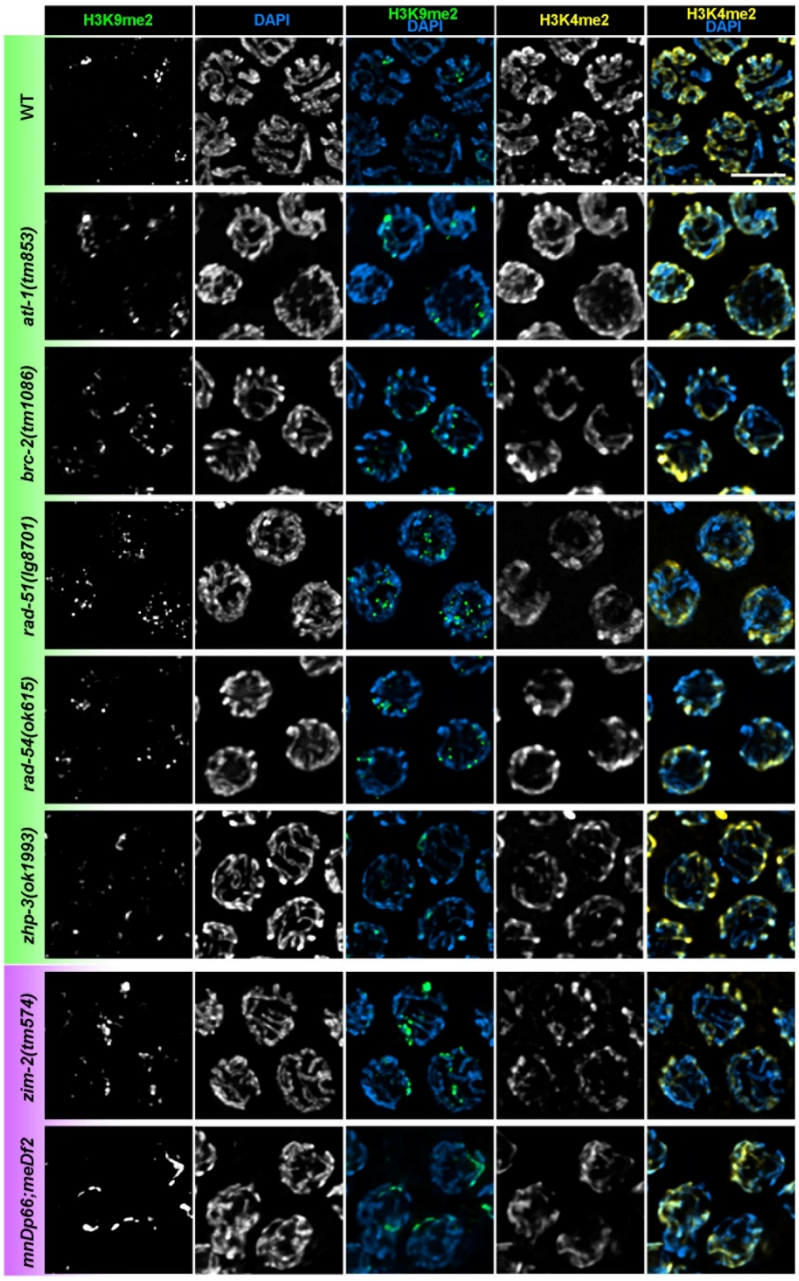
H3K9me2
DAPI
H3K9me2
DAPI
H3K4me2
H3K4me2
DAPI
WT
atl-1(tm853)
brc-2(tm1086)
rad-51(lg8701)
rad-54(ok615)
zhp-3(ok1993)
zim-2(tm574)
mnDp66;meDf2

Figure 12. Representative examples of H3K9me2 and H3K4me2 patterns in mutants from Cluster 2 (extensive asynapsis) and Cluster 3 (heterologous synapsis) of the phylogram.

Maximum intensity projection image of pachytene nuclei, stained with anti-H3K9me2 antibodies (green) and anti-H3K4me2 (yellow) antibodies. DNA is visualized with DAPI (blue). Scale bar, 5 μm.

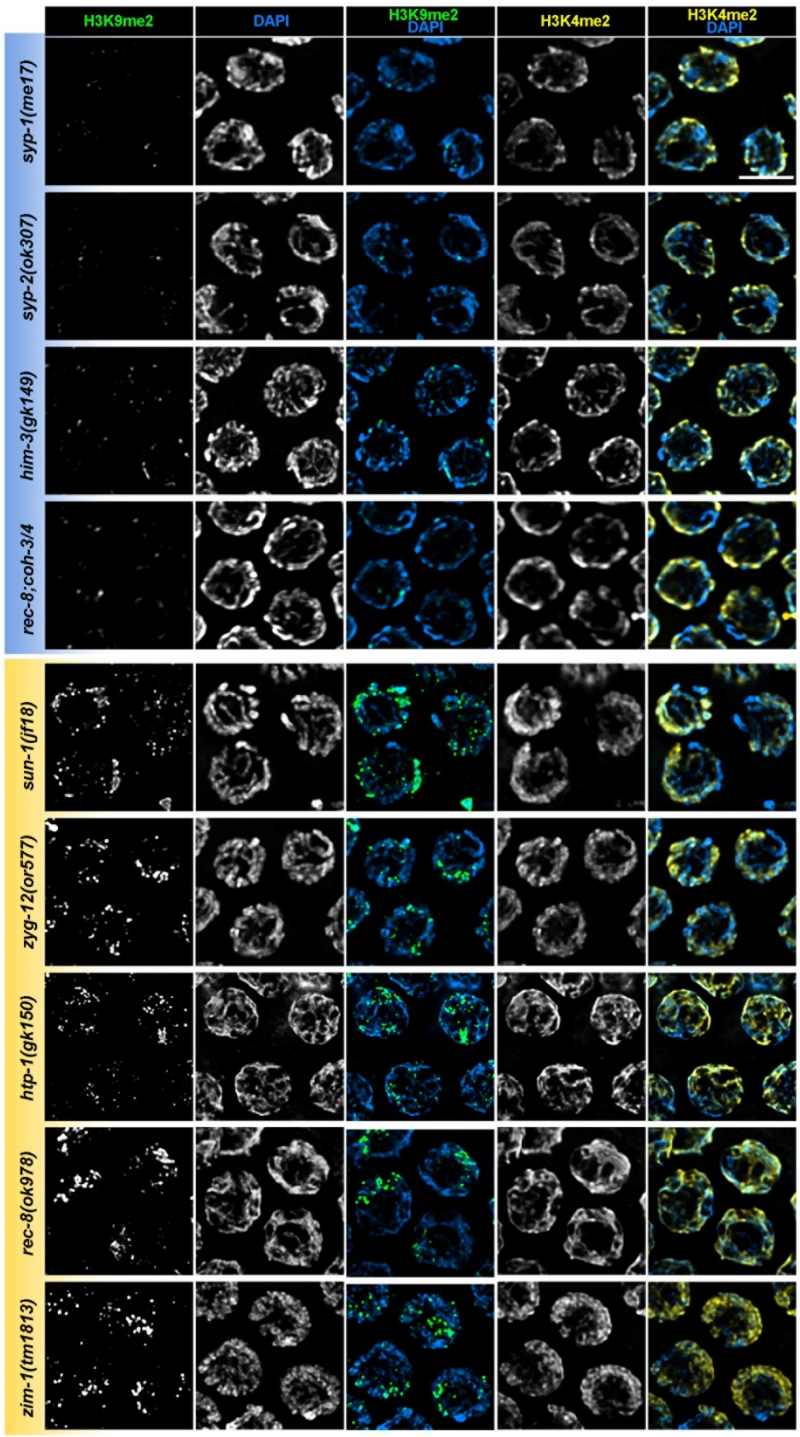
H3K9me2
DAPI
H3K9me2 DAPI
H3K4me2
H3K4me2 DAPI
syp-1(me17)
syp-2(ok307)
him-3(gk149)
rec-8;coh-3/4
sun-1(jf18)
zyg-12(or577)
htp-1(gk150)
rec-8(ok978)
zim-1(tm1813)

Figure 13. Synapsis defects specifically affect H3K9me2 distribution on chromatin of pachytene nuclei.

Representative SYP-1 and H3K9me2 patterns in pachytene nuclei from each cluster. Each panel shows a maximum intensity projection image of a single pachytene nucleus probed with anti-H3K9me2 (green), and anti-SYP-1 (red) antibodies, and DAPI (blue). Arrowheads indicate H3K9me2 foci at the tips of synapsed chromosomes. Arrows in *zim-2(tm574)* mutant show chromosome V univalents with weak/lacking SYP-1 staining and elevated H3K9me2 signal. Scale bar, 2 μm.

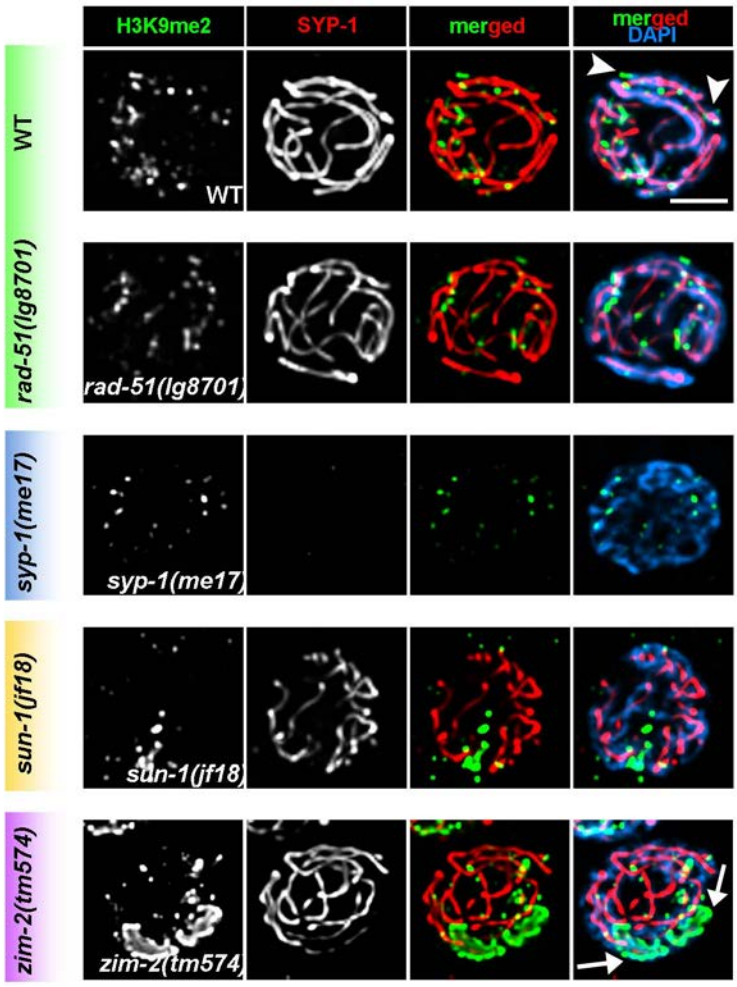
H3K9me2
SYP-1
merged
merged
DAPI
WT
WT
rad-51(lg8701)
rad-51(lg8701)
syp-1(me17)
syp-1(me17)
sun-1(jf18)
sun-1(jf18)
zim-2(tm574)
zim-2(tm574)

Figure 14. Representative examples of SYP-1 distribution and H3K9me2 patterns in mutants from Clusters 2 (extensive asynapsis) and 3 (heterologous synapsis) of the phylogram.

Maximum intensity projection image of pachytene nuclei, stained with anti-H3K9me2 antibodies (green) and anti-SYP-1 (red) antibodies. DNA is visualized with DAPI (blue). Scale bar, 5 μm.

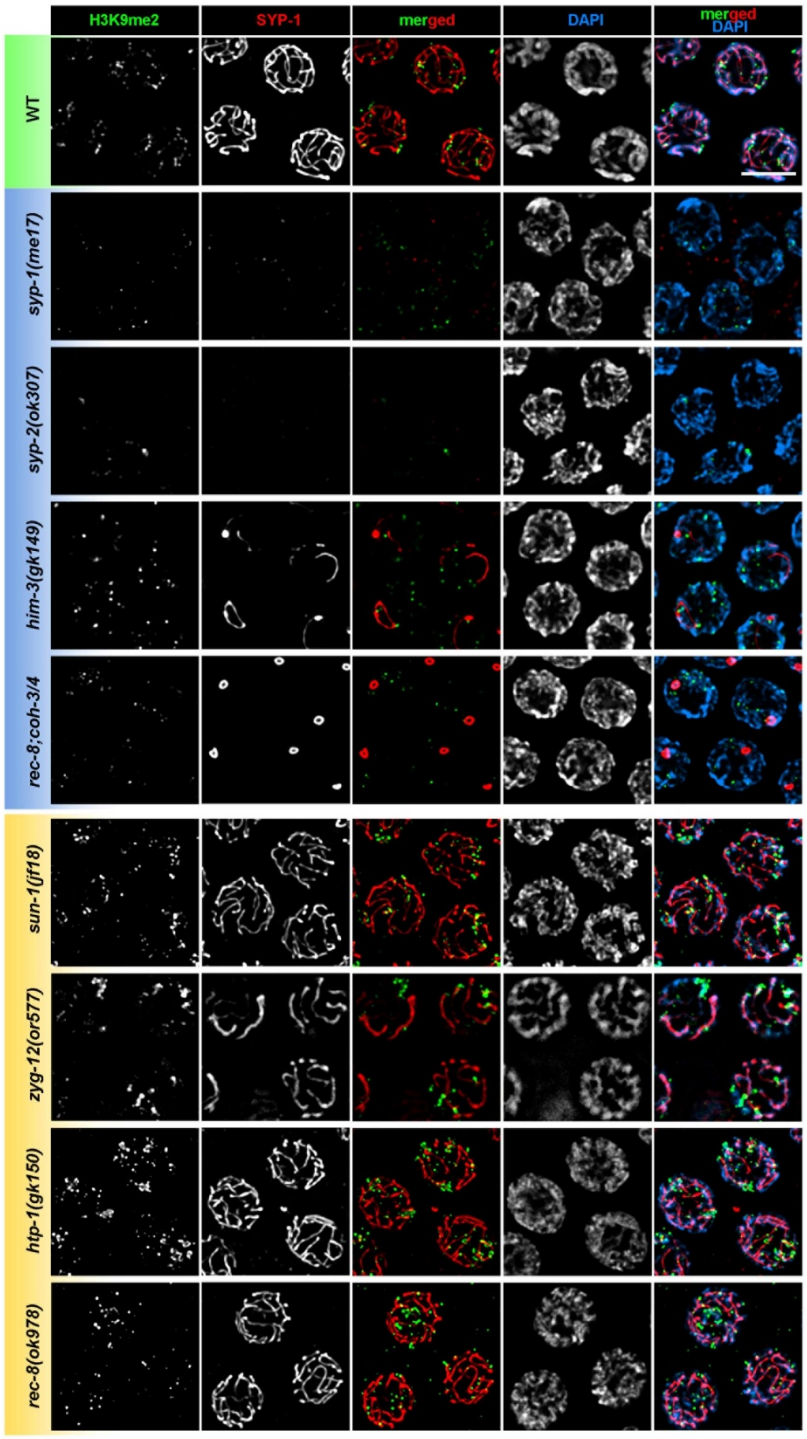
H3K9me2
SYP-1
merged
DAPI
merged
DAPI
WT
syp-1(me17)
syp-2(ok307)
him-3(gk149)
rec-8;coh-3/4
sun-1(jf18)
zyg-12(or577)
htp-1(gk150)
rec-8(ok978)

Figure 15. Dynamics of H3K4me2 at the early stages and pachytene of prophase I.

High-resolution maximum-intensity projection images of nuclei from each of the identified zones of wild-type gonad. Nuclei were stained with anti-H3K4me2 (yellow). DNA is visualized with DAPI (blue). Scale bar, 5 μm. Box highlights a nucleus used to generate montage view of H3K4me2 and DNA. tz – transition.

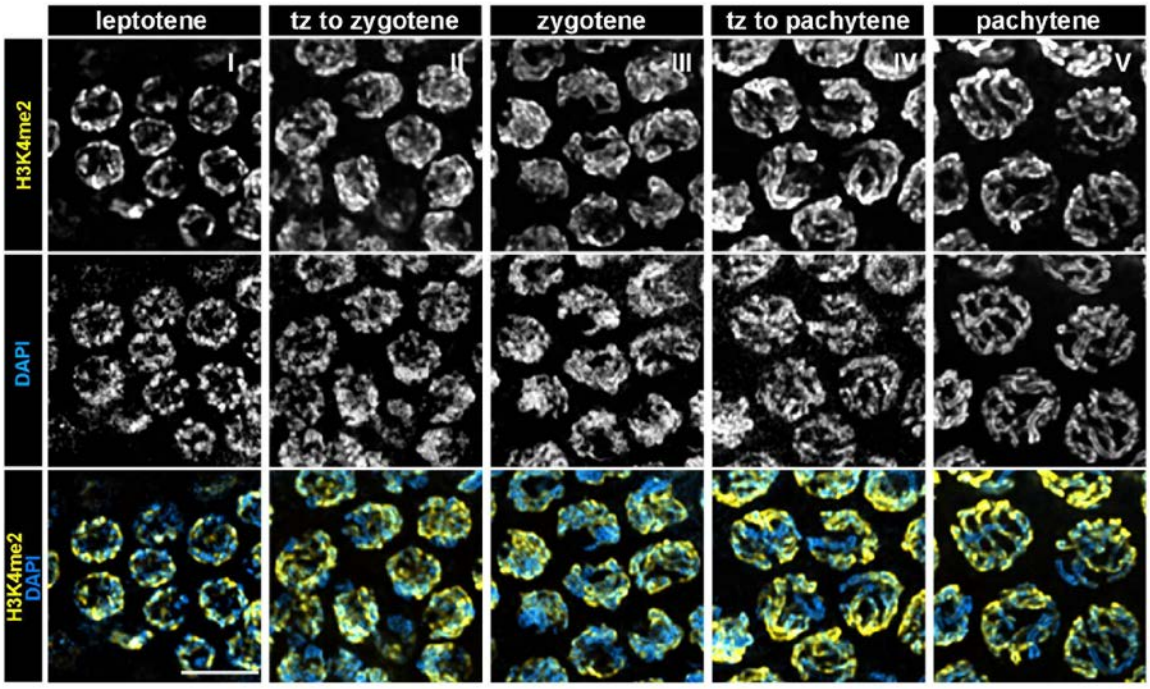
leptotene
tz to zygotene
zygotene
tz to pachytene
pachytene
I
II
III
IV
V
H3K4me2
DAPI
H3K4me2
DAPI

Figure 16. Distribution of H3K4me2 signal on synapsed bivalents in wild-type pachytene nuclei.

(A) Montage view of H3K4me2 pattern in a single pachytene nucleus. Red and green bars on the merged image represent cross-sections for intensity profiles measurements.

(B) Intensity profiles of H3K4me2 and DAPI signals at the cross-section of a pachytene autosome. Position of points along the line of the cross-section in XY plane is plotted on the X-axis.

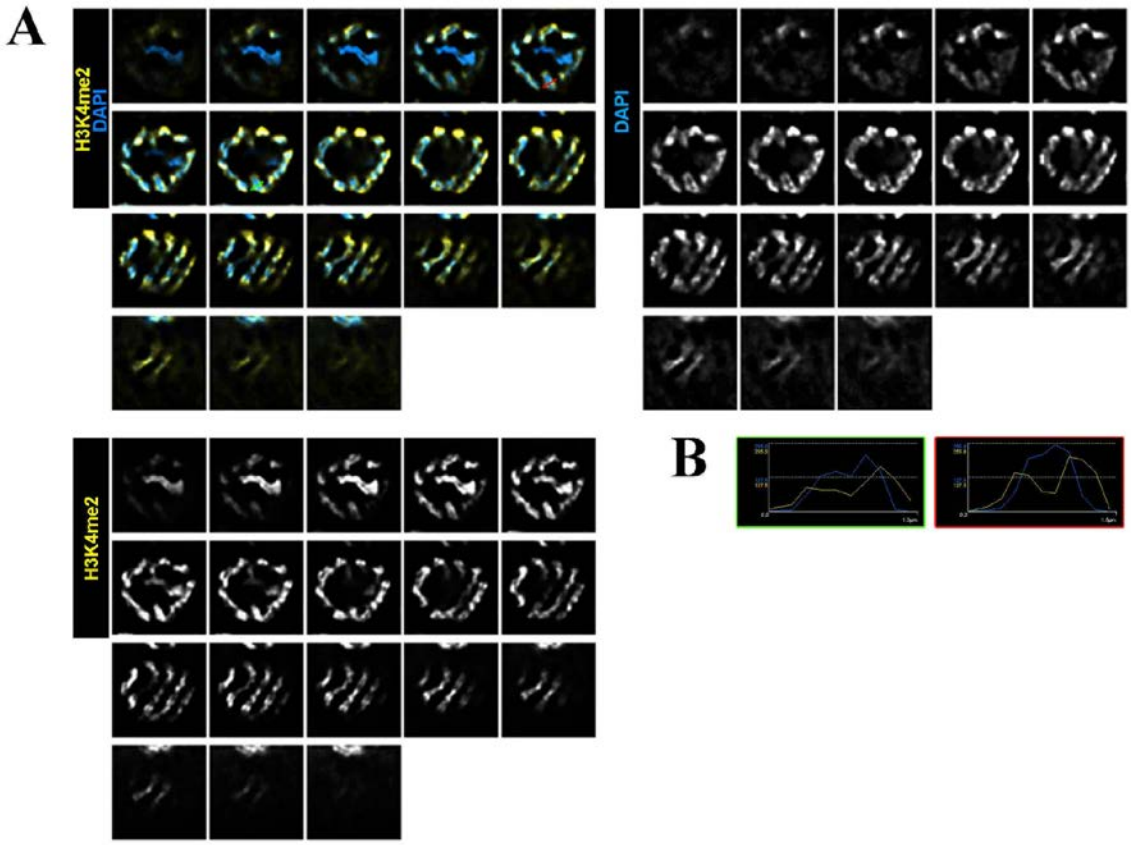
A
H3K4me2
DAPI
DAPI
H3K4me2
B

Figure 17. Identification of synapsis zones in WT prophase I.

(A) Dynamics of SC assembly in adult gonad. Top panel: Maximum-intensity projection image of the nuclei in the gonad with the SC central element visualized with anti-SYP-1 antibodies (red) and DNA (DAPI; blue). White line is the proximodistal axis of the gonad along which different states of the central elements assembly in the nucleus were scored. Another line, perpendicular to the proximodistal axis of the gonad, highlights how columns of nuclei (circled) were selected and scored within each zone of the gonad. Bottom panel: Graph depicts the number of nuclei exhibiting a particular category of SYP-1 state scored along the proximodistal axis of the gonad. Colors of the sections of the x-axis of the graph indicate the predominant category of SYP-1 state used to demarcate each zone. Scale bar, 30 μm.

(B) Distribution of nuclei by stage of SYP-1 assembly in wild-type early prophase I. (Top panel) SYP-1 is visualized with anti-SYP-1 antibody and colored according to the category of SYP-1 state in panel A. (Bottom panel) Red – anti-SYP-1; DAPI – blue. Zones of the gonad based on predominant state of SYP-1, are labeled. Scale bar, 10 μm. tz – transition.

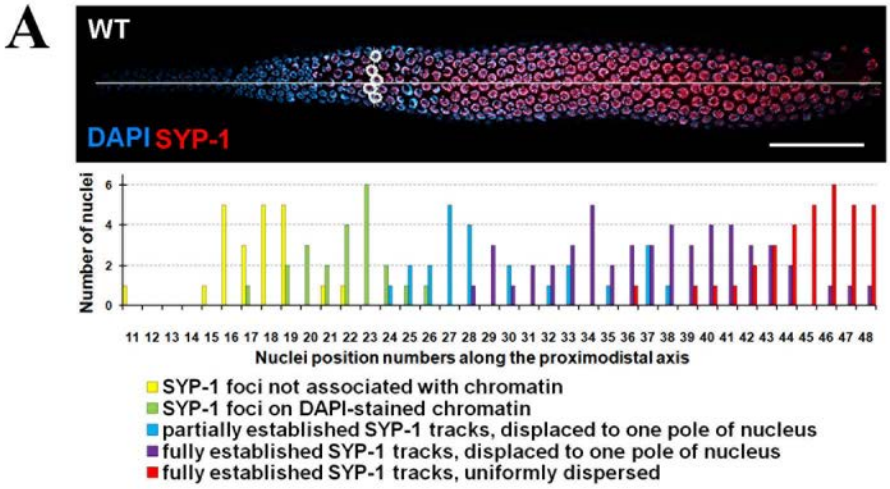
A
WT
DAPI SYP-1
Number of nuclei
0
2
4
6
11 12 13 14 15 16 17 18 19 20 21 22 23 24 25 26 27 28 29 30 31 32 33 34 35 36 37 38 39 40 41 42 43 44 45 46 47 48
Nuclei position numbers along the proximodistal axis
SYP-1 foci not associated with chromatin
SYP-1 foci on DAPI-stained chromatin
partially established SYP-1 tracks, displaced to one pole of nucleus
fully established SYP-1 tracks, displaced to one pole of nucleus
fully established SYP-1 tracks, uniformly dispersed

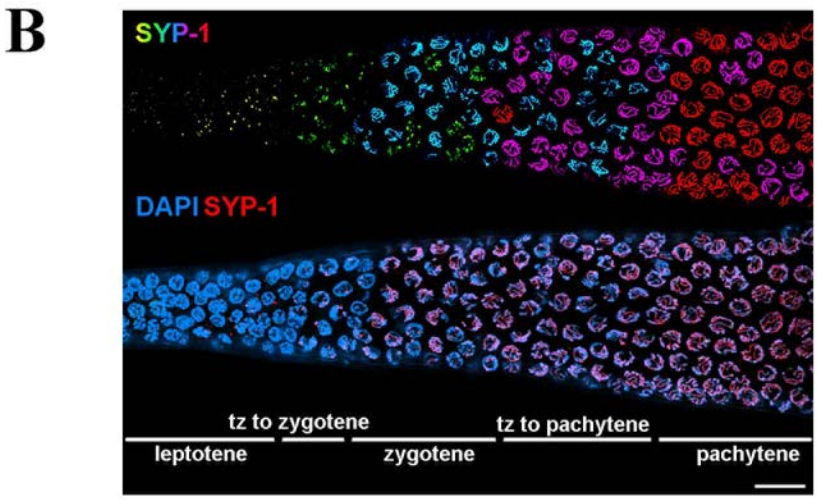
B
SYP-1
DAPI SYP-1
tz to zygotene
tz to pachytene
leptotene
zygotene
pachytene

Figure 18. Quantification of the pairing and alignment dynamics of homologs in WT prophase I.

(A) Pairing status of autosomes and X chromosome in each of the identified zones of the adult WT. Pairing centers of LG I and IV visualized with anti-ZIM-3 antibodies (purple), pairing center of X with anti-HIM-8 antibodies (orange). Blue – DAPI. Arrows point to two unpaired foci of HIM-8 in a zygotene zone nucleus that also exhibits four separated ZIM-3 foci. Arrowhead indicates nucleus with paired HIM-8 and ZIM-3 foci in a nucleus in the transition to pachytene zone of the gonad. Scale bar, 5 μm.

(B) Synapsis status of chromosome V in ovary zones. Right arm of LG V is visualized by a 5S rDNA-specific FISH (white), SC central elements of SC are visualized with anti-SYP-1 antibodies (red), DAPI – blue. Arrows point to two separated signals of the FISH probe, one of which is located on a chromosome that has some SYP-1 foci associated with it, in a transition to zygotene zone of the gonad. Arrowhead indicates a case where unpaired FISH probe signal is colocalized with SYP-1 in a zygotene zone nucleus. Inset shows region of the univalent of chromosome V with colocalization of 5S rDNA FISH and SYP-1 signals. Scale bar, 5 μm.

(C) Pairing status quantification in WT zones. (Top panel) Schematic diagram of the ovary with scoring zones highlighted by red boxes. (Bottom panel) Graph demonstrates percent of nuclei with detectable pairing center foci and paired signals in each of the corresponding zones of the gonad. N = 10 gonads. LPT – leptotene,

TzZ – transition to zygotene, ZGT – zygotene, TzP – transition to pachytene, PCH – pachytene zones of the gonad.

(D) LG V synapsis quantification by zone. Graph shows percent distribution of categories of 5S rDNA FISH and SYP-1 signals in each of the corresponding zones of the gonad. Scoring was performed in the same manner as panel D. N = 10 gonads.

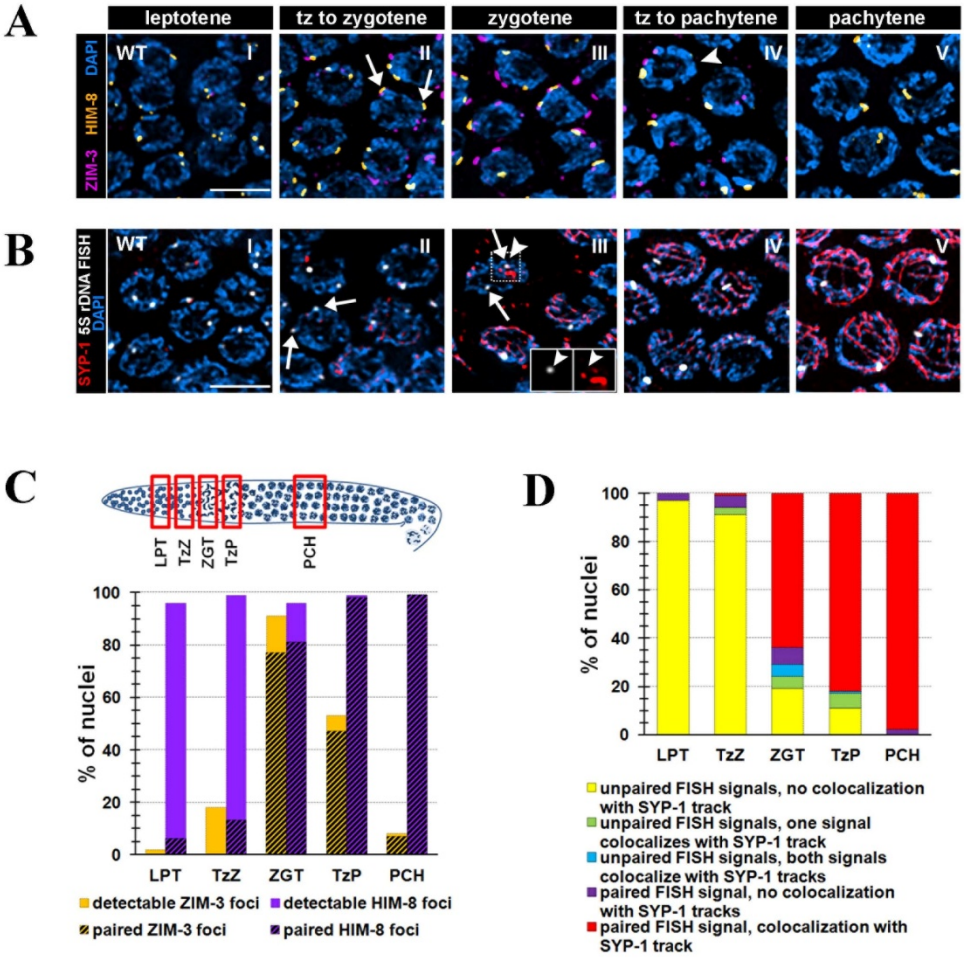
A
leptotene
tz to zygotene
zygotene
tz to pachytene
pachytene
DAPI
HIM-8
ZIM-3
WT
I
II
III
IV
V
B
SYP-1
5S rDNA FISH
DAPI
C
LPT
TzZ
ZGT
TzP
PCH
% of nuclei
detectable ZIM-3 foci
detectable HIM-8 foci
paired ZIM-3 foci
paired HIM-8 foci
D
unpaired FISH signals, no colocalization with SYP-1 track
unpaired FISH signals, one signal colocalizes with SYP-1 track
unpaired FISH signals, both signals colocalize with SYP-1 tracks
paired FISH signal, no colocalization with SYP-1 tracks
paired FISH signal, colocalization with SYP-1 track

Figure 19. H3K9me2 dynamics is linked to SC assembly in WT prophase I.

H3K9me2 dynamics and SC assembly in meiotic zones. Green – anti-H3K9me2, Red – anti-SYP-1 antibodies, Blue – DAPI. Arrows point to zygotene zone nuclei where SYP-1 signals colocalize with chromatin, yet do not form tracks, and bright H3K9me2 foci are abundant. Arrowhead indicates a nucleus in the same zone with established SYP-1 tracks with decreased H3K9me2 foci and intensity. Scale bar, 5 µm.

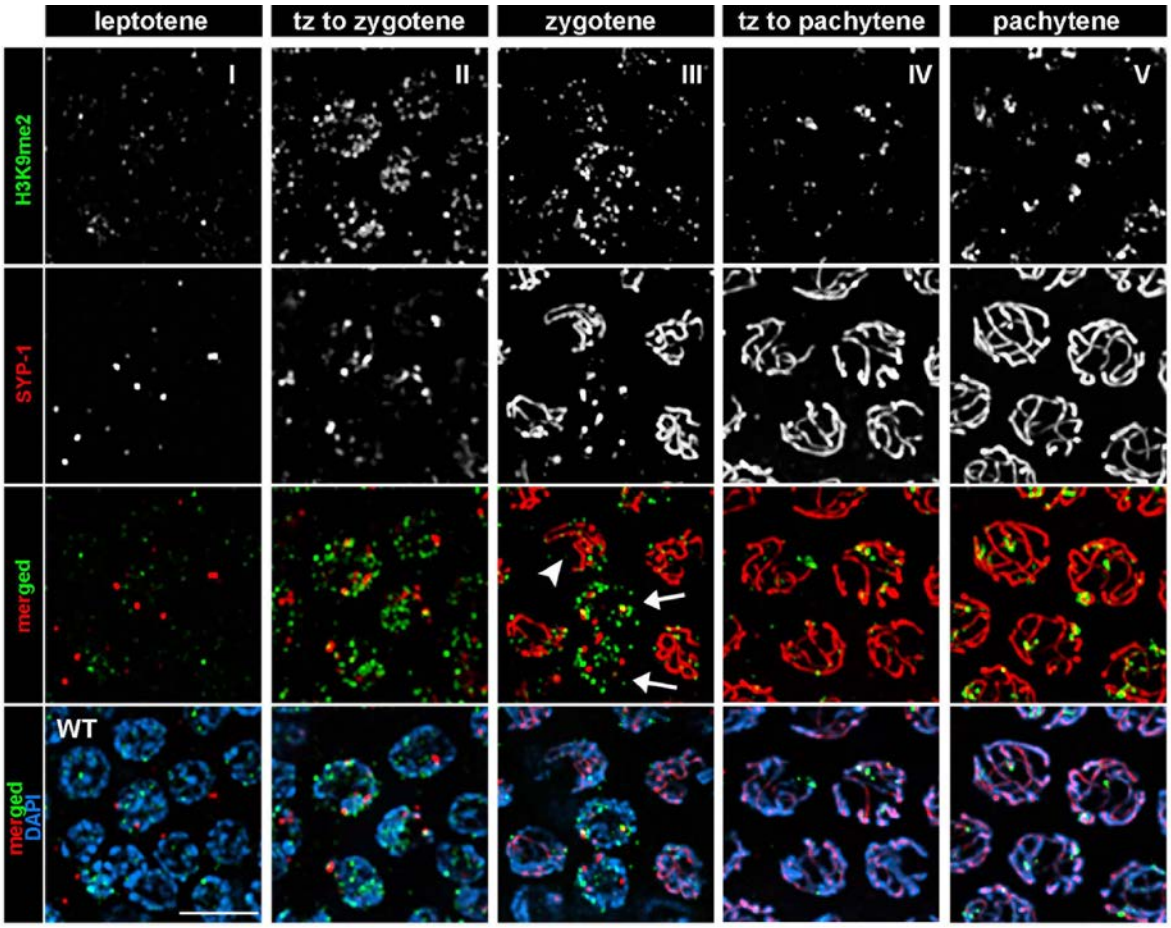
leptotene
tz to zygotene
zygotene
tz to pachytene
pachytene
I
II
III
IV
V
H3K9me2
SYP-1
merged
WT
merged
DAPI

Figure 20. Quantification of the pairing and alignment dynamics of homologs during limited asynapsis in prophase I.

(A) Quantification of the pairing status of chromosomes in *zim-2(tm574)* gonads, represented as on Figure 18C.

(B) Quantification of the synapsis status of chromosome V in *zim-2(tm574)* gonads, represented as on Figure 18D.

(C) Quantification of the pairing status of chromosomes in the gonads of wild-type animals subjected to weak *syp-2* RNAi, represented as on Figure 18C.

(D) Quantification of the synapsis status of chromosome V in weak *syp-2* RNAi animals represented as on Figure 18D.

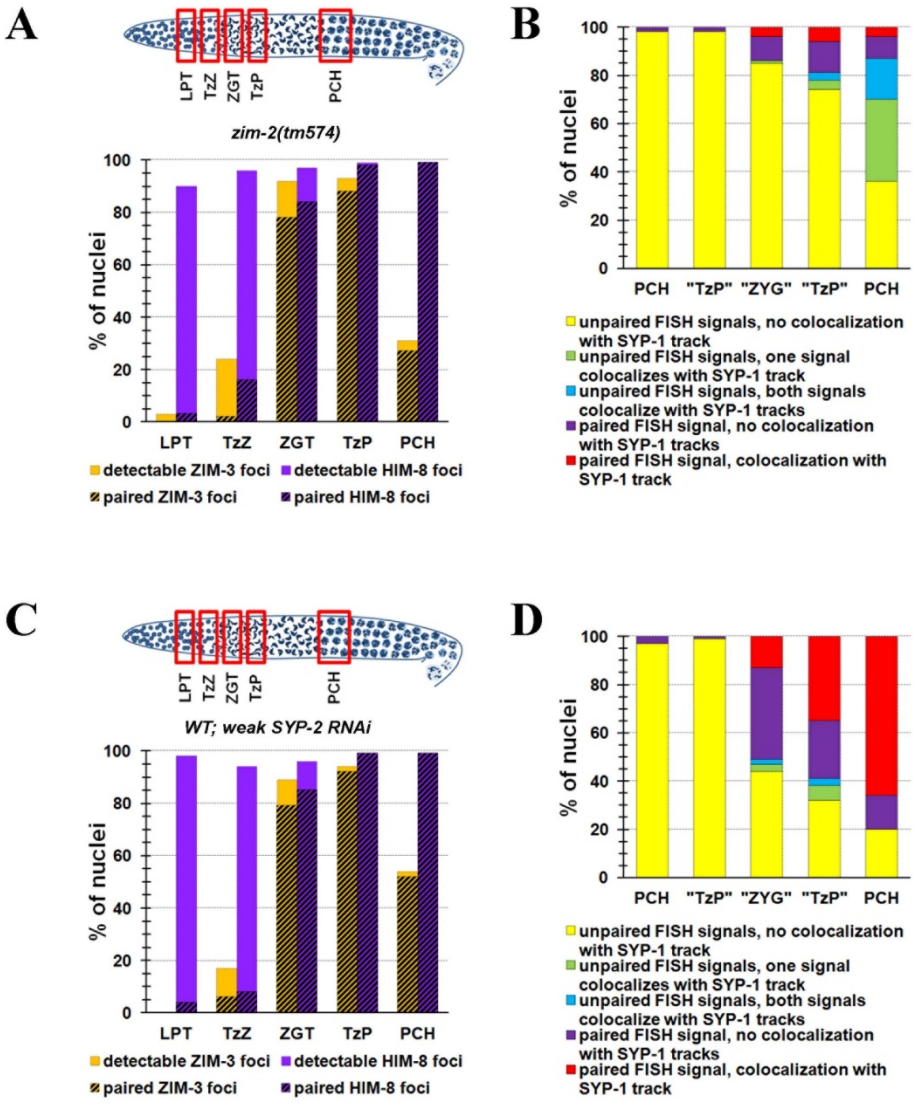
A
LPT
TzZ
ZGT
TzP
PCH
zim-2(tm574)
% of nuclei
100
80
60
40
20
0
LPT
TzZ
ZGT
TzP
PCH
detectable ZIM-3 foci
detectable HIM-8 foci
paired ZIM-3 foci
paired HIM-8 foci
B
% of nuclei
PCH
"TzP"
"ZYG"
"TzP"
PCH
unpaired FISH signals, no colocalization with SYP-1 track
unpaired FISH signals, one signal colocalizes with SYP-1 track
unpaired FISH signals, both signals colocalize with SYP-1 tracks
paired FISH signal, no colocalization with SYP-1 tracks
paired FISH signal, colocalization with SYP-1 track
C
WT; weak SYP-2 RNAi
D

Figure 21. Limited asynapsis due to a pairing defect leads to persistence of heterochromatic domains from early stages of prophase I to pachytene.

H3K9me2 dynamics in relation to the stages of the assembly of central elements of SC in *zim-2(tm574)* gonad. Arrows point to chromosomes that lack SYP-1 tracks and exhibit bright H3K9me2 foci in nuclei transitioning to pachytene. Arrowheads indicate univalents in pachytene zone that exhibit bright H3K9me2 signal along their length yet also have SYP-1 tracks. Features are indicated as on Figure 19.

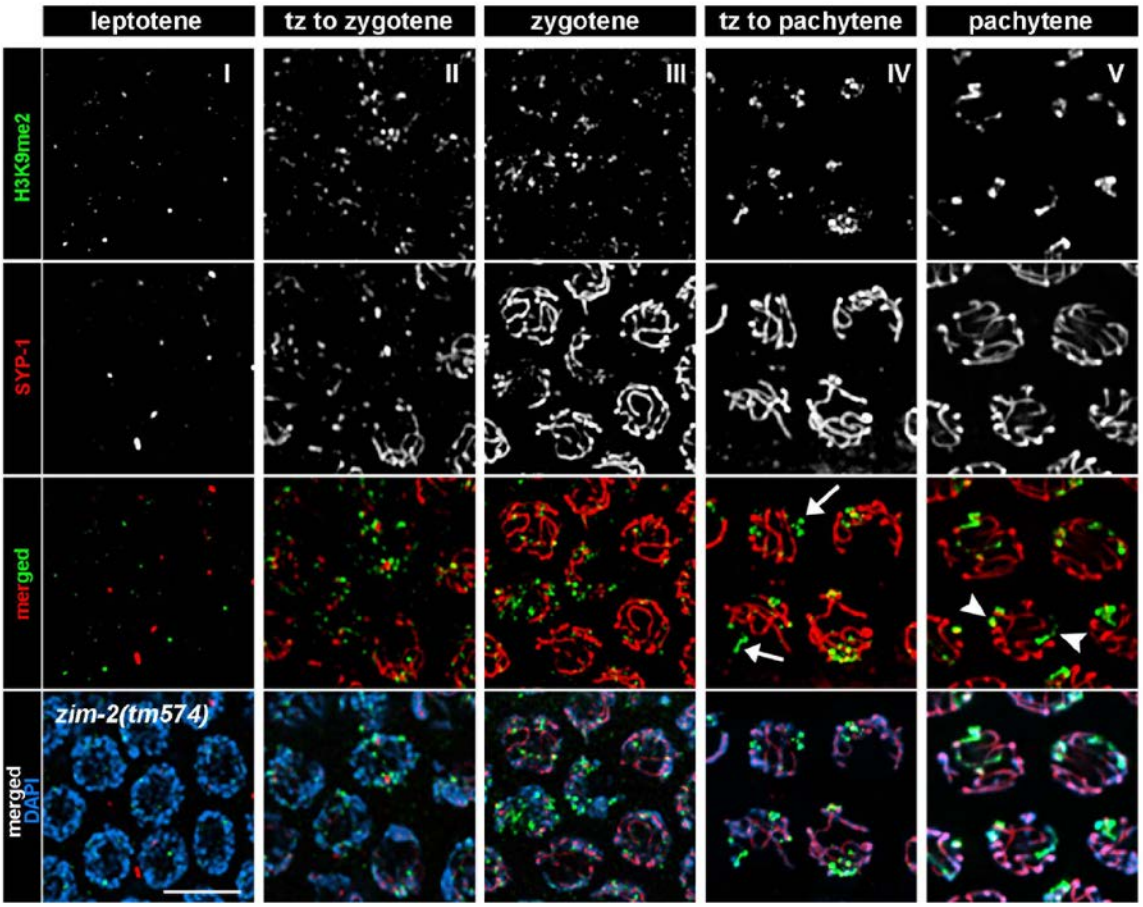
leptotene
tz to zygotene
zygotene
tz to pachytene
pachytene
I
II
III
IV
V
H3K9me2
SYP-1
merged
merged
DAPI
zim-2(tm574)

Figure 22. Limited asynapsis due to reduced levels of SC also leads to persistence of heterochromatic domains from early stages of prophase I to pachytene.

H3K9me2 and SC assembly dynamics in weak *syp-2* RNAi animals. Arrows point to chromatin enriched for H3K9me2 and lacking SYP-1 tracks in transition to or in pachytene zone nuclei of the gonad. Arrowhead indicates chromatin that has a thick SYP-1 track and is devoid of H3K9me2 signal. The inset shows a region of chromosome where chromatin with assembled short SYP-1 tracks is interspersed with chromatin enriched for H3K9me2 signal. Features are indicated as on Figure 19.

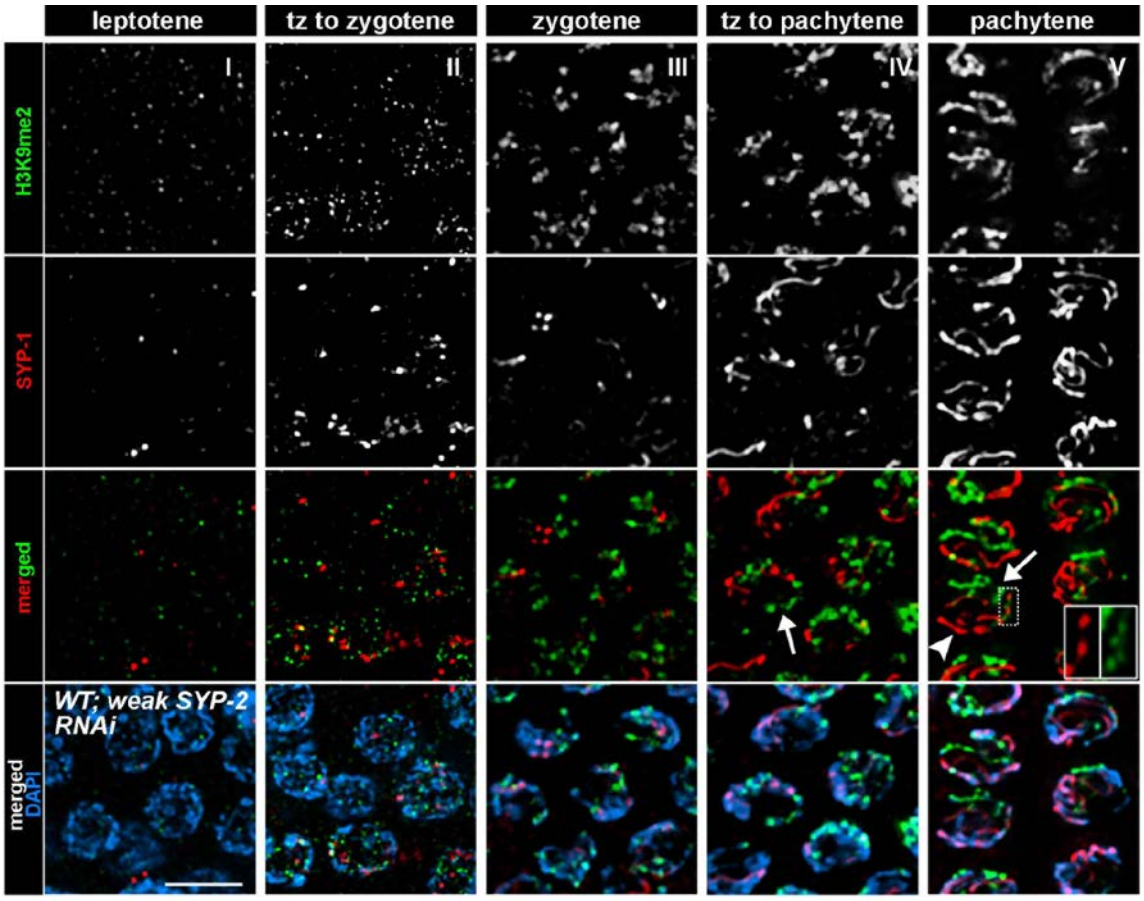
leptotene
tz to zygotene
zygotene
tz to pachytene
pachytene
I
II
III
IV
V
H3K9me2
SYP-1
merged
merged
DAPI
WT; weak SYP-2 RNAi

Figure 23. Quantification of the pairing and alignment dynamics of homologs during extensive asynapsis in prophase I.

(A) Quantification of the pairing status in strong *syp-2* RNAi animals, represented as in Figure 18C.

(B) Quantification of the synapsis status of chromosome V in strong *syp-2* RNAi animals, represented as on Figure 18D.

(C) Quantification of the pairing status of chromosomes in *zim-2(tm574)* mutant animals subjected to strong *syp-2* RNAi, represented as on Figure 18C.

(D) Quantification of LG V synapsis in *zim-2(tm574)* mutant animals subjected to strong *syp-2* RNAi, represented as on Figure 18D.

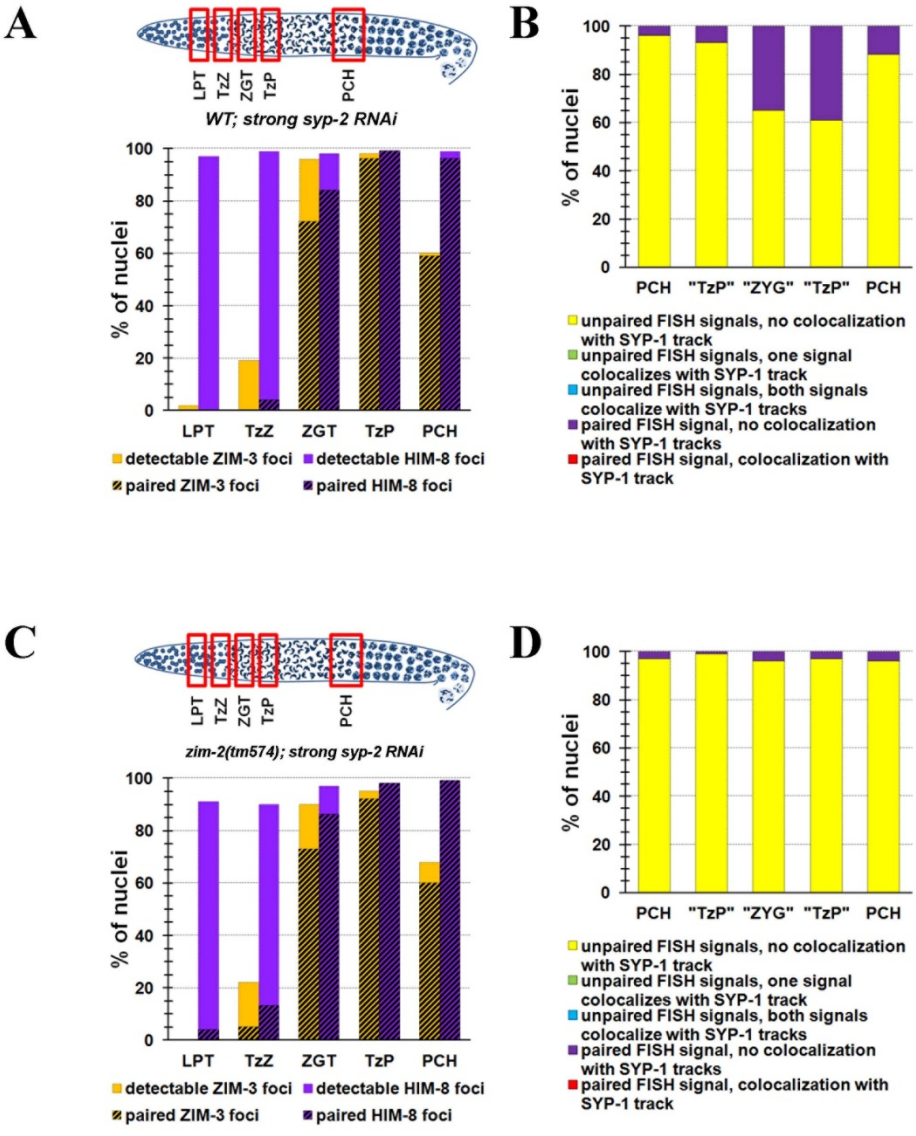
A
LPT
TzZ
ZGT
TzP
PCH
WT; strong syp-2 RNAi
% of nuclei
100
80
60
40
20
0
LPT
TzZ
ZGT
TzP
PCH
detectable ZIM-3 foci
detectable HIM-8 foci
paired ZIM-3 foci
paired HIM-8 foci
B
% of nuclei
PCH
"TzP"
"ZYG"
"TzP"
PCH
unpaired FISH signals, no colocalization with SYP-1 track
unpaired FISH signals, one signal colocalizes with SYP-1 track
unpaired FISH signals, both signals colocalize with SYP-1 tracks
paired FISH signal, no colocalization with SYP-1 tracks
paired FISH signal, colocalization with SYP-1 track
C
zim-2(tm574); strong syp-2 RNAi
D

Figure 24. SC-dependent chromatin reorganization at the onset of meiosis is required for establishment of heterochromatic domains.

Dynamics of H3K9me2 and SC central region assembly in strong *syp-2* RNAi animals. Features are indicated as in Figure 19.

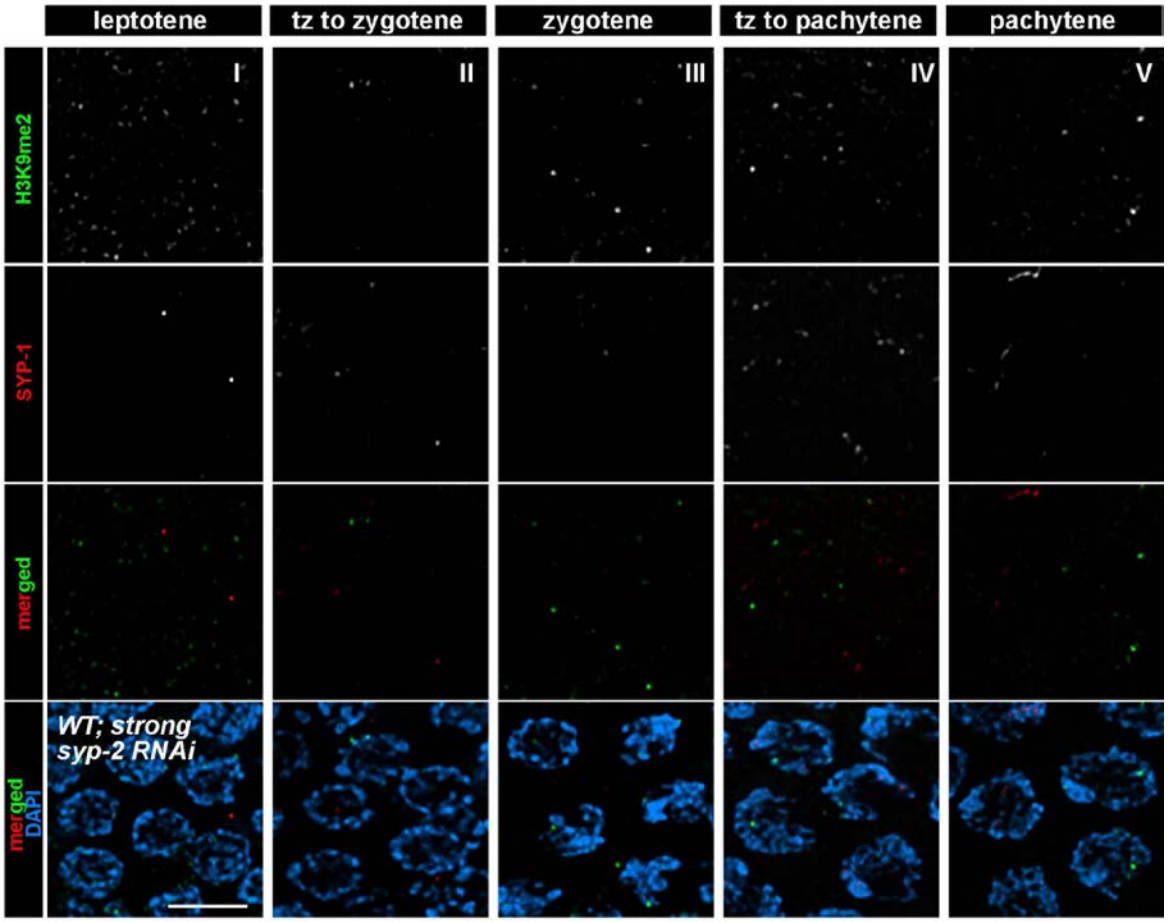
leptotene
tz to zygotene
zygotene
tz to pachytene
pachytene
I
II
III
IV
V
H3K9me2
SYP-1
merged
merged DAPI
WT; strong syp-2 RNAi

Figure 25. Failure to establish heterochromatic domains at the onset of meiosis leads to their disappearance on univalents in pachytene.

Dynamics of H3K9me2 and SC central region assembly in *zim-2(tm574)* mutant animals subjected to strong *syp-2* RNAi. Features are indicated as on Figure 19. Scale bar, 5 μm.

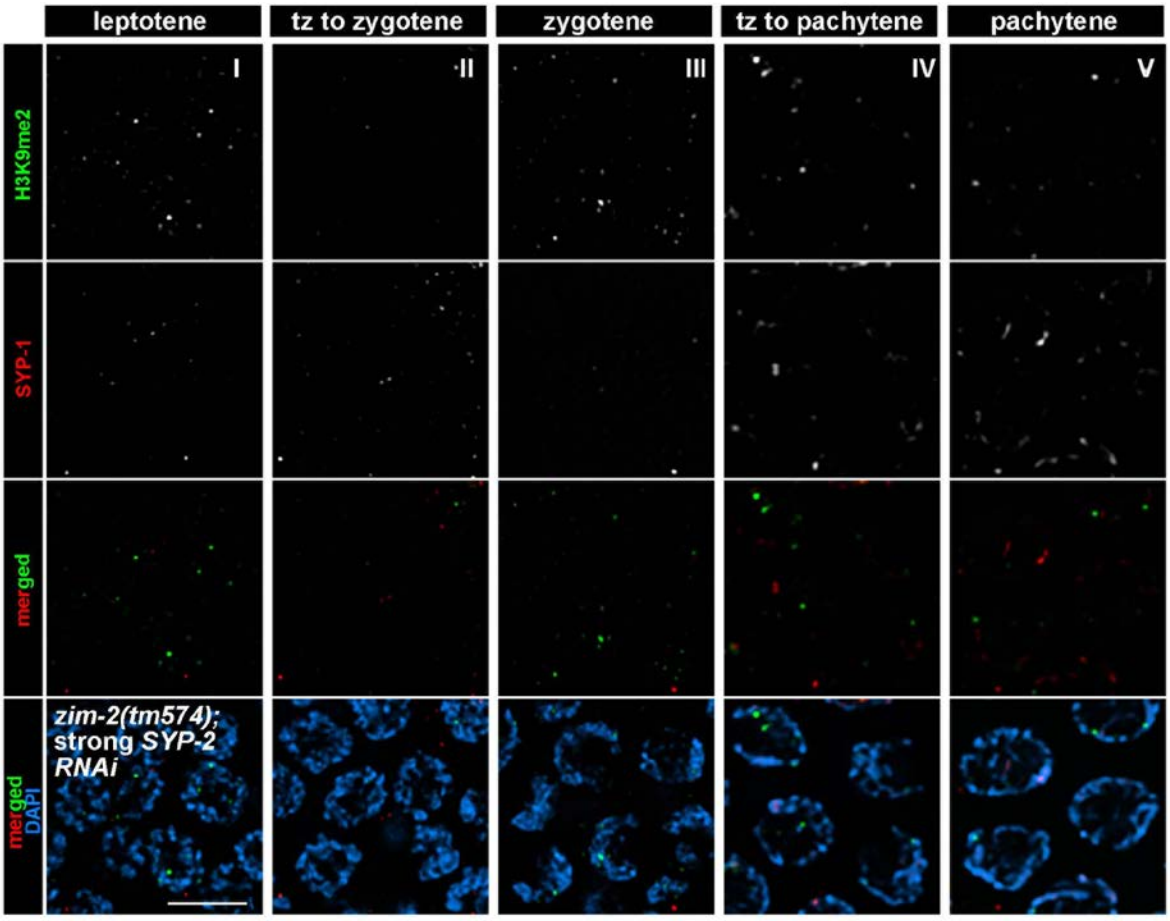
leptotene
tz to zygotene
zygotene
tz to pachytene
pachytene
I
II
III
IV
V
H3K9me2
SYP-1
merged
merged DAPI
zim-2(tm574);
strong SYP-2
RNAi

Figure 26. Quantification of DAPI-stained bivalents/univalents in diakinesis nuclei of wild-type and mutant gonads.

(A) Maximum-intensity projection images of representative nuclei with DAPI-stained chromosomes from wild-type gonads, subjected to different degrees of *syp-2* RNAi. Number of DAPI-stained bodies is indicated in the top left corner of the image, while average percent of this class of nuclei in a population is indicated in the top right corner of the image. At least 10 gonads were scored for each experimental condition.

(B) Maximum-intensity projection images of representative nuclei with DAPI-stained chromosomes from *zim-2(tm574)* gonads, subjected to *syp-2* RNAi. Number of DAPI-stained bodies is indicated in the top left corner of the image, while average percent of this class of nuclei in a population is indicated in the top right corner of the image. At least 10 gonads were scored for each experimental condition.

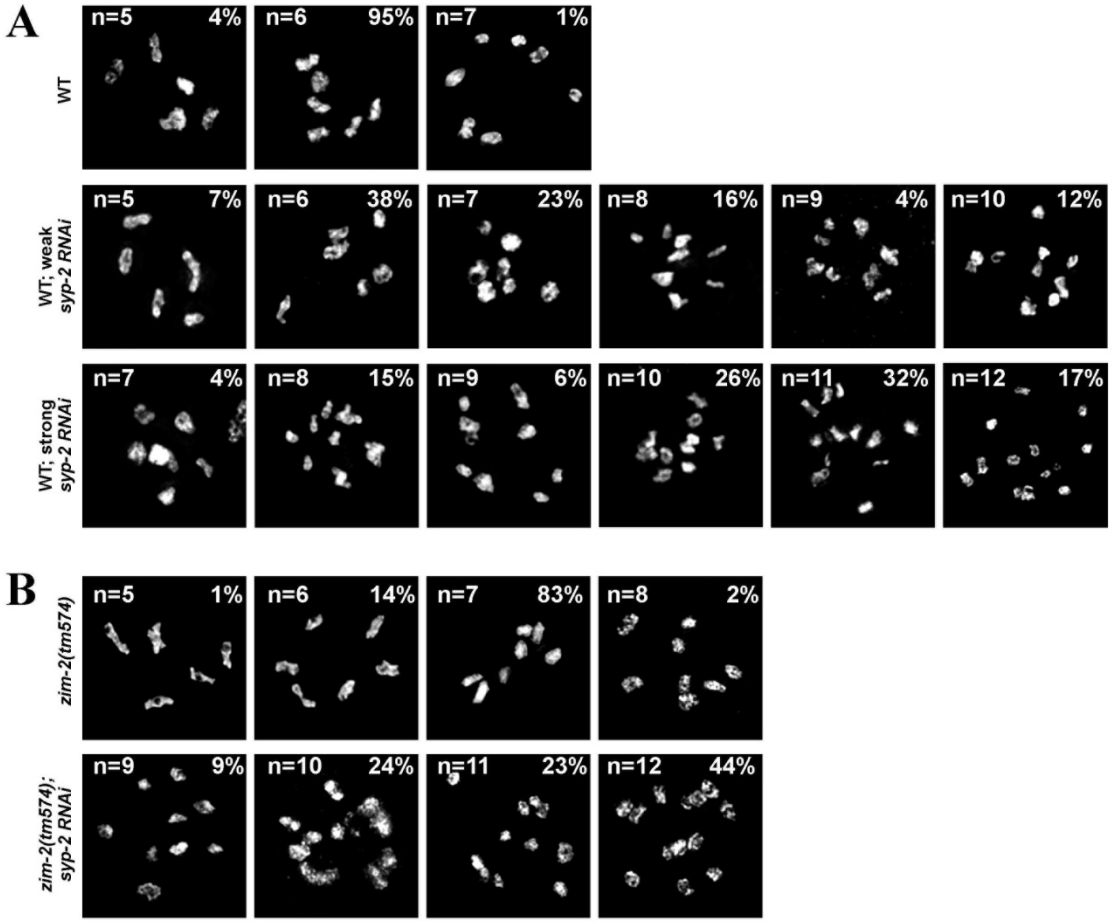
A
WT
n=5 4%
n=6 95%
n=7 1%
WT; weak syp-2 RNAi
n=5 7%
n=6 38%
n=7 23%
n=8 16%
n=9 4%
n=10 12%
WT; strong syp-2 RNAi
n=7 4%
n=8 15%
n=9 6%
n=10 26%
n=11 32%
n=12 17%
B
zim-2(tm574)
n=5 1%
n=6 14%
n=7 83%
n=8 2%
zim-2(tm574); syp-2 RNAi
n=9 9%
n=10 24%
n=11 23%
n=12 44%

Figure 27. Extensive asynapsis, caused by depletion of the axial component of SC, leads to disappearance of heterochromatic domains from univalents.

(A) High-resolution maximum-intensity projection images of pachytene nuclei of wild type and *zim-2(tm574)* gonads, subjected to *him-3* RNAi. Nuclei were stained with anti-H3K9me2 (green) and anti-SYP-1 antibodies (red). DNA is visualized with DAPI (blue). Scale bar, 5 μm.

(B) Maximum-intensity projection images of representative nuclei with DAPI-stained chromosomes from wild type and *zim-2(tm574)* gonads, subjected to *him-3* RNAi.

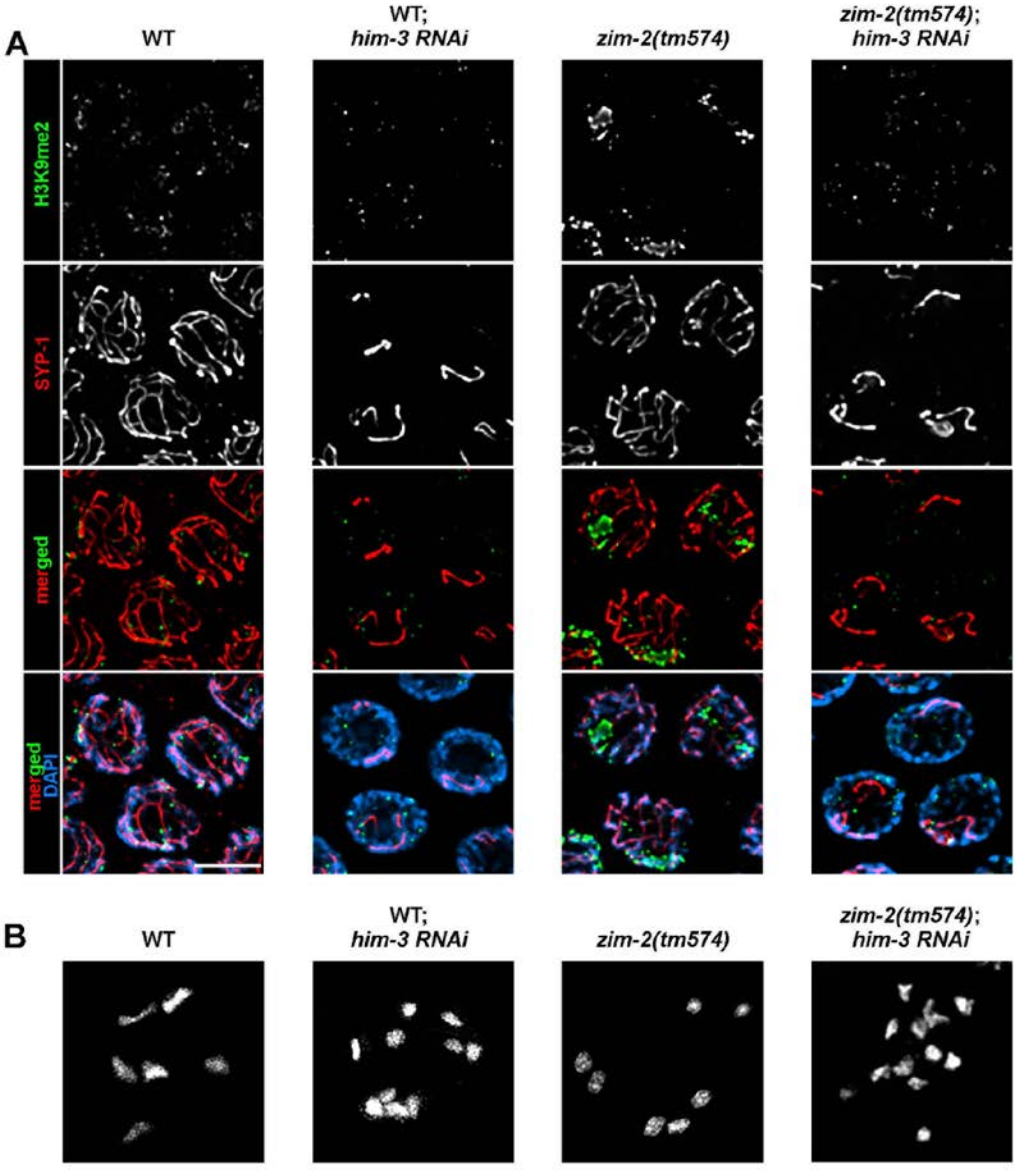
A
WT
WT;
him-3 RNAi
zim-2(tm574)
zim-2(tm574);
him-3 RNAi
H3K9me2
SYP-1
merged
merged
DAPI
B
WT
WT;
him-3 RNAi
zim-2(tm574)
zim-2(tm574);
him-3 RNAi

Figure 28. Quantification of the alignment dynamics of homologs during extensive non-homologous synapsis in prophase I.

(A) Quantification of the synapsis status of chromosome V in the ieDf2 strain, represented as on Figure 18D.

(B) Quantification of LG V synapsis in the ieDf2 strain subjected to strong *syp-2* RNAi, represented as on Figure 18D.

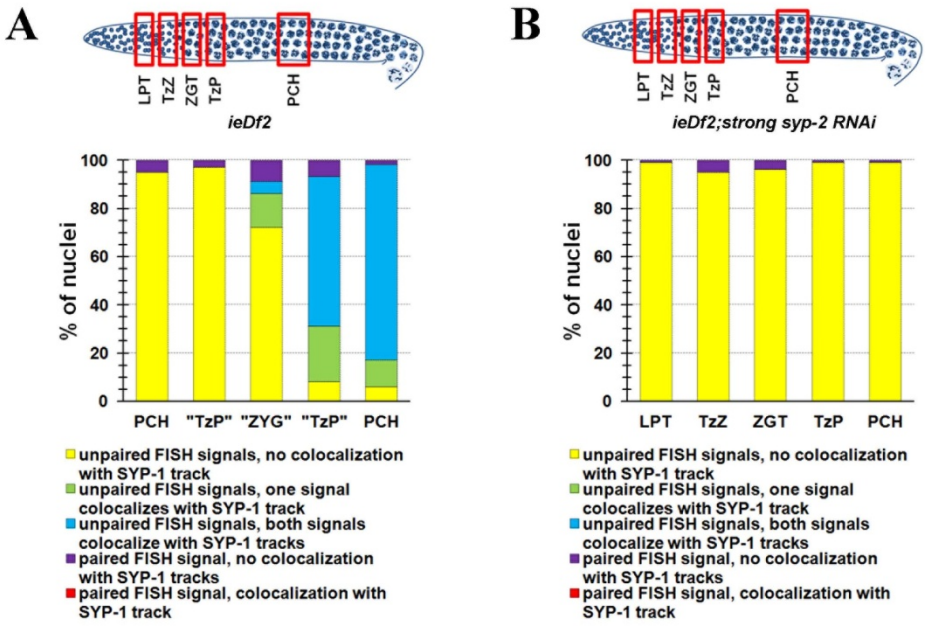
A
LPT
TzZ
ZGT
TzP
PCH
ieDf2
100
80
60
40
20
0
% of nuclei
PCH
"TzP"
"ZYG"
"TzP"
PCH
unpaired FISH signals, no colocalization with SYP-1 track
unpaired FISH signals, one signal colocalizes with SYP-1 track
unpaired FISH signals, both signals colocalize with SYP-1 tracks
paired FISH signal, no colocalization with SYP-1 tracks
paired FISH signal, colocalization with SYP-1 track
B
LPT
TzZ
ZGT
TzP
PCH
ieDf2;strong syp-2 RNAi
100
80
60
40
20
0
% of nuclei
LPT
TzZ
ZGT
TzP
PCH
unpaired FISH signals, no colocalization with SYP-1 track
unpaired FISH signals, one signal colocalizes with SYP-1 track
unpaired FISH signals, both signals colocalize with SYP-1 tracks
paired FISH signal, no colocalization with SYP-1 tracks
paired FISH signal, colocalization with SYP-1 track

Figure 29. Assembly of SC between non-homologs in early prophase I leads to disappearance of heterochromatic domains.

Dynamics of H3K9me2 and SC central region assembly in the *ieDf2* strain. Features are indicated as on Figure 19.

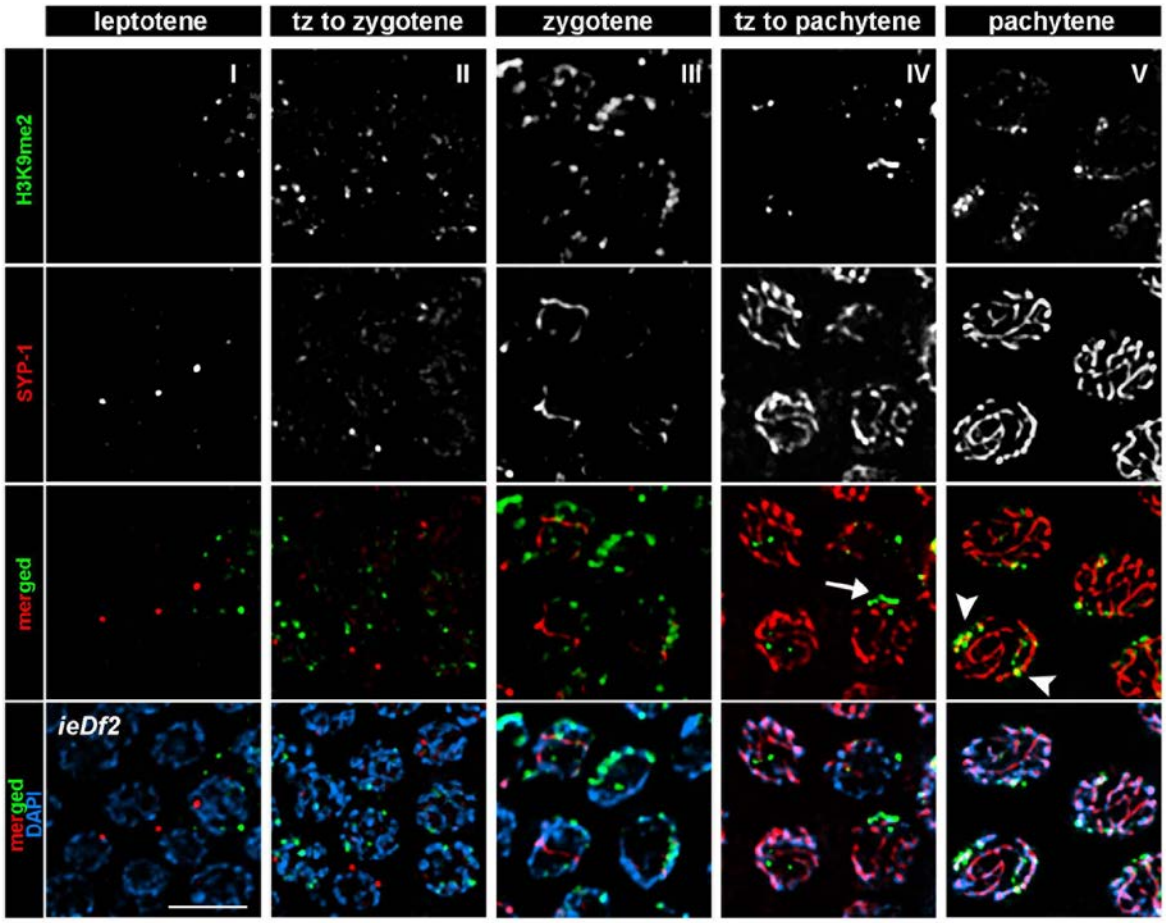
leptotene
tz to zygotene
zygotene
tz to pachytene
pachytene
I
II
III
IV
V
H3K9me2
SYP-1
merged
merged
DAPI
ieDf2

Figure 30. Remaining heterochromatic domains in a mutant with non-homologous synapsis disappear in the complete absence of central region components of SC.

H3K9me2 and SC central element assembly dynamics in the *ieDf2* strain subjected to strong *syp-2* RNAi. Features are indicated as on Figure 19.

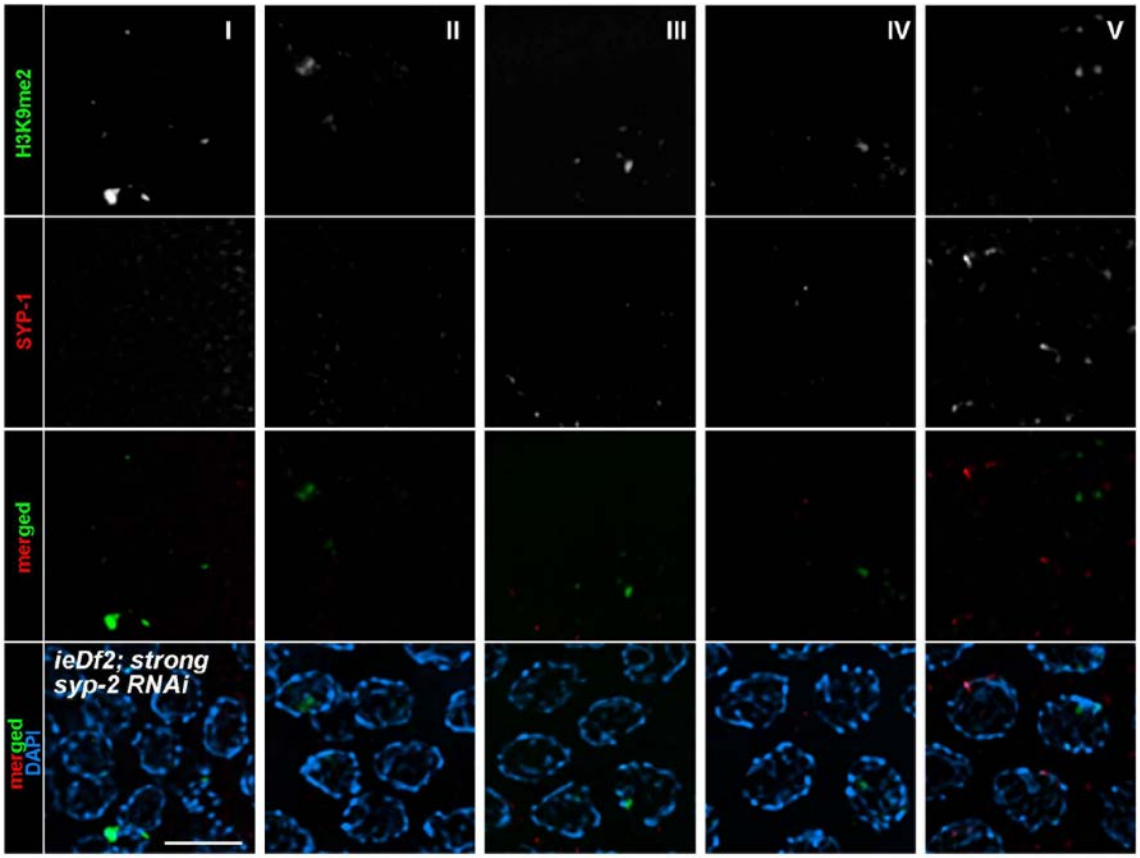
I
II
III
IV
V
H3K9me2
SYP-1
merged
merged
DAPI
ieDf2; strong
syp-2 RNAi

Figure 31. Severe depletion of the levels of central region components of SC in *sun-1(jf18)* mutant also leads to disappearance of heterochromatic domains from univalents.

High-resolution maximum-intensity projection images of pachytene nuclei of *sun-1(jf18)* gonads, subjected to *syp-2* RNAi. Nuclei were stained with anti-H3K9me2 (green) and anti-SYP-1 antibodies (red). DNA is visualized with DAPI (blue). Scale bar, 5 μm.

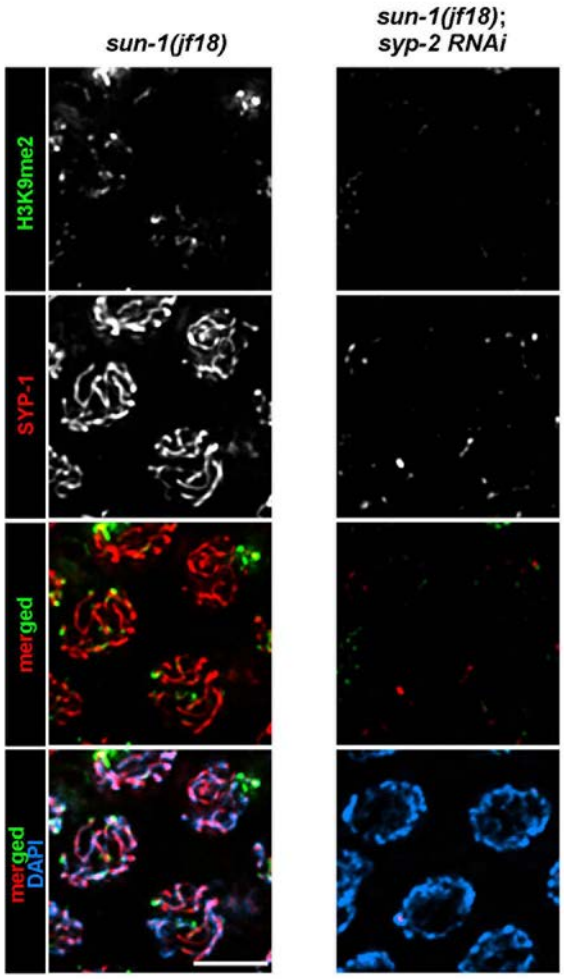
sun-1(jf18)
sun-1(jf18);
syp-2 RNAi
H3K9me2
SYP-1
merged
merged
DAPI

Figure 32. Dynein is required for the assembly of central elements of SC on univalents.

Dynamics of SC assembly in *C. elegans* gonads from adult wild-type animals grown at 16°C and 25°C on an empty RNAi vector, and *dlc-1 RNAi* gonads from animals subjected to 25°C for 12 hours and allowed to recover at 16°C for indicated periods of time. Gonads are shown as maximum-intensity projection image of the nuclei, demonstrating central elements of SC visualized with anti-SYP-1 antibodies (red) and DNA visualized with DAPI (blue). Insets show DAPI-stained diakinesis nuclei of the corresponding gonad. Graph depicts quantification of the number of nuclei with SYP-1 aggregates in each *dlc-1 RNAi* condition. Scale bar, 30 µm.

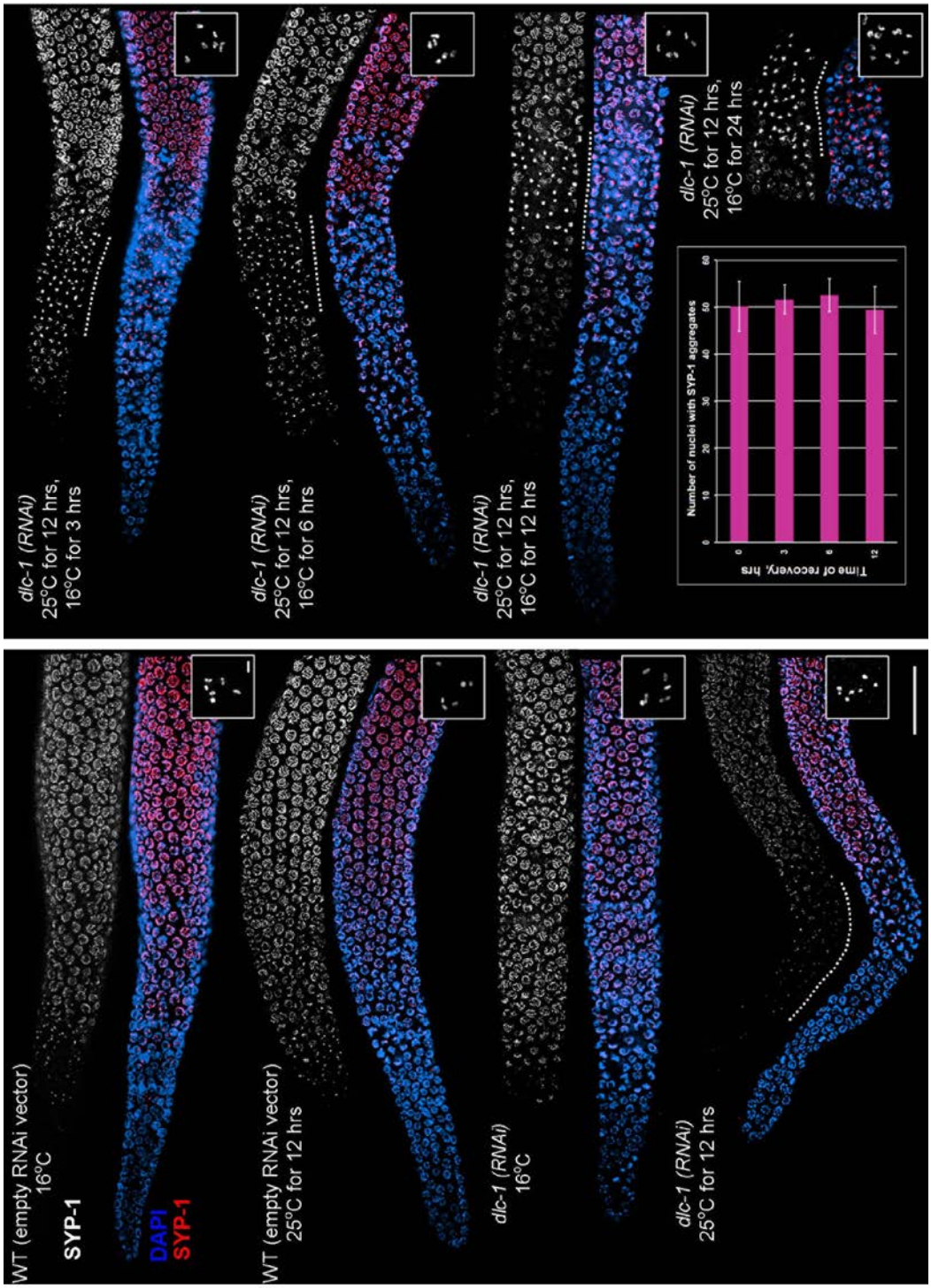
WT (empty RNAi vector)
16°C
SYP-1
DAPI
SYP-1
WT (empty RNAi vector)
25°C for 12 hrs
dlc-1 (RNAi)
16°C
dlc-1 (RNAi)
25°C for 12 hrs
dlc-1 (RNAi)
25°C for 12 hrs,
16°C for 3 hrs
dlc-1 (RNAi)
25°C for 12 hrs,
16°C for 6 hrs
dlc-1 (RNAi)
25°C for 12 hrs,
16°C for 12 hrs
dlc-1 (RNAi)
25°C for 12 hrs,
16°C for 24 hrs
Number of nuclei with SYP-1 aggregates
Time of recovery, hrs
0
10
20
30
40
50
60
0
3
6
12

Figure 33. Dynein promotes initial stages of SC assembly.

(A) Example of the distribution of nuclei at different stages of SYP-1 assembly in the region immediately proximal to the nuclei with SYP- aggregates in *dlc-1* RNAi gonads. (Top panel) Schematic diagram of the gonad with regions shown on the panels highlighted by the red boxes. (Medium panel) Maximum-intensity projection images of SYP-1 states in the regions of the gonad, shown on the top panel. SYP-1 is visualized with anti-SYP-1 antibody and colored according to the categories of SYP-1 states designated on panel C. (Bottom panel) Maximum-intensity projection images of nuclei from the same regions of the gonads, SYP-1 is shown in red, DAPI-stained DNA is show in blue. Scale bar, 5 μm.

(B) Quantification of the categories of SYP-1 states, scored in the region immediately proximal to the nuclei with SYP-1 aggregates in *dlc-1 RNAi* animals and in the corresponding region in the gonads of the control animals. A total of ten gonads were scored.

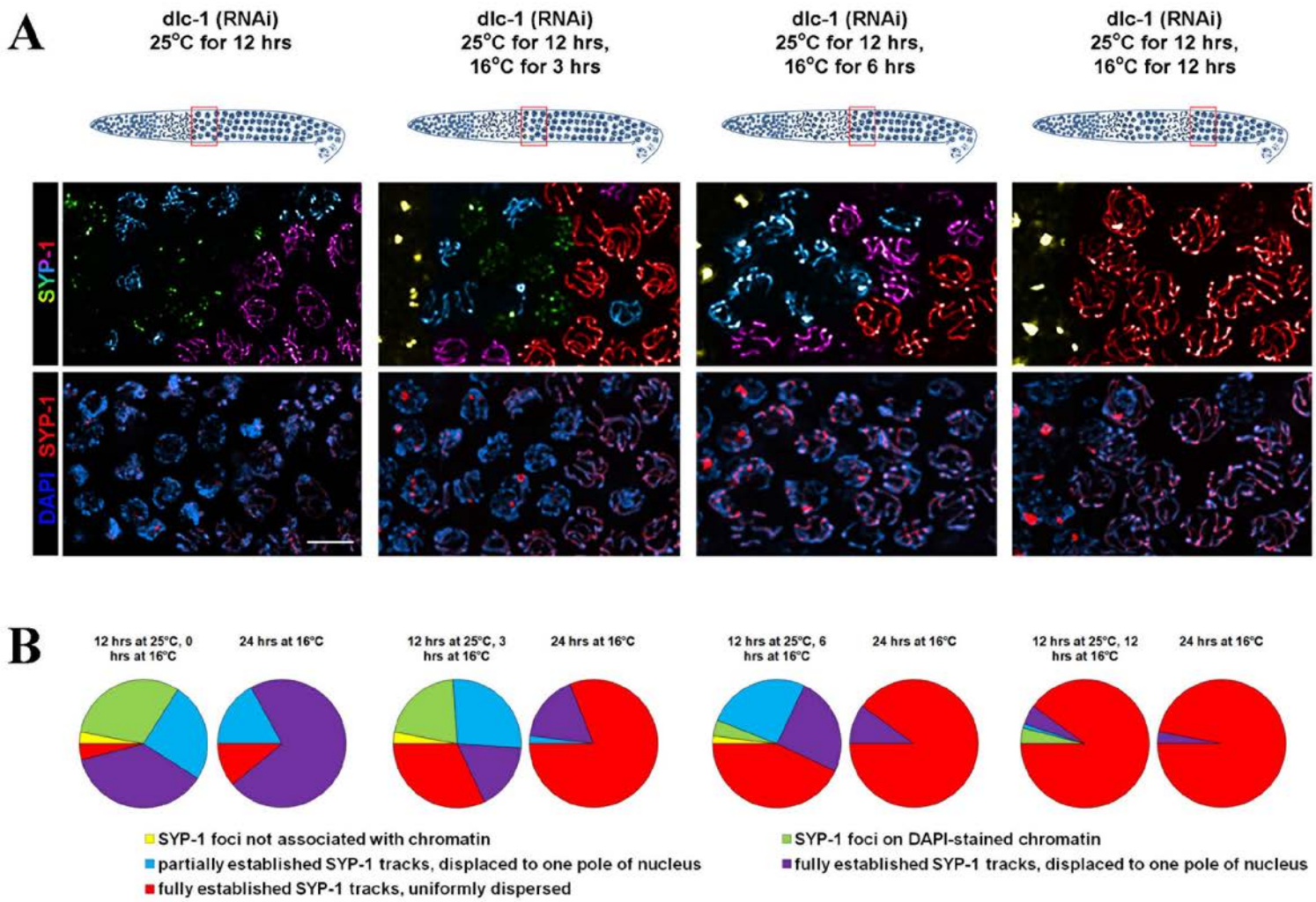
A
dlc-1 (RNAi)
25°C for 12 hrs
dlc-1 (RNAi)
25°C for 12 hrs,
16°C for 3 hrs
dlc-1 (RNAi)
25°C for 12 hrs,
16°C for 6 hrs
dlc-1 (RNAi)
25°C for 12 hrs,
16°C for 12 hrs
SYP-1
DAPI SYP-1
B
12 hrs at 25°C, 0 hrs at 16°C
24 hrs at 16°C
12 hrs at 25°C, 3 hrs at 16°C
24 hrs at 16°C
12 hrs at 25°C, 6 hrs at 16°C
24 hrs at 16°C
12 hrs at 25°C, 12 hrs at 16°C
24 hrs at 16°C
SYP-1 foci not associated with chromatin
SYP-1 foci on DAPI-stained chromatin
partially established SYP-1 tracks, displaced to one pole of nucleus
fully established SYP-1 tracks, displaced to one pole of nucleus
fully established SYP-1 tracks, uniformly dispersed

Figure 34. Quantification of the pairing and alignment dynamics of homologs upon dynein depletion in prophase I.

(A) Quantification of the pairing status of chromosomes in the gonads of *dlc-1 RNAi* animals subjected to 25°C for 12 hours and recovered at 16°C for 12 hours, represented as on Figure 18C.

(B) Quantification of the synapsis status of chromosome V in the gonads of *dlc-1 RNAi* animals subjected to 25°C for 12 hours and recovered at 16°C for 12 hour, represented as on Figure 18D.

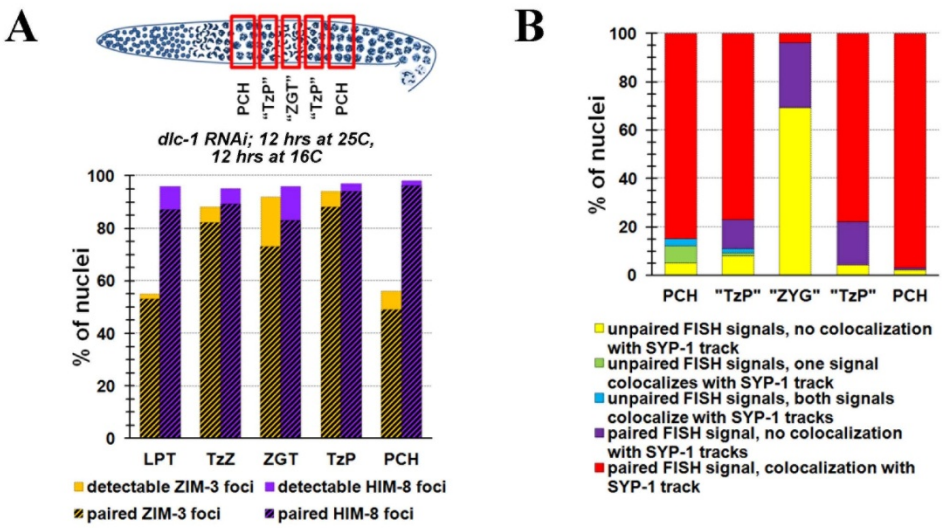
A
PCH
"TzP"
"ZGT"
"TzP"
PCH
dlc-1 RNAi; 12 hrs at 25C,
12 hrs at 16C
% of nuclei
100
80
60
40
20
0
LPT
TzZ
ZGT
TzP
PCH
detectable ZIM-3 foci
detectable HIM-8 foci
paired ZIM-3 foci
paired HIM-8 foci
B
% of nuclei
100
80
60
40
20
0
PCH
"TzP"
"ZYG"
"TzP"
PCH
unpaired FISH signals, no colocalization with SYP-1 track
unpaired FISH signals, one signal colocalizes with SYP-1 track
unpaired FISH signals, both signals colocalize with SYP-1 tracks
paired FISH signal, no colocalization with SYP-1 tracks
paired FISH signal, colocalization with SYP-1 track

Figure 35. SC-dependent dynamics of heterochromatic domains can be uncoupled from other chromatin reorganization events.

H3K9me2 dynamics in relation to the stages of the assembly of central elements of SC in the gonads of *dlc-1 RNAi* animals subjected to 25°C for 12 hours and recovered at 16°C for 12 hours. Arrows point to nuclei that exhibit association of SYP-1 foci with chromatin and elevated levels of H3K9me2 signal. Features are indicated as on Figure 19.

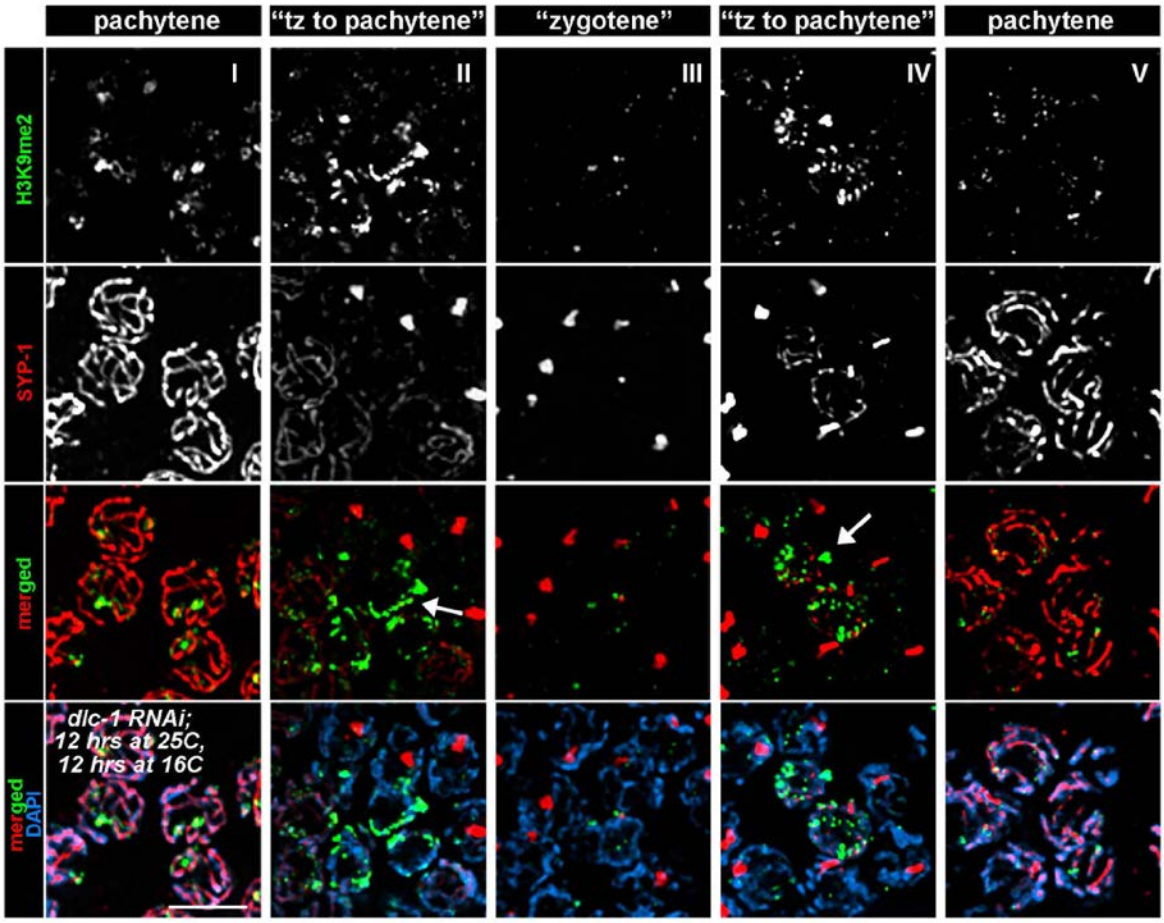
pachytene
"tz to pachytene"
"zygotene"
"tz to pachytene"
pachytene
I
II
III
IV
V
H3K9me2
SYP-1
merged
dlc-1 RNAi;
12 hrs at 25C,
12 hrs at 16C
merged
DAPI

Figure 36. Model of the effects of SYP-1 assembly on the dynamics of H3K9me2-enriched regions of chromatin.

Initiation of SYP-1 assembly on chromosome upon establishment of the connection with microtubules leads to formation of H3K9me2-enriched compartments of chromatin. Dynein-mediated movement promotes juxtaposition of homolog interfaces, stabilized by interactions of central region components of SC. Continuation of SC polymerization leads to sequestration of H3K9me2-enriched interfaces of homologs.

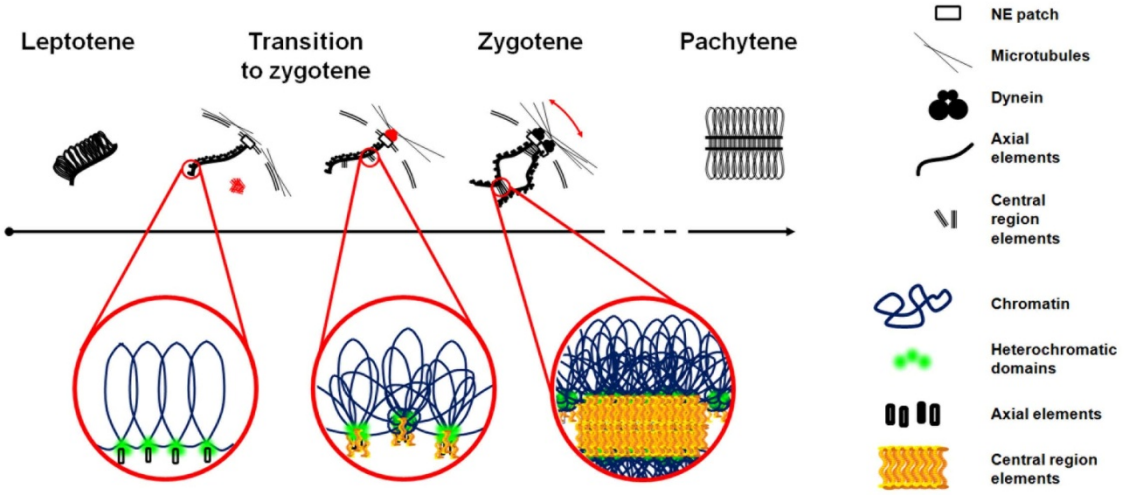
Leptotene
Transition to zygotene
Zygotene
Pachytene
NE patch
Microtubules
Dynein
Axial elements
Central region elements
Chromatin
Heterochromatic domains
Axial elements
Central region elements

CHAPTER 4

SEX-SPECIFIC DIFFERENCES IN HETEROCHROMATIN DYNAMICS IN PROPHASE I OF *C. ELEGANS*

4.1 Introduction

Comparative studies of meiosis progression during oogenesis and spermatogenesis in mammals reveal fundamental differences in several aspects of these processes. First, they are different in the timing of occurrence. While oocytes complete prophase I during foetal development and arrest until female sexual maturation, spermatogenesis is a postnatal process (Handel and Eppig, 1998). Second, oocytes undergo two stages where they arrest their development – upon completion of prophase I and in metaphase II, – while spermatocytes do not arrest at all (Morelli and Cohen, 2005). Third, the success rates of meiosis are different in males and females. This difference is especially dramatic in humans, with almost 25% of oocytes exhibiting aneuploidy (Hassold and Hunt, 2001). Such dimorphism appears to be related to different levels of quality control of the meiotic processes. In males, defective synapsis or recombination of homologs result in complete abrogation of spermatogenesis, causing apoptosis of pachytene nuclei, and eventually leading to infertility. In females, the same defects result in a range of fertility defects from subfertility, in which the number of oocytes is reduced, to complete sterility, in which follicles are completely absent (Cohen et al., 2006).

Reasons underlying the difference in the levels of fidelity of meiotic processes are not yet understood in full detail, but the contribution of mechanisms that differentially regulate homolog juxtaposition in the two sexes during prophase I and at the meiotic spindle has been demonstrated. The SC is twice longer in females than in males, suggesting different degree of chromatin compaction in the two sexes (Bojko, 1983). Traces of SC remain associated with chromosomes untill anaphase II in males, in contrast to a much earlier disappearance of SC in females (Hodges et al., 2001). The pairing and synapsis of homologs also occurs faster in

male meiosis (Roig et al., 2004). Since aneuploidy could also arise from defective placement of recombination events, sex-specific differences in the number and distribution of crossovers could also affect the fidelity of chromosome segregation (Hassold et al., 2000).

While gametogenesis in *C. elegans* is vastly different from the one of mammals in the morphology of ovaries, testes, and gametes themselves, it also exhibits sexual dimorphism. However, these differences are unique in their manifestation to *C. elegans.* First, apoptosis is absent in male meiosis (Gumienny et al., 1999). Therefore, even extensive asynapsis of homologs does not trigger their elimination (Jaramillo-Lambert et al., 2010). The timing of SC disassembly is also different, with females retaining it for a longer period of time upon completion of prophase I (Shakes et al., 2009). Finally, whereas stages in which chromosomes undergo pairing and alignment are extended in males, the overall timing of prophase I in spermatogenesis is half that in oogenesis (Jaramillo-Lambert et al., 2007).

Despite the advances in our understanding of the key differences in regulation of meiotic processes in two sexes, very little is known about any dimorphism in chromatin organization. Here we report that in *C. elegans* male chromosomes are shorter and their unsynapsed chromosomes reveal more pronounced heterochromatic domains, suggesting that meiotic chromosomes architecture could also be different between sexes.

4.2 Results

Appearance of H3K9me2 patterns on aberrant chromatin in prophase I of spermatogenesis differs from the ones of oogenesis

To understand sex-specific effects of defects in homolog pairing and synapsis on heterochromatic regions of the genome, we examined the appearance of H3K9me2 patterns

in adult males from a collection of meiosis mutants. We observed several dramatic differences in the appearance of heterochromatin on aberrant chromosomes in male spermatogenesis versus hermaphrodite oogenesis. Mutations in the axial component in *him-3(gk149)* mutant, which is defective for pairing, synapsis, and segregation of homologs, prevent association of central region components of SC with chromatin at the onset of meiosis. As a result, this mutant fails to establish heterochromatic domains on univalents during oogenesis (see Chapter 3). Consequently, pachytene nuclei in *him-3(gk149)* mutant exhibit small H3K9me2 foci on unpaired/unsynapsed chromosomes (see Figure 12, 14). Contrary to this pattern of H3K9me2 in the adult hermaphrodites, pachytene nuclei from the gonads of *him-3(gk149)* males exhibit pronounced H3K9me2 foci, scattered across the chromatin mass of univalents (Figure 37). Similarly, mutants lacking functional components of CR of the SC also have weak H3K9me2 foci in pachytene nuclei during oogenesis, yet demonstrate bright anti-H3K9me2 staining in some nuclei during spermatogenesis (Figure 37). The most intriguing difference can be observed in the appearance of heterochromatic domains in relation to the topology of pachytene chromosomes. While bright H3K9me2 domains are found on the diffuse chromatin, surrounding the condensed core of meiotic chromosome in *zim-2(tm574)* and *him-3(e1256)* nuclei undergoing oogenesis in adult hermaphrodites (Figure 11, see also (Bean et al., 2004)), H3K9me2 is mainly concentrated at the core of chromosomes in pachytene nuclei undergoing spermatogenesis in males (Figure 37). Taken together, these findings suggest that heterochromatic regions could be subjected to differential regulation during spermatogenesis versus oogenesis of *C. elegans.*

Chromatin is more compact in prophase I of spermatogenesis versus oogenesis

Next we examined whether global differences in chromatin organization between sexes could contribute to dimorphism in the appearance of H3K9me2 patterns. The SC is a major component of the meiotic scaffold and reflects changes to chromatin organization. Therefore, we measured the length of the mature SC in pachytene nuclei undergoing spermatogenesis in adult males and oogenesis in adult hermaphrodites (Figure 38A, B). Since the X chromosome does not assemble SC in males, we identified the X homolog bivalent in hermaphrodites by its more condensed chromatin and eliminated the length of SC of synapsed X bivalent in our measurements (Figure 38A, C). As a result, the total length of the autosomal SCs in pachytene nuclei of hermaphrodite oogenesis was one and a half times longer than in male spermatogenesis (Student t-test, $p<0.05$) (Figure 38D). Our results indicated that similarly to humans, SC length differs between sexes in *C. elegans*.

4.3 Discussion

Our initial comparison of H3K9me2 patterns in pachytene nuclei undergoing oogenesis and spermatogenesis in meiotic mutant revealed sex-specific differences in the intensity of H3K9me2 foci and their distribution on univalents. We have previously shown that components of RNAi machinery regulate appearance of H3K9me2 domains on chromatin in *C. elegans* meiosis (Maine et al., 2005; She et al., 2009). Therefore, one explanation of the observed dimorphism in H3K9me2 patterns could be the difference in the levels of activity of double stranded RNA-processing pathways between sexes. However, both the lone X chromosome during spermatogenesis in WT males and unpaired X chromosomes during oogenesis in *him-8(e1489)* hermaphrodites exhibit similarly bright H3K9me2 staining,

suggesting that the efficiencies of RNAi-dependent establishment of heterochromatin in the germlines of two sexes could be similar.

Next we examined another hypothesis, according to which differences in chromatin architecture contribute to the appearance of heterochromatic domains in two sexes. Our measurements of the length of SC in pachytene nuclei revealed that the average length of the total autosomal complement is 55 μm in oogenesis and 40 μm in spermatogenesis. Our data is consistent with measurements of *C. elegans* chromosomes using three-dimensional karyotype reconstructed from electron micrographs of serial sections of pachytene nuclei – male chromosomal complement was shorter than the one of hermaphrodites in both studies (Goldstein, 1982). However, we detected more dramatic differences in the lengths of chromosomes. This discrepancy could be explained by several factors, potentially contributing to the overall accuracy of the measurements based on electron micrographs. First, we utilized different fixation conditions, which could differentially impact compactness of the chromatin. Second, manual reconstruction of three-dimensional topology of chromosomes from multiple sections represents a substantial challenge due to a potential undersampling and problems with alignment of sections. Finally, sectioning whole worms for EM limits the ability of the investigator to correctly identify corresponding zones of the male and hermaphrodite gonads, thus complicating comparisons. Nonetheless, both studies are similar in recognizing the X chromosome bivalent as the shortest one. In summary, these studies indicated that male chromatin is more compactly organized, and this difference in chromatin organization could potentially contribute to the difference in the appearance of H3K9me2 foci on univalents.

Obtained results indicate that chromatin organization in *C. elegans* is different between sexes at several levels. First, pachytene chromosomes are more extended during oogenesis than spermatogenesis. Since the length of chromosomes is related to the density of chromatin loops (Zickler and Kleckner, 1999), these data also suggest differential compaction of autosomal chromatin between sexes. Second, differential organization of heterochromatic domains indicates that meiotic chromosome domain topology could also vary between sexes. These results provide important insights into the mechanisms that regulate homologous recombination in other organisms. It has been previously proposed that inter-sex variation in the SC length and the rate of recombination correlate with each other (Tease and Hultén, 2004). Indeed, the levels of recombination in human oocytes is 1.4-1.6 times greater than in spermatocytes (Broman et al., 1998; Tease et al., 2002). Similar relationship between the length of chromosomes and number of crossovers has been reported for thale cress *Arabidopsis thaliana* (Giraut et al., 2011), flatworms *Dendrocoelum lacteum* (Jones and Croft, 1989), locusts *Locusta migratoria* (Quevedo et al., 1997), zebrafish *Danio rerio* (Wallace and Wallace, 2003), and *M. musculus* (Lynn et al., 2002). However, a direct causal link between these two parameters yet remains to be established. Genetic analysis in *C. elegans* indicated that spermatocyte recombination frequencies are similar to the ones of oocytes, suggesting that degree of chromatin compactness does not impact number of crossovers (Zetka and Rose, 1990). Nonetheless, the level of crossover interference is higher in males, raising a question of the SC contribution to this difference (Meneely et al., 2002). Our study demonstrates that heterochromatin organization during spermatogenesis is different from the one during oogenesis even in the absence of the SC. Therefore, these data suggest that differences in chromosomal length and domain topology could be caused not by

the SC proteins *per se*, but by other factors contributing to differential organization of meiotic chromatin in two sexes. Comparison of proteomic profiles of sperm and oocytes chromatin in *C. elegans* yielded a set of candidate proteins that could serve as sperm-specific factors, establishing unique organization of its chromatin. Testing their contribution to chromatin organization in males should help us to identify the key factors that contribute to differences in regulation of recombination patterns between sexes. Importantly, chiasma formation in humans is skewed towards the telomeric regions in spermatocytes, while distal regions very rarely recombine in oocytes (Barlow and Hultén, 1998; Tease et al., 2002). Further insights into spermatogenesis-specific domain topology in *C. elegans* and other model organisms could also shed light into these sex-specific differences in distribution of crossover events on chromosomes.

4.4 Materials and Methods

Strains

Standard techniques were used for worm culture (Brenner, 1974). All worms were raised at 20°C, unless otherwise specified. Worms of N2 strain var. Bristol were used as wild type reference. The following alleles were used in the study: *zim-2(tm574), him-3(gk149), him-3(e1256), syp-1(me17).*

Indirect immunocytochemistry

Dissected gonads of age-matched 24 hours-post L4 adults were used for staining procedures. Whole-mount fixation and incubation with antibodies was performed as previously described (Bean et al., 2004). The following primary antibodies were used at the indicated dilutions: mouse anti-H3K9me2 (Abcam®, ab1220, 1:500), guinea pig anti-SYP-1 (a gift from A.

Villeneuve, 1:200). The following secondary antibodies at respective dilutions were used: Alexafluor™ 594 goat anti-rabbit IgG (Invitrogen™, 1:500), Alexafluor™ 488 goat anti-mouse IgG (Invitrogen™, 1:500).

Image acquisition and analysis

Images were acquired on a Leica DMRA microscope (Leica Microsystems), equipped with a cooled CCD camera (QImaging), with a 40× 1.4 or 100× 1.35 NA objectives and a voxel size of 150 nm in the x, 150 nm in the y, and 200 nm in the z planes. Image acquisition was performed using Simple PCI software (Hamamatsu Corporation).

Measurement of SC length

Measurements were performed on pachytene nuclei of adult male and hermaphrodite N2 worms. Tracing of the length of SC was performed on three dimensional volume-rendered nuclei using Simple Neurite Tracer/Fiji (Longair et al., 2011). Total five nuclei were scored per gonad.

Figure 37. Males exhibit different staining pattern of H3K9me2 on aberrant chromatin in spermatogenesis when compared to oogenesis of hermaphrodites (compare to Figure 13, 14).

Maximum intensity projection image of male pachytene nuclei, stained with anti-H3K9me2 antibodies (green) and anti-SYP-1 (red) antibodies. DNA is visualized with DAPI (blue). Scale bar, 5 µm.

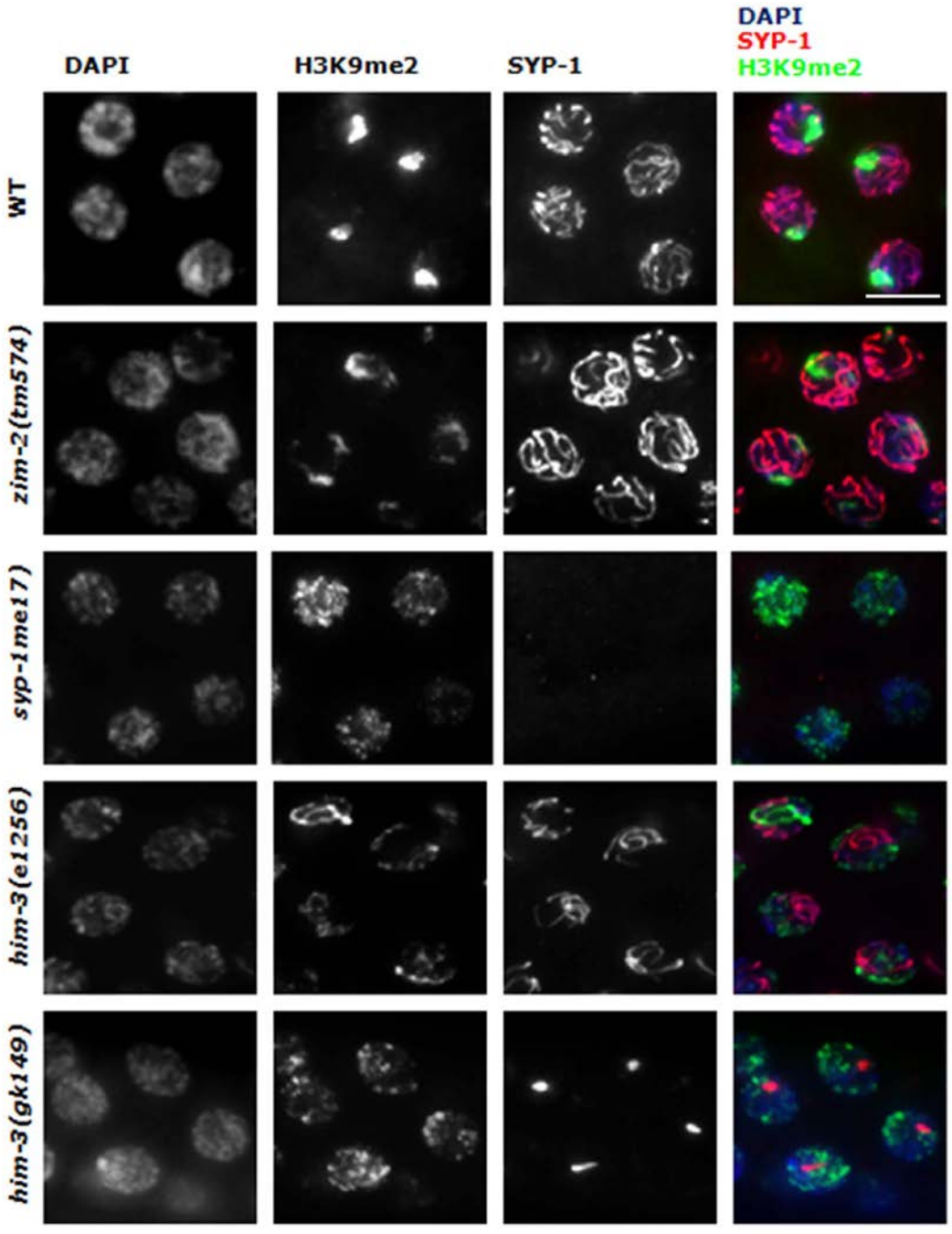
DAPI
H3K9me2
SYP-1
DAPI
SYP-1
H3K9me2
WT
zim-2(tm574)
syp-1me17)
him-3(e1256)
him-3(gk149)

Figure 38. Measurements of the SC length in pachytene nuclei during spermatogenesis versus oogenesis.

(A) An example of tracing SYP-1 tracks in the maximum intensity projection image of a single pachytene nucleus from adult hermaphrodite gonad.

(B) Same approach, but in a nucleus from adult male gonad.

(C) SYP-1 track lengths of individual bivalents in pachytene nuclei during spermatogenesis and oogenesis. ChrX – X chromosome. Aut – autosome.

(D) Total length of SYP-1 tracks of autosomal bivalents in pachytene nuclei during spermatogenesis and oogenesis. Aut+X – total length of the SC of the X chromosome and autosomes. Aut – total length of the SC of the autosomes. Oog – oogenesis. Sperm – spermatogenesis.

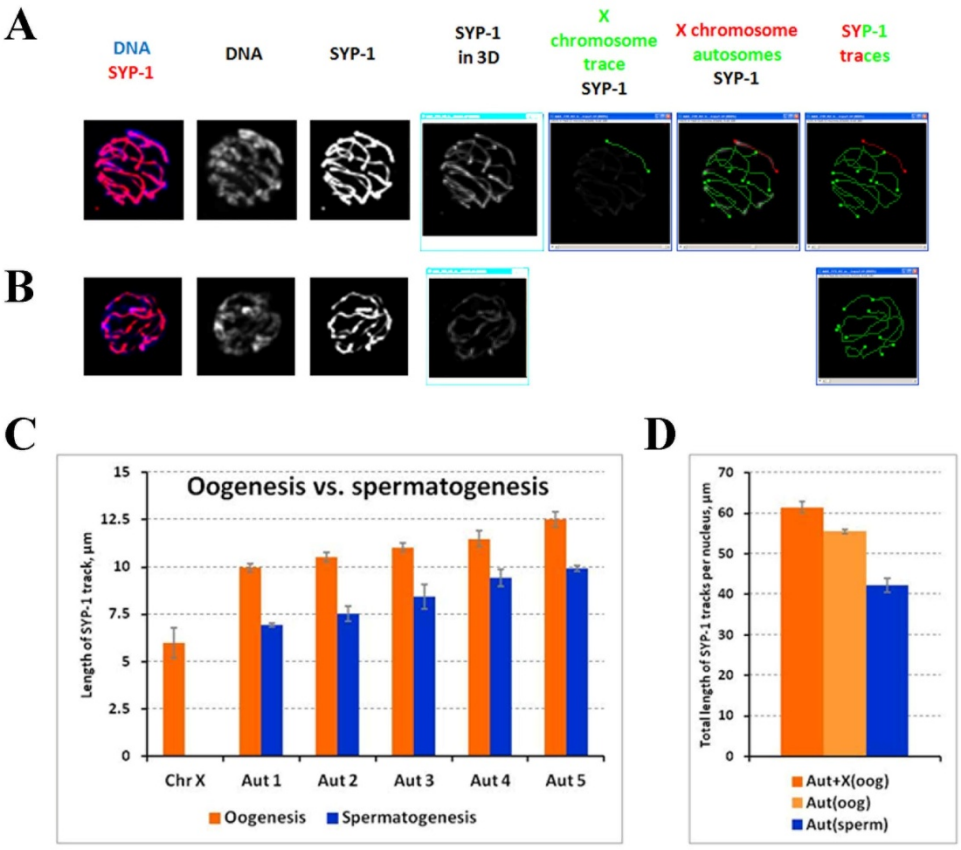
A
DNA
SYP-1
DNA
SYP-1
SYP-1
in 3D
X
chromosome
trace
SYP-1
X chromosome
autosomes
SYP-1
SYP-1
traces
B
C
Oogenesis vs. spermatogenesis
Length of SYP-1 track, µm
15
12.5
10
7.5
5
2.5
0
Chr X
Aut 1
Aut 2
Aut 3
Aut 4
Aut 5
Oogenesis
Spermatogenesis
D
Total length of SYP-1 tracks per nucleus, µm
70
60
50
40
30
20
10
0
Aut+X(oog)
Aut(oog)
Aut(sperm)

CHAPTER 5

SUMMARY AND FUTURE DIRECTIONS

In this work, I investigated heterochromatin-specific aspects of chromosome dynamics during homolog juxtaposition in *C. elegans* meiosis. Our results indicated that the appearance of heterochromatic domains on univalents during prophase I stage of oogenesis does not affect the efficiency of elimination of nuclei carrying this aberrant chromatin via apoptotic pathways. We also did not detect any effects of heterochromatinization of univalents on their transcriptional status at the onset, during and after the completion of meiosis. Examination of H3K9me2 levels in the genome of adult hermaphrodites revealed that repetitive regions of the genome, but not intergenic spaces, promoters or gene bodies, were enriched for this modification. These results are consistent with the genome-wide data, obtained for embryonic and larval stages of *C. elegans*. Interestingly, we did not detect enrichment for H3K9me2 at these loci by ChIP in mutants that carry univalents in prophase I of meiosis and exhibit elevated H3K9me2 signal on these chromosomes via immunofluorescence. Instead, our results pointed to potential contribution of changes in chromatin architecture to the appearance of heterochromatic domains on univalents. Specifically, we revealed dramatic reorganization of heterochromatic domains upon the assembly of meiotic scaffold of chromosomes, using a combination of high-resolution microscopy, data mining, and cytogenetic approaches. Based on our findings, we proposed a model where initial association of CR components of SC with chromatin causes assembly of heterochromatic domains into larger compartments, forming the interface of aligned homologs. Subsequent polymerization of SC between juxtaposed homologs, promoted by dynein-dependent movement of chromosomes, leads to sequestration of these regions. In accordance with this model, failure to achieve homolog pairing, alignment or synapsis would lead to the exposure of these regions and detection of this modification on univalents – a hallmark of several

examined *C. elegans* meiotic mutants. Interestingly, we also detected differences in organization of heterochromatic domains and overall levels of chromatin compaction between sexes.

Emerging evidence from molecular and cytogenetic studies in diverse groups of organisms suggests that packaging of the entire genome into condensed, yet transcriptionally active chromosomes, during meiosis is a key step that ensures both transcriptional readout and faithful segregation of genetic information during cell divisions. For instance, assembly of cohesins at the rDNA repeats in *S. cerevisiae* is required for prevention of non-equal sister chromatids recombination (Kobayashi et al., 2004). Remarkably, Sir2 deacetylase is involved in transcriptional repression of the locus, thus allowing the retention of cohesins and correct pairing and alignment of the repeats on sister chromatids during DSBs repair (Kobayashi and Ganley, 2005). Our findings in turn suggest that specific chromatin domains occupy unique regions within the core or at the periphery of meiotic chromatin. Therefore, they highlight the importance of studying higher-order architecture of meiotic chromatin in the context of organization of specific chromatin domains for our understanding of the mechanisms of homolog juxtaposition and fidelity of meiotic processes.

Despite the interest in this topic, the highly dynamic and transient nature of meiotic events, limited availability of the material, and a lack of suitable culturing conditions hinder studies of meiotic chromatin architecture. As a result, the governing principles and the sequence of events that lead to the establishment of the highly-organized structure of chromosomes during meiosis remain poorly understood. Therefore, development of techniques aimed at isolation of meiotic cells at specific stages of their division will provide unique advantage to examine chromatin reorganization during each of the key processes

leading to homolog juxtaposition. One of the most promising approaches is a recently established INTACT method, based on isolation of nuclei from specific tissues of an organism utilizing transgenic approach and tissue-specific promoters (Deal and Henikoff, 2010). Using this technique, one could isolate meiotic cells at different stages of their development in quantities, sufficient for any high-throughput approaches, including ChIP followed by high-throughput DNA sequencing (ChIP-seq), high-throughput cDNA sequencing (RNA-seq), and mass spectrometry analysis (Park, 2009; Wang et al., 2009).

Recent progress in sequencing technologies allows us to examine the three-dimensional organization of chromatin at an unprecedented resolution. Several studies, directed at understanding the topology of interphase nuclei, suggested hierarchical folding of chromatin fibers as a key organizational principle of genomes, yet, the underlying mechanisms of the assembly of these structures are not entirely clear (Guelen et al., 2008; Lieberman-Aiden et al., 2009). Recently, the use of chromatin confirmation capture (3C) techniques linked the topology of chromatin with organization of epigenetic domains, but left the question of the scale of these domains in different genomes open (Nora et al., 2012; Sexton et al., 2012). At the same time, details of the structure of condensed, mitotic or meiotic, chromosomes remain even more elusive (Nishino et al., 2012). Thus, the application of 3C-based approach to studies of meiotic chromatin is a promising approach for gaining insights into domanial organization of chromosomes.

Technological advances in these two areas of meiotic chromatin biology allow us to investigate several intriguing questions, raised by our work.

First, it is currently not clear what aspect of chromatin architecture of lone chromosomes triggers their transcriptional repression, while univalents that are unpaired, but present in two

copies, do not exhibit meiotic silencing. Combination of Hi-C approach with RNA Polymerase II (Pol II) ChIP-seq would allow one to determine the transcriptional activity of different regions of meiotic chromatin and the impacts that absence of SC may have on it. Results of these studies would have direct implications for understanding MSUC phenomenon and whether it is a contributing cause of sterility in mammals (Homolka et al., 2007; Reinholdt et al., 2009).

Second, it remains to be elucidated whether the gradual increase in H3K9me2 signal on univalents during their progression through pachytene stage of prophase I is caused by the expansion of chromosome territories, or active enrichment of specific regions of the genome for H3K9me2 as a result of the activity of histone methyltransferase, or both. By isolating meiotic nuclei from the gonads of *C. elegans* mutants carrying univalents at several stages during prophase I and comparing genome-wide distribution of H3K9me2 on them with wild-type bivalents devoid of H3K9me2, we could specifically determine how unpaired/unsynapsed status affects appearance of H3K9me2-enriched regions of the genome. These studies would also shed light on the dynamics of this and other histone modifications in vertebrates, where several pieces of evidence suggest that chromatin architecture *per se* could account for changes in distribution of phosphorylated form of H2AX and H3K9me2 on aberrant chromatin (Kouznetsova et al., 2009; Manterola et al., 2009).

Finally, contribution of specific position of heterochromatic domains within the chromosomal core to the prevention of nonallelic recombination requires closer examination. High-resolution maps of DSBs distribution in genomes of wild type and mutant strains of *C. elegans* carrying univalents could be obtained using high-throughput sequencing of single-strand DNA bound to RAD51 molecules. This approach would address the question whether

repetitive regions in *C. elegans* genome show reduced levels of DSBs in any topological context or their positioning at the interface of juxtaposed homologs prevents access of DSB-generating machinery to them. These studies would be particularly interesting in light of recent findings that some human repeats are enriched for binding sites of H3K4me3 histone methyltrasferase PRDM9 and therefore possess a high potential for deleterious genomic rearrangements; however, these rearrangements are prevented in normal meiosis by unknown mechanisms (Smagulova et al., 2011).

REFERENCES

Alpi, A., Pasierbek, P., Gartner, A., and Loidl, J. (2003). Genetic and cytological characterization of the recombination protein RAD-51 in Caenorhabditis elegans. Chromosoma *112*, 6–16.

Alsheimer, M. (2009). The dance floor of meiosis: evolutionary conservation of nuclear envelope attachment and dynamics of meiotic telomeres. Genome Dynamics *5*, 81–93.

Andersen, E.C., and Horvitz, H.R. (2007). Two C. elegans histone methyltransferases repress lin-3 EGF transcription to inhibit vulval development. Development *134*, 2991–2999.

Aoki, H., Sato, S., Takanami, T., Ishihara, T., Katsura, I., Takahashi, H., and Higashitani, A. (2000). Characterization of Ce-atl-1, an ATM-like gene from Caenorhabditis elegans. Molecular & General Genetics : MGG *264*, 119–126.

Baarends, W.M., Hoogerbrugge, J.W., Roest, H.P., Ooms, M., Vreeburg, J., Hoeijmakers, J.H., and Grootegoed, J.A. (1999). Histone ubiquitination and chromatin remodeling in mouse spermatogenesis. Developmental Biology *207*, 322–333.

Baarends, W.M., Wassenaar, E., van der Laan, R., Hoogerbrugge, J., Sleddens-Linkels, E., Hoeijmakers, J.H.J., de Boer, P., and Grootegoed, J.A. (2005). Silencing of unpaired chromatin and histone H2A ubiquitination in mammalian meiosis. Molecular and Cellular Biology *25*, 1041–1053.

Barbero, A.C. and J.L. (2012). Cohesins and Cohesin-Regulators in Meiosis. In Meiosis - Molecular Mechanisms and Cytogenetic Diversity, A. Swan, ed. (InTech),.

Barlow, A.L., and Hultén, M.A. (1998). Crossing over analysis at pachytene in man. European Journal of Human Genetics : EJHG *6*, 350–358.

Barzel, A., and Kupiec, M. (2008). Finding a match: how do homologous sequences get together for recombination? Nat Rev Genet *9*, 27–37.

Baudat, F., Manova, K., Yuen, J.P., Jasin, M., and Keeney, S. (2000). Chromosome synapsis defects and sexually dimorphic meiotic progression in mice lacking Spo11. Molecular Cell *6*, 989–998.

Bean, C.J., Schaner, C.E., and Kelly, W.G. (2004). Meiotic pairing and imprinted X chromatin assembly in Caenorhabditis elegans. Nat Genet *36*, 100–105.

Beisel, C., and Paro, R. (2011). Silencing chromatin: comparing modes and mechanisms. Nature Reviews. Genetics *12*, 123–135.

Bessler, J.B., Andersen, E.C., and Villeneuve, A.M. (2010). Differential localization and independent acquisition of the H3K9me2 and H3K9me3 chromatin modifications in the Caenorhabditis elegans adult germ line. PLoS Genetics *6*, e1000830.

Bhalla, N., and Dernburg, A.F. (2005). A conserved checkpoint monitors meiotic chromosome synapsis in Caenorhabditis elegans. Science *310*, 1683–1686.

Bhalla, N., and Dernburg, A.F. (2008). Prelude to a division. Annu Rev Cell Dev Biol *24*, 397–424.

Bishop, D.K., Park, D., Xu, L., and Kleckner, N. (1992). DMC1: a meiosis-specific yeast homolog of E. coli recA required for recombination, synaptonemal complex formation, and cell cycle progression. Cell *69*, 439–456.

Blat, Y., Protacio, R.U., Hunter, N., and Kleckner, N. (2002). Physical and functional interactions among basic chromosome organizational features govern early steps of meiotic chiasma formation. Cell *111*, 791–802.

Bojko, M. (1983). Human meiosis VIII. Chromosome pairing and formation of the synaptonemal complex in oocytes. Carlsberg Research Communications *48*, 457–483.

Borde, V., Robine, N., Lin, W., Bonfils, S., Géli, V., and Nicolas, A. (2009). Histone H3 lysine 4 trimethylation marks meiotic recombination initiation sites. The EMBO Journal *28*, 99–111.

Brenner, S. (1974). The genetics of Caenorhabditis elegans. Genetics *77*, 71–94.

Brick, K., Smagulova, F., Khil, P., Camerini-Otero, R.D., and Petukhova, G.V. (2012). Genetic recombination is directed away from functional genomic elements in mice. Nature.

Broman, K.W., Murray, J.C., Sheffield, V.C., White, R.L., and Weber, J.L. (1998). Comprehensive human genetic maps: individual and sex-specific variation in recombination. American Journal of Human Genetics *63*, 861–869.

Brown, M.S., Zanders, S., and Alani, E. (2011). Sustained and rapid chromosome movements are critical for chromosome pairing and meiotic progression in budding yeast. Genetics *188*, 21–32.

Buard, J., Barthès, P., Grey, C., and de Massy, B. (2009). Distinct histone modifications define initiation and repair of meiotic recombination in the mouse. The EMBO Journal *28*, 2616–2624.

Burgoyne, P.S., Mahadevaiah, S.K., and Turner, J.M.A. (2009). The consequences of asynapsis for mammalian meiosis. Nature Reviews. Genetics *10*, 207–216.

Chan, R.C., Severson, A.F., and Meyer, B.J. (2004). Condensin restructures chromosomes in preparation for meiotic divisions. The Journal of Cell Biology *167*, 613–625.

Checchi, P.M., and Engebrecht, J. (2011). Caenorhabditis elegans histone methyltransferase MET-2 shields the male X chromosome from checkpoint machinery and mediates meiotic sex chromosome inactivation. PLoS Genetics *7*, e1002267.

Claycomb, J.M., Batista, P.J., Pang, K.M., Gu, W., Vasale, J.J., van Wolfswinkel, J.C., Chaves, D.A., Shirayama, M., Mitani, S., Ketting, R.F., et al. (2009). The Argonaute CSR-1 and its 22G-RNA cofactors are required for holocentric chromosome segregation. Cell *139*, 123–134.

Cohen, P.E., Pollack, S.E., and Pollard, J.W. (2006). Genetic analysis of chromosome pairing, recombination, and cell cycle control during first meiotic prophase in mammals. Endocrine Reviews *27*, 398–426.

Colaiácovo, M.P., MacQueen, A.J., Martinez-Perez, E., McDonald, K., Adamo, A., La Volpe, A., and Villeneuve, A.M. (2003). Synaptonemal complex assembly in C. elegans is dispensable for loading strand-exchange proteins but critical for proper completion of recombination. Developmental Cell *5*, 463–474.

Colas, I., Shaw, P., Prieto, P., Wanous, M., Spielmeyer, W., Mago, R., and Moore, G. (2008). Effective chromosome pairing requires chromatin remodeling at the onset of meiosis. Proceedings of the National Academy of Sciences of the United States of America *105*, 6075–6080.

Contrino, S., Smith, R.N., Butano, D., Carr, A., Hu, F., Lyne, R., Rutherford, K., Kalderimis, A., Sullivan, J., Carbon, S., et al. (2012). modMine: flexible access to modENCODE data. Nucleic Acids Research *40*, D1082–8.

Couteau, F., Guerry, F., Muller, F., and Palladino, F. (2002). A heterochromatin protein 1 homologue in Caenorhabditis elegans acts in germline and vulval development. EMBO Reports *3*, 235–241.

Couteau, F., Nabeshima, K., Villeneuve, A., and Zetka, M. (2004). A component of C. elegans meiotic chromosome axes at the interface of homolog alignment, synapsis, nuclear reorganization, and recombination. Curr Biol *14*, 585–592.

Couteau, F., and Zetka, M. (2005). HTP-1 coordinates synaptonemal complex assembly with homolog alignment during meiosis in C. elegans. Genes Dev *19*, 2744–2756.

Couteau, F., and Zetka, M. (2011). DNA damage during meiosis induces chromatin remodeling and synaptonemal complex disassembly. Developmental Cell *20*, 353–363.

Cowell, I.G., Aucott, R., Mahadevaiah, S.K., Burgoyne, P.S., Huskisson, N., Bongiorni, S., Prantera, G., Fanti, L., Pimpinelli, S., Wu, R., et al. (2002). Heterochromatin, HP1 and methylation at lysine 9 of histone H3 in animals. Chromosoma *111*, 22–36.

Deal, R.B., and Henikoff, S. (2010). A simple method for gene expression and chromatin profiling of individual cell types within a tissue. Developmental Cell *18*, 1030–1040.

Dernburg, A.F. (2012). RNA plays meiotic matchmaker. Science (New York, N.Y.) *336*, 681–682.

Dernburg, A.F., McDonald, K., Moulder, G., Barstead, R., Dresser, M., and Villeneuve, A.M. (1998). Meiotic recombination in C. elegans initiates by a conserved mechanism and is dispensable for homologous chromosome synapsis. Cell *94*, 387–398.

Ding, D.-Q., Okamasa, K., Yamane, M., Tsutsumi, C., Haraguchi, T., Yamamoto, M., and Hiraoka, Y. (2012). Meiosis-specific noncoding RNA mediates robust pairing of homologous chromosomes in meiosis. Science (New York, N.Y.) *336*, 732–736.

Ding, D.-Q., Yamamoto, A., Haraguchi, T., and Hiraoka, Y. (2004). Dynamics of homologous chromosome pairing during meiotic prophase in fission yeast. Developmental Cell *6*, 329–341.

Ferguson, K.A., Chow, V., and Ma, S. (2008). Silencing of unpaired meiotic chromosomes and altered recombination patterns in an azoospermic carrier of a t(8;13) reciprocal translocation. Hum Reprod *23*, 988–995.

Fraune, J., Schramm, S., Alsheimer, M., and Benavente, R. (2012). The mammalian synaptonemal complex: Protein components, assembly and role in meiotic recombination. Experimental Cell Research *318*, 1340–1346.

Gartner, A., Milstein, S., Ahmed, S., Hodgkin, J., and Hengartner, M.O. (2000). A conserved checkpoint pathway mediates DNA damage--induced apoptosis and cell cycle arrest in C. elegans. Mol Cell *5*, 435–443.

Gerstein, M.B., Lu, Z.J., Van Nostrand, E.L., Cheng, C., Arshinoff, B.I., Liu, T., Yip, K.Y., Robilotto, R., Rechtsteiner, A., Ikegami, K., et al. (2010). Integrative analysis of the Caenorhabditis elegans genome by the modENCODE project. Science (New York, N.Y.) *330*, 1775–1787.

Ghabrial, A., and Schüpbach, T. (1999). Activation of a meiotic checkpoint regulates translation of Gurken during Drosophila oogenesis. Nature Cell Biology *1*, 354–357.

Giraut, L., Falque, M., Drouaud, J., Pereira, L., Martin, O.C., and Mézard, C. (2011). Genome-wide crossover distribution in Arabidopsis thaliana meiosis reveals sex-specific patterns along chromosomes. PLoS Genetics *7*, e1002354.

Glory, E., and Murphy, R.F. (2007). Automated subcellular location determination and high-throughput microscopy. Developmental Cell *12*, 7–16.

Goldstein, P. (1982). The synaptonemal complexes of Caenorhabditis elegans: pachytene karyotype analysis of male and hermaphrodite wild-type and him mutants. Chromosoma *86*, 577–593.

Goodyer, W., Kaitna, S., Couteau, F., Ward, J.D., Boulton, S.J., and Zetka, M. (2008). HTP-3 links DSB formation with homolog pairing and crossing over during C. elegans meiosis. Dev Cell *14*, 263–274.

Gottlieb, S., and Esposito, R.E. (1989). A new role for a yeast transcriptional silencer gene, SIR2, in regulation of recombination in ribosomal DNA. Cell *56*, 771–776.

Grewal, S.I.S., and Jia, S. (2007). Heterochromatin revisited. Nat Rev Genet *8*, 35–46.

Grishok, A., Sinskey, J.L., and Sharp, P.A. (2005). Transcriptional silencing of a transgene by RNAi in the soma of C. elegans. Genes & Development *19*, 683–696.

Guelen, L., Pagie, L., Brasset, E., Meuleman, W., Faza, M.B., Talhout, W., Eussen, B.H., de Klein, A., Wessels, L., de Laat, W., et al. (2008). Domain organization of human chromosomes revealed by mapping of nuclear lamina interactions. Nature *453*, 948–951.

Guioli, S., Lovell-Badge, R., and Turner, J.M.A. (2012). Error-Prone ZW Pairing and No Evidence for Meiotic Sex Chromosome Inactivation in the Chicken Germ Line. PLoS Genetics *8*, e1002560.

Gumienny, T.L., Lambie, E., Hartwieg, E., Horvitz, H.R., and Hengartner, M.O. (1999). Genetic control of programmed cell death in the Caenorhabditis elegans hermaphrodite germline. Development (Cambridge, England) *126*, 1011–1022.

Hagstrom, K.A., Holmes, V.F., Cozzarelli, N.R., and Meyer, B.J. (2002). C. elegans condensin promotes mitotic chromosome architecture, centromere organization, and sister chromatid segregation during mitosis and meiosis. Genes & Development *16*, 729–742.

Handel, M.A., and Eppig, J.J. (1998). Sexual dimorphism in the regulation of mammalian meiosis. Current Topics in Developmental Biology *37*, 333–358.

Handel, M.A., and Schimenti, J.C. (2010). Genetics of mammalian meiosis: regulation, dynamics and impact on fertility. Nature Reviews. Genetics *11*, 124–136.

Harper, N.C., Rillo, R., Jover-Gil, S., Assaf, Z.J., Bhalla, N., and Dernburg, A.F. (2011). Pairing centers recruit a Polo-like kinase to orchestrate meiotic chromosome dynamics in C. elegans. Developmental Cell *21*, 934–947.

Hartl, T.A., Sweeney, S.J., Knepler, P.J., and Bosco, G. (2008). Condensin II resolves chromosomal associations to enable anaphase I segregation in Drosophila male meiosis. PLoS Genetics *4*, e1000228.

Hassold, T., Hall, H., and Hunt, P. (2007). The origin of human aneuploidy: where we have been, where we are going. Human Molecular Genetics *16 Spec No*, R203–8.

Hassold, T., and Hunt, P. (2001). To err (meiotically) is human: the genesis of human aneuploidy. Nature Reviews. Genetics *2*, 280–291.

Hassold, T., Sherman, S., and Hunt, P. (2000). Counting cross-overs: characterizing meiotic recombination in mammals. Human Molecular Genetics *9*, 2409–2419.

Hayashi, M., Mlynarczyk-Evans, S., and Villeneuve, A.M. (2010). The synaptonemal complex shapes the crossover landscape through cooperative assembly, crossover promotion and crossover inhibition during Caenorhabditis elegans meiosis. Genetics *186*, 45–58.

Henry, J.M., Camahort, R., Rice, D.A., Florens, L., Swanson, S.K., Washburn, M.P., and Gerton, J.L. (2006). Mnd1/Hop2 facilitates Dmc1-dependent interhomolog crossover formation in meiosis of budding yeast. Molecular and Cellular Biology *26*, 2913–2923.

Hernández-Hernández, A., Rincón-Arano, H., Recillas-Targa, F., Ortiz, R., Valdes-Quezada, C., Echeverría, O.M., Benavente, R., and Vázquez-Nin, G.H. (2008). Differential distribution and association of repeat DNA sequences in the lateral element of the synaptonemal complex in rat spermatocytes. Chromosoma *117*, 77–87.

Hirano, T. (2002). The ABCs of SMC proteins: two-armed ATPases for chromosome condensation, cohesion, and repair. Genes & Development *16*, 399–414.

Hirano, T. (2005). Condensins: organizing and segregating the genome. Current Biology : CB *15*, R265–75.

Hiraoka, Y., and Dernburg, A.F. (2009). The SUN rises on meiotic chromosome dynamics. Developmental Cell *17*, 598–605.

Hochwagen, A., and Amon, A. (2006). Checking your breaks: surveillance mechanisms of meiotic recombination. Curr Biol *16*, R217–28.

Hodges, C.A., LeMaire-Adkins, R., and Hunt, P.A. (2001). Coordinating the segregation of sister chromatids during the first meiotic division: evidence for sexual dimorphism. Journal of Cell Science *114*, 2417–2426.

Hodgkin, J., Horvitz, H.R., and Brenner, S. (1979). Nondisjunction Mutants of the Nematode CAENORHABDITIS ELEGANS. Genetics *91*, 67–94.

Hollingsworth, N.M., Goetsch, L., and Byers, B. (1990). The HOP1 gene encodes a meiosis-specific component of yeast chromosomes. Cell *61*, 73–84.

Homolka, D., Ivanek, R., Capkova, J., Jansa, P., and Forejt, J. (2007). Chromosomal rearrangement interferes with meiotic X chromosome inactivation. Genome Research *17*, 1431–1437.

Ikegami, K., Egelhofer, T.A., Strome, S., and Lieb, J.D. (2010). Caenorhabditis elegans chromosome arms are anchored to the nuclear membrane via discontinuous association with LEM-2. Genome Biology *11*, R120.

Inagaki, A., Schoenmakers, S., and Baarends, W.M. (2010). DNA double strand break repair, chromosome synapsis and transcriptional silencing in meiosis. Epigenetics : Official Journal of the DNA Methylation Society *5*, 255–266.

Jantsch, V., Pasierbek, P., Mueller, M.M., Schweizer, D., Jantsch, M., and Loidl, J. (2004). Targeted gene knockout reveals a role in meiotic recombination for ZHP-3, a Zip3-related protein in Caenorhabditis elegans. Molecular and Cellular Biology *24*, 7998–8006.

Jaramillo-Lambert, A., Ellefson, M., Villeneuve, A.M., and Engebrecht, J. (2007). Differential timing of S phases, X chromosome replication, and meiotic prophase in the C. elegans germ line. Developmental Biology *308*, 206–221.

Jaramillo-Lambert, A., and Engebrecht, J. (2010). A single unpaired and transcriptionally silenced X chromosome locally precludes checkpoint signaling in the Caenorhabditis elegans germ line. Genetics *184*, 613–628.

Jaramillo-Lambert, A., Harigaya, Y., Vitt, J., Villeneuve, A., and Engebrecht, J. (2010). Meiotic errors activate checkpoints that improve gamete quality without triggering apoptosis in male germ cells. Current Biology : CB *20*, 2078–2089.

John, B. (1990). Meiosis (Cambridge: Cambridge University Press).

Jones, G.H., and Croft, J.A. (1989). Chromosome pairing and chiasma formation in spermatocytes and oocytes of Dendrocoelum lactem (Turbellaria, Tricladida); a cytogenetical and ultrastructural study. Heredity *63*, 97–106.

Joyce, E.F., and McKim, K.S. (2007). When specialized sites are important for synapsis and the distribution of crossovers. Bioessays *29*, 217–226.

Katz, D.J., Edwards, T.M., Reinke, V., and Kelly, W.G. (2009). A C. elegans LSD1 demethylase contributes to germline immortality by reprogramming epigenetic memory. Cell *137*, 308–320.

Kauppi, L., Barchi, M., Baudat, F., Romanienko, P.J., Keeney, S., and Jasin, M. (2011). Distinct properties of the XY pseudoautosomal region crucial for male meiosis. Science (New York, N.Y.) *331*, 916–920.

Kelly, K.O., Dernburg, A.F., Stanfield, G.M., and Villeneuve, A.M. (2000). Caenorhabditis elegans msh-5 is required for both normal and radiation-induced meiotic crossing over but not for completion of meiosis. Genetics *156*, 617–630.

Kelly, W.G., and Aramayo, R. (2007). Meiotic silencing and the epigenetics of sex. Chromosome Research : an International Journal on the Molecular, Supramolecular and Evolutionary Aspects of Chromosome Biology *15*, 633–651.

Kelly, W.G., Schaner, C.E., Dernburg, A.F., Lee, M.-H.H., Kim, S.K., Villeneuve, A.M., and Reinke, V. (2002). X-chromosome silencing in the germline of C. elegans. Development *129*, 479–492.

Khalil, A.M., Boyar, F.Z., and Driscoll, D.J. (2004). Dynamic histone modifications mark sex chromosome inactivation and reactivation during mammalian spermatogenesis. Proceedings of the National Academy of Sciences of the United States of America *101*, 16583–16587.

Kimble, J.E., and White, J.G. (1981). On the control of germ cell development in Caenorhabditis elegans. Developmental Biology *81*, 208–219.

Kleckner, N. (2006). Chiasma formation: chromatin/axis interplay and the role(s) of the synaptonemal complex. Chromosoma *115*, 175–194.

Kobayashi, T., and Ganley, A.R.D. (2005). Recombination regulation by transcription-induced cohesin dissociation in rDNA repeats. Science (New York, N.Y.) *309*, 1581–1584.

Kobayashi, T., Horiuchi, T., Tongaonkar, P., Vu, L., and Nomura, M. (2004). SIR2 regulates recombination between different rDNA repeats, but not recombination within individual rRNA genes in yeast. Cell *117*, 441–453.

Koszul, R., and Kleckner, N. (2009). Dynamic chromosome movements during meiosis: a way to eliminate unwanted connections? Trends in Cell Biology *19*, 716–724.

Kouzarides, T. (2007). Chromatin modifications and their function. Cell *128*, 693–705.

Kouznetsova, A., Wang, H., Bellani, M., Camerini-Otero, R.D., Jessberger, R., and Höög, C. (2009). BRCA1-mediated chromatin silencing is limited to oocytes with a small number of asynapsed chromosomes. Journal of Cell Science *122*, 2446–2452.

Krauss, V. (2008). Glimpses of evolution: heterochromatic histone H3K9 methyltransferases left its marks behind. Genetica *133*, 93–106.

Kupiec, M., and Petes, T.D. (1988). Meiotic recombination between repeated transposable elements in Saccharomyces cerevisiae. Molecular and Cellular Biology *8*, 2942–2954.

Labella, S., Woglar, A., Jantsch, V., and Zetka, M. (2011). Polo kinases establish links between meiotic chromosomes and cytoskeletal forces essential for homolog pairing. Developmental Cell *21*, 948–958.

Lammers, J.H., Offenberg, H.H., van Aalderen, M., Vink, A.C., Dietrich, A.J., and Heyting, C. (1994). The gene encoding a major component of the lateral elements of synaptonemal complexes of the rat is related to X-linked lymphocyte-regulated genes. Molecular and Cellular Biology *14*, 1137–1146.

Lee, C.-Y., Conrad, M.N., and Dresser, M.E. (2012). Meiotic chromosome pairing is promoted by telomere-led chromosome movements independent of bouquet formation. PLoS Genetics *8*, e1002730.

Lee, J., Ogushi, S., Saitou, M., and Hirano, T. (2011). Condensins I and II are essential for construction of bivalent chromosomes in mouse oocytes. Molecular Biology of the Cell *22*, 3465–3477.

Li, T., and Kelly, W.G. (2011). A role for Set1/MLL-related components in epigenetic regulation of the Caenorhabditis elegans germ line. PLoS Genetics *7*, e1001349.

Lichten, M. (2001). Meiotic recombination: Breaking the genome to save it. Current Biology *11*, R253–R256.

Lichten, M., Borts, R.H., and Haber, J.E. (1987). Meiotic gene conversion and crossing over between dispersed homologous sequences occurs frequently in Saccharomyces cerevisiae. Genetics *115*, 233–246.

Lichten, M., and de Massy, B. (2011). The impressionistic landscape of meiotic recombination. Cell *147*, 267–270.

Lieberman-Aiden, E., van Berkum, N.L., Williams, L., Imakaev, M., Ragoczy, T., Telling, A., Amit, I., Lajoie, B.R., Sabo, P.J., Dorschner, M.O., et al. (2009). Comprehensive mapping of long-range interactions reveals folding principles of the human genome. Science (New York, N.Y.) *326*, 289–293.

Longair, M.H., Baker, D.A., and Armstrong, J.D. (2011). Simple Neurite Tracer: open source software for reconstruction, visualization and analysis of neuronal processes. Bioinformatics (Oxford, England) *27*, 2453–2454.

Lui, D.Y., and Colaiácovo, M.P. (2013). Meiotic Development in Caenorhabditis elegans. Advances in Experimental Medicine and Biology *757*, 133–170.

Lydall, D., Nikolsky, Y., Bishop, D.K., and Weinert, T. (1996). A meiotic recombination checkpoint controlled by mitotic checkpoint genes. Nature *383*, 840–843.

Lynn, A., Koehler, K.E., Judis, L., Chan, E.R., Cherry, J.P., Schwartz, S., Seftel, A., Hunt, P.A., and Hassold, T.J. (2002). Covariation of synaptonemal complex length and mammalian meiotic exchange rates. Science (New York, N.Y.) *296*, 2222–2225.

MacQueen, A.J., Colaiácovo, M.P., McDonald, K., Villeneuve, A.M., and Colaiacovo, M.P. (2002). Synapsis-dependent and -independent mechanisms stabilize homolog pairing during meiotic prophase in C. elegans. Genes Dev *16*, 2428–2442.

MacQueen, A.J., Phillips, C.M., Bhalla, N., Weiser, P., Villeneuve, A.M., and Dernburg, A.F. (2005). Chromosome sites play dual roles to establish homologous synapsis during meiosis in C. elegans. Cell *123*, 1037–1050.

MacQueen, A.J., and Villeneuve, A.M. (2001). Nuclear reorganization and homologous chromosome pairing during meiotic prophase require C. elegans chk-2. Genes & Development *15*, 1674–1687.

Mahadevaiah, S.K., Bourc'his, D., de Rooij, D.G., Bestor, T.H., Turner, J.M.A., and Burgoyne, P.S. (2008). Extensive meiotic asynapsis in mice antagonises meiotic silencing of unsynapsed chromatin and consequently disrupts meiotic sex chromosome inactivation. The Journal of Cell Biology *182*, 263–276.

Mahadevaiah, S.K., Turner, J.M., Baudat, F., Rogakou, E.P., de Boer, P., Blanco-Rodríguez, J., Jasin, M., Keeney, S., Bonner, W.M., and Burgoyne, P.S. (2001). Recombinational DNA double-strand breaks in mice precede synapsis. Nature Genetics *27*, 271–276.

Maine, E.M., Hauth, J., Ratliff, T., Vought, V.E., She, X., and Kelly, W.G. (2005). EGO-1, a putative RNA-dependent RNA polymerase, is required for heterochromatin assembly on unpaired dna during C. elegans meiosis. Curr Biol *15*, 1972–1978.

Manheim, E.A., and McKim, K.S. (2003). The Synaptonemal complex component C(2)M regulates meiotic crossing over in Drosophila. Current Biology : CB *13*, 276–285.

Manterola, M., Page, J., Vasco, C., Berríos, S., Parra, M.T., Viera, A., Rufas, J.S., Zuccotti, M., Garagna, S., and Fernández-Donoso, R. (2009). A high incidence of meiotic silencing of unsynapsed chromatin is not associated with substantial pachytene loss in heterozygous male mice carrying multiple simple robertsonian translocations. PLoS Genetics *5*, e1000625.

Martin, C., and Zhang, Y. (2005). The diverse functions of histone lysine methylation. Nat Rev Mol Cell Biol *6*, 838–849.

Martin, J.S., Winkelmann, N., Petalcorin, M.I.R., McIlwraith, M.J., and Boulton, S.J. (2005). RAD-51-dependent and -independent roles of a Caenorhabditis elegans BRCA2-related protein during DNA double-strand break repair. Molecular and Cellular Biology *25*, 3127–3139.

Martinez-Perez, E., and Villeneuve, A.M. (2005). HTP-1-dependent constraints coordinate homolog pairing and synapsis and promote chiasma formation during C. elegans meiosis. Genes & Development *19*, 2727–2743.

McKim, K.S. (1998). Meiotic Synapsis in the Absence of Recombination. Science *279*, 876–878.

Meneely, P.M., Farago, A.F., and Kauffman, T.M. (2002). Crossover distribution and high interference for both the X chromosome and an autosome during oogenesis and spermatogenesis in Caenorhabditis elegans. Genetics *162*, 1169–1177.

Mets, D.G., and Meyer, B.J. (2009). Condensins regulate meiotic DNA break distribution, thus crossover frequency, by controlling chromosome structure. Cell *139*, 73–86.

Meuwissen, R.L., Offenberg, H.H., Dietrich, A.J., Riesewijk, A., van Iersel, M., and Heyting, C. (1992). A coiled-coil related protein specific for synapsed regions of meiotic prophase chromosomes. The EMBO Journal *11*, 5091–5100.

Mieczkowski, P.A., Dominska, M., Buck, M.J., Lieb, J.D., and Petes, T.D. (2007). Loss of a histone deacetylase dramatically alters the genomic distribution of Spo11p-catalyzed DNA breaks in Saccharomyces cerevisiae. Proceedings of the National Academy of Sciences of the United States of America *104*, 3955–3960.

Moens, P.B. (1968). The structure and function of the synaptinemal complex in Lilium longiflorum sporocytes. Chromosoma *23*, 418–451.

Moens, P.B. (1969). The fine structure of meiotic chromosome polarization and pairing in Locusta migratoria spermatocytes. Chromosoma *28*, 1–25.

Morelli, M. a, and Cohen, P.E. (2005). Not all germ cells are created equal: aspects of sexual dimorphism in mammalian meiosis. Reproduction (Cambridge, England) *130*, 761–781.

Moses, M.J. (1968). Synaptinemal Complex. Annual Review of Genetics *2*, 363–412.

Nabeshima, K., Mlynarczyk-Evans, S., and Villeneuve, A.M. (2011). Chromosome painting reveals asynaptic full alignment of homologs and HIM-8-dependent remodeling of X chromosome territories during Caenorhabditis elegans meiosis. PLoS Genetics *7*, e1002231.

Nishino, Y., Eltsov, M., Joti, Y., Ito, K., Takata, H., Takahashi, Y., Hihara, S., Frangakis, A.S., Imamoto, N., Ishikawa, T., et al. (2012). Human mitotic chromosomes consist predominantly of irregularly folded nucleosome fibres without a 30-nm chromatin structure. The EMBO Journal *31*, 1644–1653.

Nora, E.P., Lajoie, B.R., Schulz, E.G., Giorgetti, L., Okamoto, I., Servant, N., Piolot, T., van Berkum, N.L., Meisig, J., Sedat, J., et al. (2012). Spatial partitioning of the regulatory landscape of the X-inactivation centre. Nature *485*, 381–385.

Oliver-Bonet, M., Benet, J., Sun, F., Navarro, J., Abad, C., Liehr, T., Starke, H., Greene, C., Ko, E., and Martin, R.H. (2005). Meiotic studies in two human reciprocal translocations and their association with spermatogenic failure. Hum Reprod *20*, 683–688.

Ollinger, R., Alsheimer, M., and Benavente, R. (2005). Mammalian protein SCP1 forms synaptonemal complex-like structures in the absence of meiotic chromosomes. Molecular Biology of the Cell *16*, 212–217.

Ortiz, R., Echeverría, O.M., Ubaldo, E., Carlos, A., Scassellati, C., and Vázquez-Nin, G.H. (2002). Cytochemical study of the distribution of RNA and DNA in the synaptonemal complex of guinea-pig and rat spermatocytes. European Journal of Histochemistry : EJH *46*, 133–142.

Page, S.L., and Hawley, R.S. (2001). c(3)G encodes a Drosophila synaptonemal complex protein. Genes & Development *15*, 3130–3143.

Page, S.L., and Hawley, R.S. (2004). The genetics and molecular biology of the synaptonemal complex. Annual Review of Cell and Developmental Biology *20*, 525–558.

Paigen, K., and Petkov, P. (2010). Mammalian recombination hot spots: properties, control and evolution. Nature Reviews. Genetics *11*, 221–233.

Pan, J., Sasaki, M., Kniewel, R., Murakami, H., Blitzblau, H.G., Tischfield, S.E., Zhu, X., Neale, M.J., Jasin, M., Socci, N.D., et al. (2011). A hierarchical combination of factors shapes the genome-wide topography of yeast meiotic recombination initiation. Cell *144*, 719–731.

Panizza, S., Mendoza, M.A., Berlinger, M., Huang, L., Nicolas, A., Shirahige, K., and Klein, F. (2011). Spo11-Accessory Proteins Link Double-Strand Break Sites to the Chromosome Axis in Early Meiotic Recombination. Cell *146*, 372–383.

Park, P.J. (2009). ChIP-seq: advantages and challenges of a maturing technology. Nature Reviews. Genetics *10*, 669–680.

Pasierbek, P., Jantsch, M., Melcher, M., Schleiffer, A., Schweizer, D., and Loidl, J. (2001). A Caenorhabditis elegans cohesion protein with functions in meiotic chromosome pairing and disjunction. Genes & Development *15*, 1349–1360.

Passarge, E. (1979). Emil Heitz and the concept of heterochromatin: longitudinal chromosome differentiation was recognized fifty years ago. American Journal of Human Genetics *31*, 106–115.

Pawlowski, W.P., and Cande, W.Z. (2005). Coordinating the events of the meiotic prophase. Trends in Cell Biology *15*, 674–681.

Pearlman, R.E., Tsao, N., and Moens, P.B. (1992). Synaptonemal complexes from DNase-treated rat pachytene chromosomes contain (GT)n and LINE/SINE sequences. Genetics *130*, 865–872.

Penkner, A., Tang, L., Novatchkova, M., Ladurner, M., Fridkin, A., Gruenbaum, Y., Schweizer, D., Loidl, J., and Jantsch, V. (2007). The nuclear envelope protein Matefin/SUN-1 is required for homologous pairing in C. elegans meiosis. Developmental Cell *12*, 873–885.

Penkner, A.M., Fridkin, A., Gloggnitzer, J., Baudrimont, A., Machacek, T., Woglar, A., Csaszar, E., Pasierbek, P., Ammerer, G., Gruenbaum, Y., et al. (2009). Meiotic chromosome homology search involves modifications of the nuclear envelope protein Matefin/SUN-1. Cell *139*, 920–933.

Peters, A.H., O'Carroll, D., Scherthan, H., Mechtler, K., Sauer, S., Schöfer, C., Weipoltshammer, K., Pagani, M., Lachner, M., Kohlmaier, A., et al. (2001). Loss of the Suv39h histone methyltransferases impairs mammalian heterochromatin and genome stability. Cell *107*, 323–337.

Petes, T.D. (2001). Meiotic recombination hot spots and cold spots. Nature Reviews. Genetics *2*, 360–369.

Phillips, C.M., and Dernburg, A.F. (2006). A family of zinc-finger proteins is required for chromosome-specific pairing and synapsis during meiosis in C. elegans. Developmental Cell *11*, 817–829.

Phillips, C.M., Wong, C., Bhalla, N., Carlton, P.M., Weiser, P., Meneely, P.M., and Dernburg, A.F. (2005). HIM-8 binds to the X chromosome pairing center and mediates chromosome-specific meiotic synapsis. Cell *123*, 1051–1063.

Prieto, P., Shaw, P., and Moore, G. (2004). Homologue recognition during meiosis is associated with a change in chromatin conformation. Nature Cell Biology *6*, 906–908.

Quevedo, C., Cerro, A.L.D., Santos, J.L., and Jones, G.H. (1997). Correlated variation of chiasma frequency and synaptonemal complex length in Locusta migratoria. Heredity *78*, 515–519.

Reinholdt, L.G., Czechanski, A., Kamdar, S., King, B.L., Sun, F., and Handel, M.A. (2009). Meiotic behavior of aneuploid chromatin in mouse models of Down syndrome. Chromosoma *118*, 723–736.

Reinke, V., Gil, I.S., Ward, S., and Kazmer, K. (2004). Genome-wide germline-enriched and sex-biased expression profiles in Caenorhabditis elegans. Development (Cambridge, England) *131*, 311–323.

Reinke, V., Smith, H.E., Nance, J., Wang, J., Van Doren, C., Begley, R., Jones, S.J., Davis, E.B., Scherer, S., Ward, S., et al. (2000). A global profile of germline gene expression in C. elegans. Molecular Cell *6*, 605–616.

Reuben, M., and Lin, R. (2002). Germline X chromosomes exhibit contrasting patterns of histone H3 methylation in Caenorhabditis elegans. Developmental Biology *245*, 71–82.

Roig, I., Liebe, B., Egozcue, J., Cabero, L., Garcia, M., and Scherthan, H. (2004). Female-specific features of recombinational double-stranded DNA repair in relation to synapsis and telomere dynamics in human oocytes. Chromosoma *113*, 22–33.

Rousseeuw, P. (1987). Silhouettes: A graphical aid to the interpretation and validation of cluster analysis. Journal of Computational and Applied Mathematics *20*, 53–65.

San Filippo, J., Sung, P., and Klein, H. (2008). Mechanism of eukaryotic homologous recombination. Annu Rev Biochem *77*, 229–257.

Sato, A., Isaac, B., Phillips, C.M., Rillo, R., Carlton, P.M., Wynne, D.J., Kasad, R.A., and Dernburg, A.F. (2009). Cytoskeletal forces span the nuclear envelope to coordinate meiotic chromosome pairing and synapsis. Cell *139*, 907–919.

Schlecht, H.B., Lichten, M., and Goldman, A.S.H. (2004). Compartmentalization of the yeast meiotic nucleus revealed by analysis of ectopic recombination. Genetics *168*, 1189–1203.

Schoenmakers, S., Wassenaar, E., Hoogerbrugge, J.W., Laven, J.S.E., Grootegoed, J.A., and Baarends, W.M. (2009). Female meiotic sex chromosome inactivation in chicken. PLoS Genetics *5*, e1000466.

Severson, A.F., Ling, L., van Zuylen, V., and Meyer, B.J. (2009). The axial element protein HTP-3 promotes cohesin loading and meiotic axis assembly in C. elegans to implement the meiotic program of chromosome segregation. Genes & Development *23*, 1763–1778.

Sexton, T., Yaffe, E., Kenigsberg, E., Bantignies, F., Leblanc, B., Hoichman, M., Parrinello, H., Tanay, A., and Cavalli, G. (2012). Three-dimensional folding and functional organization principles of the Drosophila genome. Cell *148*, 458–472.

Shakes, D.C., Wu, J.-C., Sadler, P.L., Laprade, K., Moore, L.L., Noritake, A., and Chu, D.S. (2009). Spermatogenesis-specific features of the meiotic program in Caenorhabditis elegans. PLoS Genetics *5*, e1000611.

She, X., Xu, X., Fedotov, A., Kelly, W.G., and Maine, E.M. (2009). Regulation of heterochromatin assembly on unpaired chromosomes during Caenorhabditis elegans meiosis by components of a small RNA-mediated pathway. PLoS Genetics *5*, e1000624.

Sijen, T., and Plasterk, R.H.A. (2003). Transposon silencing in the Caenorhabditis elegans germ line by natural RNAi. Nature *426*, 310–314.

Smagulova, F., Gregoretti, I.V., Brick, K., Khil, P., Camerini-Otero, R.D., and Petukhova, G.V. (2011). Genome-wide analysis reveals novel molecular features of mouse recombination hotspots. Nature *472*, 375–378.

Smith, A.V., and Roeder, G.S. (1997). The yeast Red1 protein localizes to the cores of meiotic chromosomes. The Journal of Cell Biology *136*, 957–967.

Smolikov, S., Eizinger, A., Hurlburt, A., Rogers, E., Villeneuve, A.M., and Colaiácovo, M.P. (2007a). Synapsis-defective mutants reveal a correlation between chromosome conformation and the mode of double-strand break repair during Caenorhabditis elegans meiosis. Genetics *176*, 2027–2033.

Smolikov, S., Eizinger, A., Schild-Prufert, K., Hurlburt, A., McDonald, K., Engebrecht, J., Villeneuve, A.M., Colaiacovo, M.P., and Colaiácovo, M.P. (2007b). SYP-3 restricts synaptonemal complex assembly to bridge paired chromosome axes during meiosis in Caenorhabditis elegans. Genetics *176*, 2015–2025.

Smolikov, S., Schild-Prüfert, K., and Colaiácovo, M.P. (2009). A yeast two-hybrid screen for SYP-3 interactors identifies SYP-4, a component required for synaptonemal complex assembly and chiasma formation in Caenorhabditis elegans meiosis. PLoS Genetics *5*, e1000669.

Solari, A.J. (1974). The behavior of the XY pair in mammals. Int Rev Cytol *38*, 273–317.

Sumner, A. (2003). Chromosomes : organization and function (Malden MA ;;Oxford: Blackwell Pub.).

Suzuki, R., and Shimodaira, H. (2006). Pvclust: an R package for assessing the uncertainty in hierarchical clustering. Bioinformatics (Oxford, England) *22*, 1540–1542.

Sym, M., Engebrecht, J.A., and Roeder, G.S. (1993). ZIP1 is a synaptonemal complex protein required for meiotic chromosome synapsis. Cell *72*, 365–378.

Sym, M., and Roeder, G.S. (1994). Crossover interference is abolished in the absence of a synaptonemal complex protein. Cell *79*, 283–292.

Tachibana, M., Nozaki, M., Takeda, N., and Shinkai, Y. (2007). Functional dynamics of H3K9 methylation during meiotic prophase progression. The EMBO Journal *26*, 3346–3359.

Tang, S.-J. (2011). A Model of DNA Repeat-Assembled Mitotic Chromosomal Skeleton. Genes *2*, 661–670.

Tease, C., Hartshorne, G.M., and Hultén, M.A. (2002). Patterns of meiotic recombination in human fetal oocytes. American Journal of Human Genetics *70*, 1469–1479.

Tease, C., and Hultén, M.A. (2004). Inter-sex variation in synaptonemal complex lengths largely determine the different recombination rates in male and female germ cells. Cytogenetic and Genome Research *107*, 208–215.

Tsai, J.-H., and McKee, B.D. (2011). Homologous pairing and the role of pairing centers in meiosis. Journal of Cell Science *124*, 1955–1963.

Turner, J.M., Mahadevaiah, S.K., Fernandez-Capetillo, O., Nussenzweig, A., Xu, X., Deng, C.X., and Burgoyne, P.S. (2005). Silencing of unsynapsed meiotic chromosomes in the mouse. Nat Genet *37*, 41–47.

Turner, J.M. a (2007). Meiotic sex chromosome inactivation. Development (Cambridge, England) *134*, 1823–1831.

Turner, J.M.A., Aprelikova, O., Xu, X., Wang, R., Kim, S., Chandramouli, G.V.R., Barrett, J.C., Burgoyne, P.S., and Deng, C.-X. (2004). BRCA1, histone H2AX phosphorylation, and male meiotic sex chromosome inactivation. Current Biology : CB *14*, 2135–2142.

Vader, G., Blitzblau, H.G., Tame, M.A., Falk, J.E., Curtin, L., and Hochwagen, A. (2011). Protection of repetitive DNA borders from self-induced meiotic instability. Nature *477*, 115–119.

Villeneuve, A.M. (1994). A cis-acting locus that promotes crossing over between X chromosomes in Caenorhabditis elegans. Genetics *136*, 887–902.

Voelkel-Meiman, K., Moustafa, S.S., Lefrançois, P., Villeneuve, A.M., and Macqueen, A.J. (2012). Full-Length Synaptonemal Complex Grows Continuously during Meiotic Prophase in Budding Yeast. PLoS Genetics *8*, e1002993.

Wagner, C.R., Kuervers, L., Baillie, D.L., and Yanowitz, J.L. (2010). xnd-1 regulates the global recombination landscape in Caenorhabditis elegans. Nature *467*, 839–843.

Wallace, B.M.N., and Wallace, H. (2003). Synaptonemal complex karyotype of zebrafish. Heredity *90*, 136–140.

Wang, Z., Gerstein, M., and Snyder, M. (2009). RNA-Seq: a revolutionary tool for transcriptomics. Nature Reviews. Genetics *10*, 57–63.

Westergaard, M., and von Wettstein, D. (1972). The synaptinemal complex. Annual Review of Genetics *6*, 71–110.

von Wettstein, D., Rasmussen, S.W., and Holm, P.B. (1984). The synaptonemal complex in genetic segregation. Annual Review of Genetics *18*, 331–413.

White, M. (1973). Animal cytology and evolution (Cambridge [Eng.]: University Press).

Wood, A.J., Severson, A.F., and Meyer, B.J. (2010). Condensin and cohesin complexity: the expanding repertoire of functions. Nature Reviews. Genetics *11*, 391–404.

Wu, H.-Y., and Burgess, S.M. (2006). Two distinct surveillance mechanisms monitor meiotic chromosome metabolism in budding yeast. Current Biology : CB *16*, 2473–2479.

Wynne, D.J., Rog, O., Carlton, P.M., and Dernburg, A.F. (2012). Dynein-dependent processive chromosome motions promote homologous pairing in C. elegans meiosis. The Journal of Cell Biology *196*, 47–64.

Yang, F., and Wang, P.J. (2009). The Mammalian synaptonemal complex: a scaffold and beyond. Genome Dynamics *5*, 69–80.

Yu, H.-G., and Koshland, D.E. (2003). Meiotic condensin is required for proper chromosome compaction, SC assembly, and resolution of recombination-dependent chromosome linkages. The Journal of Cell Biology *163*, 937–947.

Yuan, L., Pelttari, J., Brundell, E., Björkroth, B., Zhao, J., Liu, J.G., Brismar, H., Daneholt, B., and Höög, C. (1998). The synaptonemal complex protein SCP3 can form multistranded, cross-striated fibers in vivo. The Journal of Cell Biology *142*, 331–339.

Zarkower, D. (2006). Somatic sex determination. WormBook : the Online Review of C. Elegans Biology 1–12.

Zetka, M.C., Kawasaki, I., Strome, S., and Müller, F. (1999). Synapsis and chiasma formation in Caenorhabditis elegans require HIM-3, a meiotic chromosome core component that functions in chromosome segregation. Genes & Development *13*, 2258–2270.

Zetka, M.C., and Rose, A.M. (1990). Sex-related differences in crossing over in Caenorhabditis elegans. Genetics *126*, 355–363.

Zickler, D. (2006). From early homologue recognition to synaptonemal complex formation. Chromosoma *115*, 158–174.

Zickler, D., and Kleckner, N. (1998). The leptotene-zygotene transition of meiosis. Annual Review of Genetics *32*, 619–697.

Zickler, D., and Kleckner, N. (1999). Meiotic chromosomes: integrating structure and function. Annual Review of Genetics *33*, 603–754.